Novel anti-glioblastoma therapeutic vaccines based on optimal stimulation of tumor specific CD4+ T helper cells

Andrea GATTA

Ph.D. in Experimental and Translational Medicine
XXXVI Cycle

Under the Supervision of
Prof. Greta FORLANI

Laboratories of General Pathology and Immunology
"Giovanna Tosi"

Department of Medicine and Surgery
University of Insubria

Coordinator:
Prof. Mauro FASANO

February 2024

Abstract

Glioblastoma (GBM) is the most malignant tumor of the central nervous system. Current treatments based on surgery, chemotherapy, and radiotherapy, and more recently on selected immunological approaches, unfortunately produce dismal outcomes, and less than 2% of patients survive after 5 years. Thus, there is an urgent need for new therapeutic strategies.

The immune response against tumor starts with the cell-to-cell contact between professional antigen presenting cells (APC), and CD4+ T helper cells (TH). This is mainly attributable to the interaction between the T cell receptor (TCR), present on TH and the tumor-associated antigens (TAAs), expressed on MHC-II surface of APC. TH cells are fundamental for optimal induction of both humoral and cellular effector mechanisms. Considering the importance of TH cell activation in the adaptive immune response against tumor, our laboratory has undertaken, an approach whereby tumor cells are genetically modified to express MHC-II molecules with the idea that they may act as surrogate APCs for self-antigen presentation. This is possible through the transfection in tumor cells of CIITA, the major controller of MHC-II gene expression. Whitin this frame, my PhD program has been mainly focused on demonstrating the efficacy of CIITA-based vaccination strategy in GBM.

Firstly, I have used the GL261 murine GBM model. Results revealed that mice injected with GL261-CIITA express de novo MHC class II molecules and reject or strongly retard tumor growth as a consequence of rapid infiltration of the tumor by CD4+ and CD8+ T cells. Importantly, mice vaccinated with GL261-CIITA cells by injection in the right brain hemisphere strongly reject parental GL261 tumors injected in the opposite brain hemisphere, indicating not only the acquisition of anti-tumor immune memory but also the capacity of immune T cells to migrate within the brain, overcoming the blood–brain barrier.

To evaluate the efficacy of our vaccination strategy with GL261-CIITA in eliciting a long-lasting protection, an Overall Survival (OS) study was performed. The Kaplan-Meier survival analysis confirmed a significant prolonged OS in mice intracranially injected with GL261-CIITA. Furthermore, data revealed that CIITA vaccination elicited a strong memory immune response able to protect also against parental tumor challenge.

To better recapitulate the immunosuppressive feature of human glioblastoma, GL261 and GL261-CIITA were also cultured *in vitro* to generate neurospheres (NS). The approach with GMB neurospheres confirmed the efficacy of CIITA-tumor transfection in inducing an effective adaptive immune response.

At this point, it was crucial to assess whether the adaptive immunity generated in the GL261 GBM model system after modification with CIITA could be extendable to other murine GBM cell lines. To this end a detailed characterization of CT-2A tumor cell line has been conducted. The higher tumorigenicity and invasiveness make CT-2A a versatile model more similar to human GBM. Results clearly showed that CT-2A-CIITA tumor cells could be rejected or strongly delayed in their *in vivo* growth when injected into syngeneic immunocompetent mice, thus establishing the generality of the anti-tumor protection by modification of tumor cells with CIITA.

To evaluate if generalized protection from GBM tumor growth was a consequence of an adaptive immune response against shared tumor antigens between distinct GBM cells, mice were vaccinated with GL261-CIITA and challenged with CT-2A cells. Importantly, the results showed an efficient CT-2A tumor rejection.

These results established for the first time the existence of shared immunogenic antigens between two distinct GBM cell lines amenable to an identification by molecular analysis of the corresponding immunopeptidomes.

Finally, I investigated whether an oncolytic Herpes Simplex virus (oHSV-1) could be used *in vivo* in our murine GBM tumor models to reduce tumor growth, as a preliminary step to construct HSV viral vectors containing

also CIITA to synergize the immunogenic potential of optimal tumor peptide generation and presentation to tumor specific TH cells. To do so, in collaboration with the University of Padova, I tested an oHSV-1 in our GL261 GBM model. Results shown a significant prolongation of mice survival after injection with the oncolytic HSV-1 virus. To assess whether oncolytic treatment was able not only to induce tumor cell lysis but also to generate an efficient anti-tumor immune response, oHSV-1-treated mice were challenged with GL261 in the opposite hemisphere. Of extreme interest, all challenged mice completely rejected the tumor. Thus, it appears likely that treatment of tumors with oHSV-1 induces cell death liberating in the inflamed tumor milieu relevant immunogenic tumor antigens captured by antigen presenting cells responsible of the following activation and further maturation of tumor-specific CD4+ and particularly CD8+ T cells. Overall, these data open new avenues for exploring the immunotherapeutic potential of HSV-1 in the context of Glioblastoma treatment and warrant further investigation into the underlying mechanisms driving this observed immune response.

Index

Introduction

General features of glioblastomas (GBM): WHO classification, epidemiology and risk factors

Glioblastoma (GBM) is the most aggressive and deadly form brain cancer in adults, known as a highly immunosuppressive tumor [1].
The World Health Organisation (WHO) developed a universally accepted system for the classification of brain tumours. This classification includes a histological grading system (I-IV), which indicates the differentiation status of the tumour, its malignant potential, the response to treatment and the survival of the patient [2]. According to the malignancy, there are four different grades of glioma tumours: grade I tumors, such as pilocytic astrocytomas and gangliocytomas; grade II and III gliomas consist of diffuse and anaplastic astrocytomas, oligodendrogliomas and anaplastic gangliogliomas [2]. Grade IV astrocytomas or glioblastoma multiforme (GBM) is characterised by aggressive invasion, diffuse infiltration of the surrounding brain tissue, strong vascularisation, necrosis, high proliferation. It can arise de novo as primary GBM or can evolve from a lower-grade tumour (secondary GBM). Median survival after diagnosis is 14 months, with less than 3 to 5% of patients surviving longer than 5 years. Without treatment, average survival is about 3 months [3,4] Genetic predisposition has been observed in 5-10 % of glioma cases [5]. There are some rare genetic syndromes associated with an increased risk of glioma: neurofibromatosis 1 and 2, tuberous sclerosis, retinoblastoma (RB) 1, Li-Fraumeni syndrome, Turcot's syndrome, and Hippel-Lindau syndrome [6,7].

Cellular origin of GBM

The cellular origin is a major determinant of the molecular subtype and may contribute to tumor development (8). Consistent with this concept and confirmed by GBM mouse models, the cellular origin might significantly contribute to specific GBM tumorigenic pattern. Indeed, the direction of GBM research, has been strongly influenced by the discovery of GBM-initiating cells (GICs), characterized by strong tumorigenic ability and by resistance to irradiation and anticancer drugs such as temozolomide (TMZ) (9,10**).** Literature data reveal that the GBM may originate from three different cell types: neural stem cells (NSCs), NSC-derived astrocytes and oligodendrocyte precursor cells (OPCs). NSCs are ubiquitously present into the CNS, especially during embryonic development, leading to the neuronal differentiation (11) into radial glial progenitor cells (RPGs), which further differentiate into neurons and oligodendrocyte progenitor cells (OPCs). A restricted subset of NSCs are found in adulthood in specific regions such as the subventricular zone (SVZ) of the lateral ventricle and the subgranular zone (SGZ) of the dentate gyrus in the hippocampus (12,13). Considering the self-renewal and the high proliferative properties of NSCs associated with their presence in adult brain, it has been hypothesized that the NSCs in the SVZ could be the main source of de novo specific GBM-driver mutations. Several studies have been conducted to confirm these hypotheses.
Among them, Hopewell and colleagues illustrated in murine models that tumors were frequently induced from the VZ/SVZ when tumor promoters, such as 3,4-benzpyrene and 20-methylcholanthrene, were injected into various regions (14**).** Kondo et al. induced NSCs and OPCs to transform in GICs after the combination of oncogenic Ras overexpression and p53 inhibition (15–17). The same authors also disclosed that OPCs can lose

their native characteristics and acquire NSC features (reversion) during transformation processes ([18,19]). Another group induced malignant glioma in mice after the transplantation of NSCs constitutively expressing the active form of EGFR ([20]). Finally, Liu and collaborators found, through mutant–mosaic analysis with a double-marker (MADM) mouse model, an aberrant cell growth derived from OPCs but not from NSC-derived lineages ([21]). Overall, these findings suggest that NSCs, OPCs and astrocytes are possible cells of origin for GBM and that probably non-NSCs may acquire NSC characteristics in their transformation process, contributing to tumour heterogeneity, including GICs and differentiation marker-positive cancer cells (Figure 1).

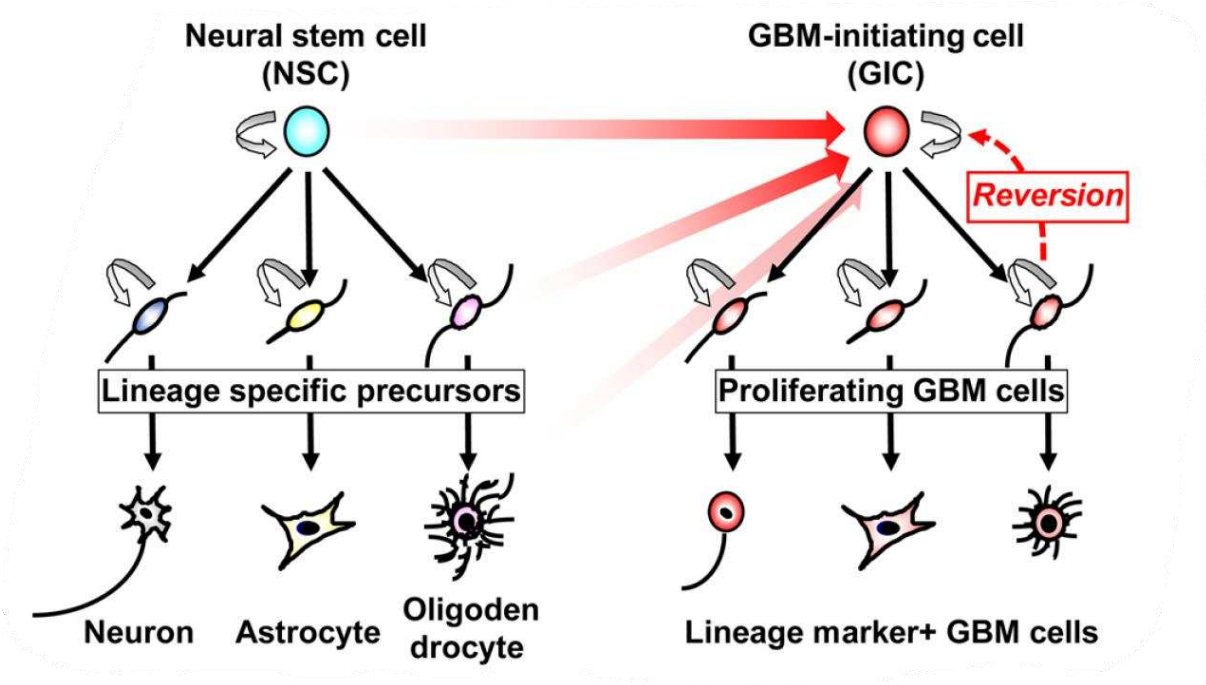

Fig. 1 | Tumour heterogeneity is generated by cell of origin, genetic mutation/epigenetic regulation and tumour environment factors. Neural stem cells (NSCs) self-renew and generate mature neurons, astrocytes and oligodendrocytes via proliferating precursor cells (left). Similarly, glioblastoma-initiating cells (GICs) self-renew and generate differentiation marker-positive cancer cells. NSCs, oligodendrocyte precursor cells (OPCs) and astrocytes, GIC cells of origin, transform into at least 3 types of GICs when these cells acquire genetic mutations/epigenetic changes. It should be noted that OPCs acquire NSC characteristics and lose their specific characteristics in the transformation process (reversion). From [22].

The cancer stem cell hypothesis represents an important advancement in the understanding of GBM origin, opening new perspectives for new therapeutic modalities to find a cure for a lethal disease. Despite intensive research, however, the definitive identity of GICs still remains elusive.

GBM heterogeneity

Thanks to developments in high-throughput analysis over the decades, GBM has been categorized according to their mutational, transcriptional, or epigenetic profiles. Within a single tumor, heterogeneity is characterized by distinctive genetic or gene expression profiles among different cell subpopulations ([23,24]). Currently, few studies have investigated into the clonal architecture of gliomas, revealing the mutational heterogeneity that characterizes GBM ([25]).

In order to improve the knowledge of the factors driving the evolution of GBM tumors and consequent resistance to treatment, the Cancer Genome Atlas Consortium (TCGA) performed high-dimensional profiling

and molecular classification of nearly 600 GBM tumors. ([26–29]). Common mutations in genes including *TP53, EGFR, IDH1, and PTEN* were found in TCGA, together with the frequent and concurrent presence of abnormalities in the RB, and receptor tyrosine kinase pathways.
Transcriptome analysis also revealed four GBM subtypes, identified as classical (CL), mesenchymal (MES), neural (NE), and proneural (PN), that were strongly related to genomic abnormalities ([27,30]) (Figure 2).

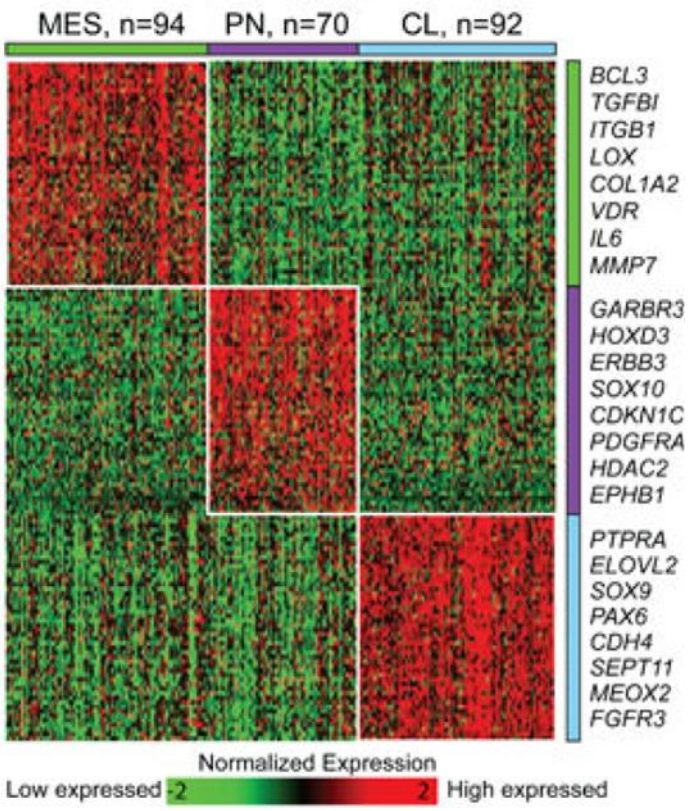

Figure 2 | Molecular classification of IDH-WT GBMs. Heatmap of 50-gene signatures by gene expression subtype. For each subtype, representative genes are provided ([30]).

The transcriptional glioma subtypes, defined by tumor-intrinsic gene clustering, strongly overlapped with the proneural, classical, and mesenchymal subtypes, however the neural subtype was identified as normal neural lineage contamination ([30]). Although distinct genetic alterations are related to each subtype, there is a significant plasticity among them: within the same tumors, multiple subtypes coexist, and shift in subtypes can occur over time ([24,31]).
Combining single-cell RNA-sequencing (scRNA-seq) from several GBM patients and analysis of over 400 TCGA bulk specimens, Neftel et al. discovered that malignant cells in GBM exist in a restricted set of cellular states: neural progenitor-like (NPC-like), oligodendrocyte-progenitor like (OPC-like), astrocyte-like (AC-like), and mesenchymal like (MES-like) ([32]). Every glioblastoma sample contains cells in multiple states, with the potential to proliferate or transition to other states. The relative frequency of each state can vary between tumors. This plasticity could be attributed to clonal variation, stem-like reprogramming, or the acquisition of new genetic and epigenetic abnormalities ([33]) (Figure 3).
Neftel et al. also discovered a wide distribution within tumors, with each state being most common in certain tumors and less prevalent in others. This suggests that other factors may also affect proliferation and transition rates. Particularly, a steady state distribution is defined by certain transition rates that are determined by specific genetic factors. EGFR aberrations, which are associated to a relative abundance of AC-

like cells, appear to be a crucial genetic factor. Similarly, Chr5q deletions and NF1 alterations impact the frequency of MES-like states, whereas amplifications of CDK4 and PDGFRA are strictly related to the NPC-like and OPC-like states, respectively ([32]).

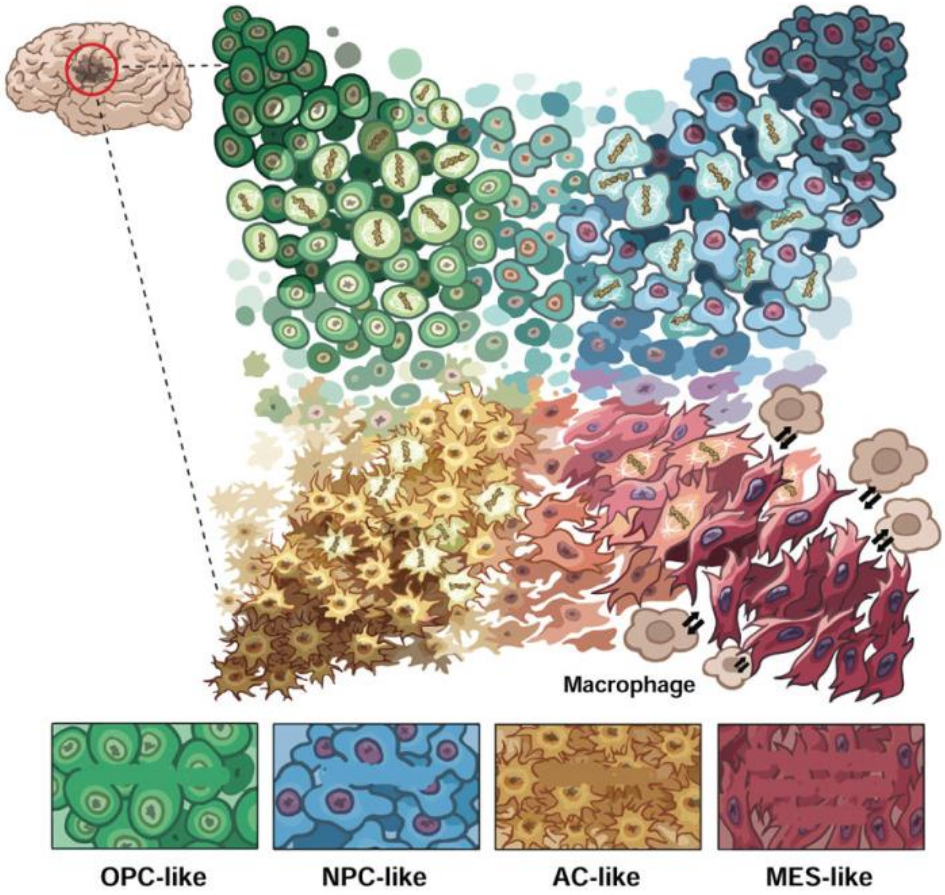

Figure 3 | Cellular transitions in glioblastoma. This model represents the cellular states of glioblastoma and their genetic and micro-environmental factors. Lighter or darker tones denote the strength of each program. Transitions between the four states are represented by intermediate states. ([32])

For instance, PN and CL tumors frequently display a MES phenotype upon recurrence, and treatment also improves the mesenchymal gene signature. These findings suggest that the MES transition (also known as epithelial to mesenchymal (MES)-like), is linked to tumor progression and therapy resistance ([34–36]). In both primary and recurrent tumor settings, patients with the MES subtype typically have worse survival rates compared to patients with other subtypes. Interestingly, when compared to PN and CL subtypes, non-neoplastic cells are extensively infiltrated into MES subtype tumors ([30]). Moreover, MES tumors exhibit high levels of necrosis and high expression of angiogenic markers. The most prevalent genetic alterations include neurofibromatosis type 1 gene (NF1) copy number loss or mutation and significant increased expression of regulators of the MES subtype, including STAT3, CEBPB, and TAZ ([27,37,38])**.** Specifically, CEBPB and STAT3 are identified as master regulators and synergistic initiators of mesenchymal transformation. While the removal of both CEBPB and STAT3 in glioma cells results in the collapse of the mesenchymal signature and a decrease in tumor aggressiveness, their ectopic co-expression reprogrammes neural stem cells along the aberrant mesenchymal lineage. Notably, Carro et al. identified the transcriptional repressor ZBTB18 (a.k.a ZNF238) (Figure 4). In a following up study, the authors strongly validated ZBTB18 as a potential negative regulator of the MGES in GBM ([33]).

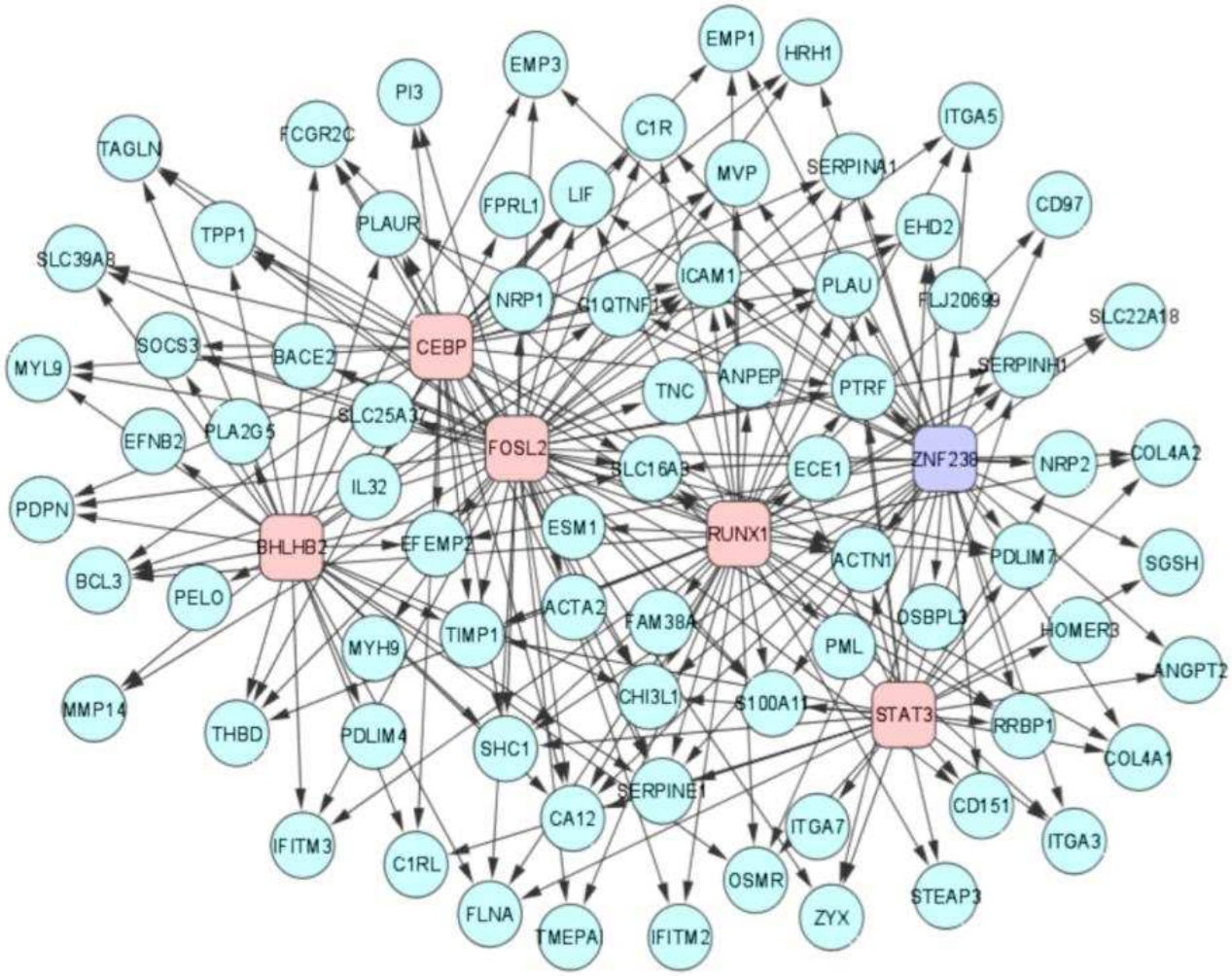

Figure 4 | Six transcription factors control the mesenchymal signature of high-grade gliomas. Six transcription factors control the mesenchymal signature of high-grade gliomas. TFs associated with activation of MGES targets are shown in pink, and those associated with repression are in purple. The MGES targets that are controlled by these TFs are shown in cyan. According to the results of the study, the six transcription factors control 74% of the genes in the mesenchymal signature of high-grade gliomas ([38]).

ZBTB18: a negative regulator of GBM mesenchymal genes

ZBTB18 (RP58 or ZNF238) belongs to the BTB/POZ-ZF [Broad complex, Tramtrack, Bric à brac (BTB) or poxvirus and zing finger (POZ)-zinc finger] protein family, which also includes B-cell lymphoma 6 (BCL-6), promyelocytic leukemia zinc finger (PLZF), and hypermethylated in cancer 1 (HIC-1). These proteins are involved in the development and/or formation of cancer ([39]). The four zinc fingers of ZBTB18 are found at the COOH-terminal region of the protein, while the BTB/POZ domain is found at the NH2-terminal region and is highly conserved across humans, mice, and zebrafish. According to Hill et al**.**, human ZBTB18 is located on chromosome 1q44 in a region that is deleted in patients with microcephaly ([40]). This could suggest a role of ZBTB18 in coordinating the production of mature differentiated cells, that compose the bulk of the brain. Indeed, previous findings have identified ZBTB18 as a factor highly expressed in postmitotic granule neuron precursors (GNPs) and differentiated neurons. In contrast, in mouse gliomas and human GBM cell lines, ZBTB18 is lost or downregulated, and implicated as a putative tumor suppressor in the brain ([41])**.** Neural-specific knock-out experiments demonstrated that loss of ZBTB18 in the central nervous system (CNS) leads to a severe impairment of neurogenesis, resulting in a remarkable postnatal small-brain phenotype.

According to Xiang et al., ZBTB18 regulates the fate and differentiation of cortical cells at the early corticogenesis stages, allowing normal brain growth ([42]). Indeed, several studies confirmed the role of ZBTB18 on neuronal development, differentiation, and maturation ([43,44]). In humans, ZBTB18 alterations are linked to macrocephaly, microcephaly, intellectual disability, and epilepsy ([45–48]).

The 58KD zinc finger protein is also associated to the regulation of the PI3K pathway, which is involved in several cellular processes, including B cell activation. Particularly, ZBTB18 directly binds enhancer/promoter regions of genes encoding class I PI3K regulatory subunits, subsequently limiting their expression, dampening PI3K signaling and suppressing plasma cells (PC) responses. Following activation, ZBTB18 was gradually downregulated by dividing B cells, allowing gradual amplification of PI3K signals and supporting PC differentiation ([49]).

Wang and collaborators suggested that a decline in the activity of the transcriptional repressor ZBTB18 defines metastasis-competent cancer cells in mouse models. Restoration of ZBTB18 activity reduces chromatin accessibility at the promoters of genes that drive metastasis, such as Tgfbr2, and this prevents TGFβ1 pathway activation and consequently reduces cell migration and invasion. Besides repressing the expression of metastatic genes, ZBTB18 also induces widespread chromatin closing, a global epigenetic adaptation previously linked to reduced phenotypic flexibility. Thus, ZBTB18 is a potent chromatin regulator, and the loss of its activity enhances chromatin accessibility and transcriptional adaptations that promote the phenotypic changes required for metastasis ([50]).

According to Fedele et al., ZBTB18 is primarily expressed in proneural GBMs and low-grade gliomas in comparison to mesenchymal GBMs, when it is less expressed ([33]). This finding is consistent with previous studies of ZBTB18 as a transcription factor, negatively associated with mesenchymal GBMs ([38]).

Additionally, the authors discovered that loss of ZBTB18 contributes to the aggressive phenotype of glioblastoma, by regulating markers associated with poor prognosis. Conversely, restoring ZBTB18 expression reverses the phenotype and impairs tumorigenesis. This was also confirmed by in vivo experiments in which ZBTB18 expression prolonged animal survival by delaying or inhibiting tumor formation. Particularly, data suggest that ZBTB18 attenuates the expression of EMT-related genes and time-to-tumor progression in GBM ([51,52]).

In order to elucidate the mechanism of ZBTB18 downregulation in GBM, in silico analysis of the ZBTB18 promoter was performed. Results revealed the presence of two CpG islands, suggesting that DNA hypermethylation could play a role in the transcriptional repression of ZBTB18, thereby promoting phenotype-driven tumor progression towards a more mesenchymal phenotype. These finding suggest a strong association between ZBTB18 promoter hypermethylation and mesenchymal GBM subtype, implying that ZBTB18 silencing by promoter methylation is a specific hallmark of this unfavourable GBM subtype.

ZBTB18 was also identified as a novel colorectal tumor suppressor gene. In fact, reintroducing ZBTB18 into colon cancer cells significantly reduced proliferation in vitro and in a subcutaneous xenograft mouse model. According to immunohistochemical analysis, ZBTB18 is frequently lost or reduced in colorectal tumors. The reduction of ZBTB18 expression was found to be associated with lymph node metastasis and a lower prognosis for patients with locally advanced colorectal cancer ([53]).

Pathogenesis & clinical presentation

Among the major pathways of glioma genesis, one is involved in mutations of the isocitrate dehydrogenase (IDH), a key enzyme in the tricyclic acid cycle. The mutated IDH1/2 gene is responsible of the synthesis of an oncometabolite, which interferes with several cellular processes, including DNA methylation ([54]). Interestingly, the IDH wild type glioblastomas (90-95% of all GBM) show the worst prognosis and treatment response, if compared to the mutated variant ([55,56]). IDH1 R132H represents a tumor-specific antigen, for this reason immunotherapy trials currently aim at vaccination to induce antitumor immunoreactions ([57]). GBM harbour other genetic alterations, mainly affecting three signalling pathways: receptor tyrosine kinase (RTK), retinoblastoma (RB1), and p53. Most alterations that affect the RTK family are EGFR amplifications and PTEN deletions/mutations in 40-50% of cases, PDGFRA (10-18%), phosphatidylinositol-3-OH kinase (PI3K) and NF1 alterations in 15-25% of cases. In the RB1 pathway, alterations include mutations/deletions of CDKN2A/p16 (52%) and amplifications of CDK4 in 10-15% of cases. In the p53 signalling pathway, the most frequent alterations involves CDKN2B/ARF (49%), TP53 (28-35%) and MDM2 amplification (7-14%) ([58–60]). Mutations in the promoter region of the telomerase reverse transcriptase (TERT), were detected in 70–80% of GBM cases. The presence of TERT mutation is commonly associated with poor outcome and can itself contribute to gliomagenesis ([61]). Alpha-thalassemia C-linked mental retardation (ATRX) mutations are found in approximately 30% of pediatric GBM and in 6% of adult glioblastoma. Because nuclear ATRX is diminished in tumors with the ALT phenotype, ATRX immunohistochemistry has become useful in identifying potential IDH mutants, H3F3A alterations or secondary GBM ([62,63]). Methylation of the MGMT promoter region results in decreased MGMT activity, which in turn results in decreased tumor resistance to alkylating agent therapy with TMZ and is therefore a predictive molecular marker. Approximately 40% of all primary GBM carry a methylated promoter ([64,65]). In general, a staged approach to therapeutically relevant molecular analysis is guided by factors such as the GBM subtype, patient's age, tumor location, and staining results. This includes the analysis of the 1p19q codeletion, MGMT promoter methylation, H3F3A screening, TERT promoter, and IDH hotspot mutations (Figure 5).

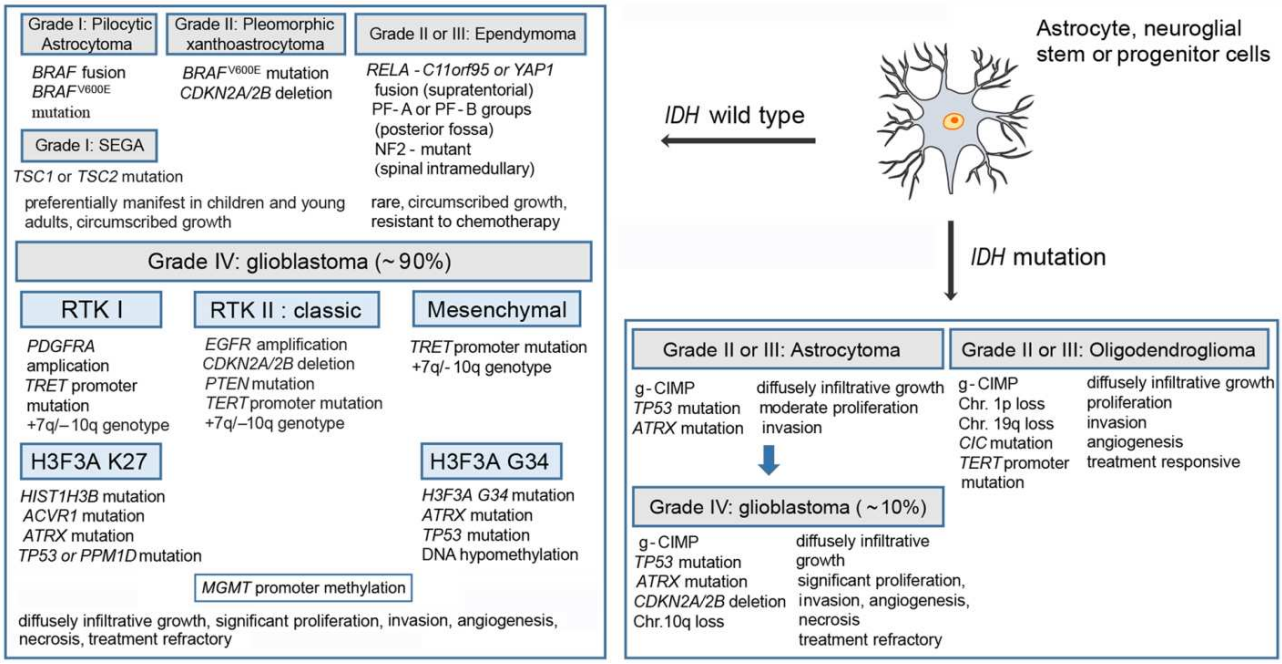

Figure 5 | Genetic and epigenetic alterations in the genesis of gliomas. Shown are the relationships between the molecular lesions and pathobiology in the different types of gliomas. IDH, socitrate dehydrogenase; RELA, transcription factor p65; CDKN, cyclin-

dependent kinase inhibitor; YAP1, YES-associated protein 1; PF, posterior fossa; NF2, neurofibromin 2; SEGA, subependymal giant cell astrocytoma; TSC, tuberous sclerosis; RTK, receptor tyrosine kinase; PDGFRA, platelet-derived growth factor receptor-α; TERT, telomerase reverse transcriptase; PTEN, phosphatase and tensin homologue; EGFR, epidermal growth factor receptor; H3F3A, histone H3.3; HIST1H3B, histone H3.1; ACVR1, activin A receptor 1; ATRX, α-thalassemia/mental retardation syndrome X-linked; TP53, tumour protein p53; PPM1D, protein phosphatase 1D; MGMT, O-6-methylguanine-DNA methyltransferase; g-CIMP, glioma CpG island methylator phenotype; Chr., chromosome; CIC, Drosophila homologue of capicua; Those IDH-mutant glioblastomas derived by progression from pre-existing lower grade astrocytomas (blue arrow) are tend to manifest in younger patients (≤50 years of age) compared with IDH wild-type tumors. From [66]

Typically, the first clinical signs are linked to an increase of intracranial pressure: headache, nausea and vomiting, and papilledema. Other symptoms include confusion, personality changes, memory loss, and epileptic seizures ([67]). Magnetic resonance imaging (RM) or computed tomography (TC) are needed when persistent neurological symptoms are observed. The detection of an increasing mass with surrounding oedema suggests the presence of malignant glioma. Nevertheless, the diagnosis can be only histopathologically confirmed at the tumor surgical debulking ([67]) (Figure 6).

Figure 6 | Glioblastoma multiforme, RM. T1 weighted RM sequences with (A) or without (B) contrast agent. T1 sequences shows a left parieto-occipital mass with perilesional oedema on FLAIR sequence (C). Adapted from ([68]).

Current standard of care

The gold standard of treatment for GBM is surgery, followed by a combination of daily RT (radiotherapy) and oral CT (chemotherapy) for six weeks. RT regimen is given in 2 daily fractions of 60 Gray (Gy) combined with 75 mg of Temozolomide (TMZ) per square meter of body-surface area. An additional six cycles of adjuvant CT is required by using 150-200 mg (per square meter of body-surface area) of TMZ five days a month ([69,70]). TMZ, an alkylating prodrug, when is converted into the active compound adds methyl groups to DNA in specific positions, including to O 6 -guanin residues. If DNA damage is not repaired, it will lead to tumor cell death ([71,72]). It is administered orally and well tolerated; main toxicity includes nausea, vomiting, and myelosuppression ([73]). Usually, in case of recurrence, it can be given in combination with other cytotoxic drugs, cytostatic agents and signal transduction modulators.

Carmustine (BCNU), an old alkylating agent used in GBM therapy, is administered locally in the surgical area (e.g. by Gliadel Wafers) or systemically i.v. Side effects include nausea, vomiting, pulmonary fibrosis, myelosuppression, seizures and cerebral oedema. It is usually reserved for treatment at progression in addition to the PCV (Procarbazine, Lomustine, Vincristine) combination treatment ([73–76]).

Recently, tumour treating fields (TTFields; Optune) are devices that specifically deliver electric fields to the tumour location to disrupt cancer cell division. TTFields have currently emerged as an FDA-approved treatment for both recurrent and newly diagnosed GBM ([77]). Nevertheless, the patient survival is still very low, and the disease is basically incurable due to the high recurrence rate. This failure is mainly attributed to

GBM molecular heterogeneity that results in tumour evasion pathways against pharmacological treatments. Advances in glioblastoma multiforme therapy are highly required in way to simultaneously improve the patient survival and reduce the side effects of medical treatment. Recent advances in glioma biology are promising for development of newly therapeutics strategies that specifically target the tumor compartment ([78,79]).

Novel approaches in GBM therapy

It is well known that GBM stem cells (GSCs) are the main responsible of GBM drug resistance, because of their high malignant properties such as the pluripotency, the high proliferation rate and the genetic instability. Studying them from a cellular and molecular point of view represent an important challenge to identify specific targets for each individual patient. Therefore, a broad search is underway for new and targeted therapies, such as molecular target therapy & immunotherapy representing a valid and important element for personalized medicine (PM).

Targeted Therapy

Typically, inhibitors are designed to specifically target a single biomarker or a group of biomarkers that exhibit significant upregulation in cancerous tissues compared to healthy ones. Generally, these inhibitors are developed for either extracellular targets such as cell surface receptors or intracellular components involved in signaling and activation of oncogenic pathways ([80]).

Target therapy includes different kinds of EGFR inhibitors, such as cetuximab (Erbitux) a recombinant monoclonal anti-body against EGFR that blocks the EGF binding and prevents receptor activation ([81,82]). The EGFR tyrosine kinase inhibitors, such as gefitinib (Iressa) and erlotinib (Tarceva), inhibit activation of the receptor-coupled tyrosine kinase ([83]).

MET/HGFR (Mesenchymal epithelial transition/hepatocyte growth factor receptor) is a proto-oncogene, having a key role in the tumor proliferation and growth. Onartuzumab and Cabozatinib are respectively a monoclonal antibody and a tyrosine kinase inhibitor of MET and have been shown to inhibit GBM growth in preclinical studies ([84,85]).

EphA3 receptor is highly expressed in GBM, promoting its tumorigenicity. A monoclonal antibody that binds the EphA3 globular ephrin-binding domain has been developed, and the humanised version (ifabotuzumab) is currently in Phase 0/1 clinical trial ([86]).

The PI3K/Akt signalling pathway plays a critical role in the regulation of signal transduction, mediating several processes in GBM, including proliferation, survival and angiogenesis. Buparlisib, a pan PI3K inhibitor, reduces GBM cell growth both *in vitro* and *in vivo*. It is currently in phase II clinical trial ([87,88]).

In the management of GBM, the most important class of vascular targeting drugs is the angiogenesis inhibitors. One of such inhibitors, bevacizumab (Avastin), has already been approved in the USA for monotherapy of GBM after progression. Bevacizumab is a monoclonal antibody that binds to secreted VEGF-A, that prevent it from the interaction with VEGFR-2 to exert its proangiogenic effects ([89]). Bevacizumab's side effects most commonly include hypertension and leukopenia ([90,91]). Alternatives to the anti VEGF-A monoclonal antibodies in GBM therapy include the PDGFR tyrosine kinase inhibitors (e.g. dasatinib - SPRYCEL®), the fibroblast growth factor receptor tyrosine kinase inhibitors (e.g. brivanib) and the αvβ3/αvβ5

integrin inhibitor cilengitide ([92,93]). Since PARP enzyme is important for DNA repair, PARP inhibitors represent an effective therapy in combination with alkylating agents. Several combination treatments are in preclinical and clinical trials, such as Veliparib-TMZ ([94]) Additional PARP inhibitors meriting further clinical study include niraparib and talazoparib ([95,96]). Another type of drug carrier that are suggested for the glioblastoma therapy are targeted protein toxins. The first consists of modified bacterial toxins to avoid unspecific binding to healty mammalian cells and conjugated to a targeting molecule. Examples of clinical phase drugs include a modified diphtheria toxin conjugated to transferrin (Tf-CRM107 - TransMID) as well as interleukin-4 PE38KDEL and interleukin-13 PE38QQR (Cintredekin besudotox) ([97]). Targeted liposomes are another type of drug carriers that have been suggested for therapy of glioblastoma multiforme. An advantage of using this technology, compared to drug/protein conjugates is that a massive drug amount can be transported by a single carrier, and also many types of drugs can be encapsulated ([98]). An interesting example include doxorubicin-liposomes. These are targeted to the transferrin receptor and to the interleukin receptors, both overexpressed on the surface of GBM cells ([99,100]). Additional molecular targets for inhibitors include myeloid cell leukemia-1 (MCL-1), and topoisomerase I inhibitors. MCL-1 is associated with PTEN deletion/mutation which occurs in 30–60% of GBM patients ([101]). Another biomarker under investigation is mTOR. Temsirolimus and everolimus are small molecular inhibitors that have been developed for mTOR which plays a role in glioma induction, growth, and progression ([102]).

Immune therapy

Lack of efficiency and development of resistance are the main limitations found with molecular targeted and antiangiogenic drugs. Therefore, it is necessary to further optimize them to achieve the desired effects. A further promising strategy to tackle GBM is based on immunotherapeutic approaches which have recently been shown to produces important success in various forms of cancer. They are based on the individual's activation of effector mechanisms mediated by crucial cells of the immune system, the lymphocytes. Traditionally, it was generally thought that the absence of a lymphatic drainage system and the presence of the blood brain barrier (BBB) render the central nervous system (CNS) an immune-privileged organ ([103]). Recent findings, however, have shown the existence of a CNS lymphatic network ([104],[105]). Consequently, in the last few years, immunotherapy is quickly becoming a possible option in GBM therapy. There are mainly four types of immunotherapies that may possibly apply to treat gliomas: Immune checkpoint blockade (ICBs), Chimeric antigen receptor T (CAR-T) cell therapies, vaccines, and oncolytic virus (OV) treatment ([106,107]) (Figure 7).

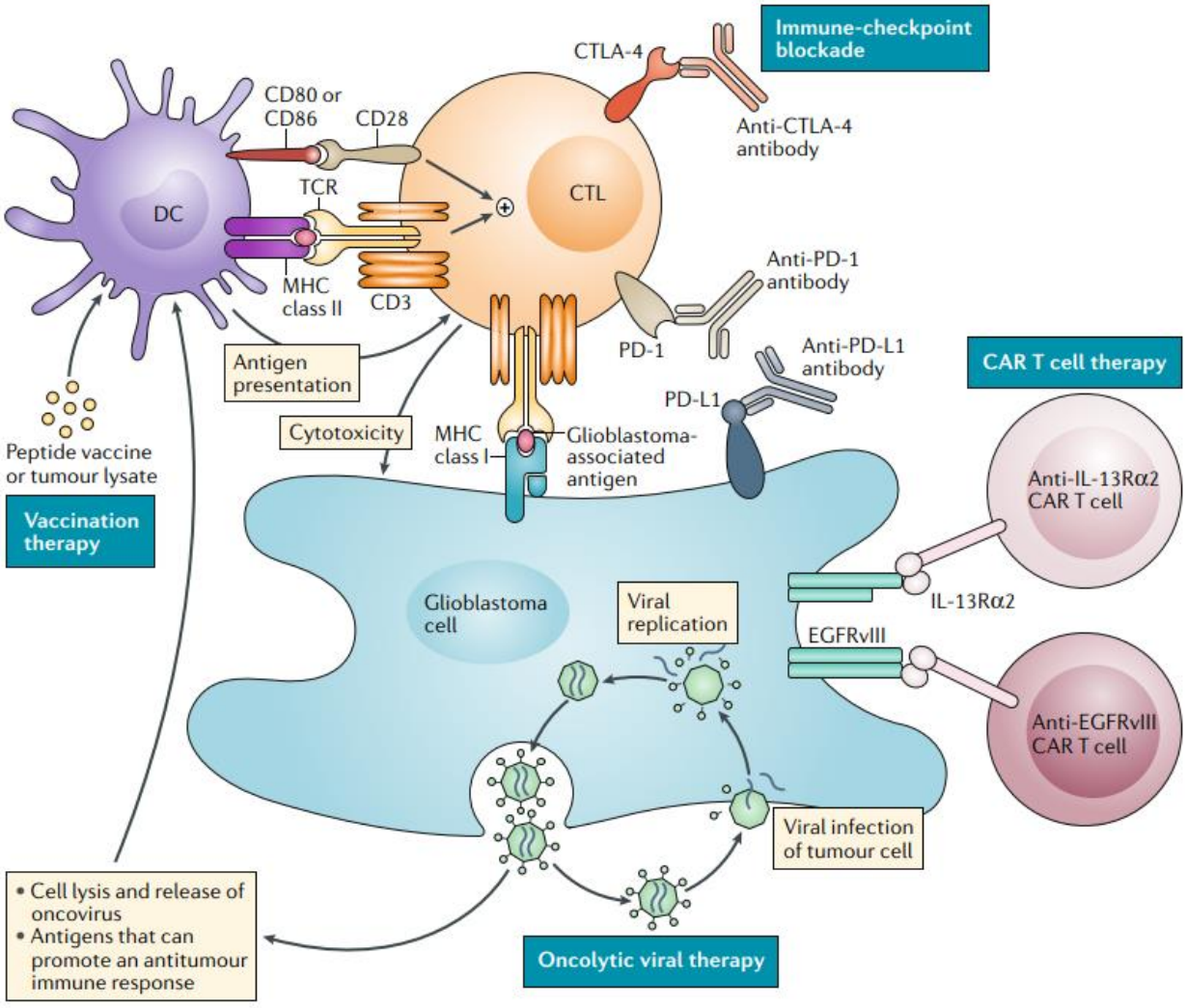

Figure 7 | Current immunotherapy modalities for the treatment of glioblastoma. Glioblastoma vaccine therapy relies on dendritic cell (DC)-mediated presentation of glioblastoma-associated peptides, antigens, or epitopes derived from tumour lysates to T cells of the adaptive immune system through MHC class II–T cell receptor (TCR) (signal 1) and CD80 and/or CD86–CD28 (signal 2) interactions. The cytotoxic T lymphocytes (CTLs) that are subsequently activated interrogate and destroy tumour cells containing glioblastoma-associated antigens presented on MHC class I molecules. However, tumour cells often evade destruction by CTLs through upregulation of immune-checkpoint ligands, such as programmed cell death 1 ligand 1 (PD-L1) that can bind complementary receptors on the CTLs, such as programmed cell death protein 1 (PD-1) to cause suppression of lymphocyte activation. Immune-checkpoint blockade with monoclonal antibodies effectively prevents this interaction. Similarly, antibody-mediated blockade of cytotoxic T lymphocyte protein 4 (CTLA-4), an inhibitory immune-checkpoint molecule that binds CD80 and CD86 and prevents their interaction with CD28, can promote T cell priming by DCs. Glioblastoma-associated antigens, including IL-13 receptor subunit-α2 (IL-13Rα2) and EGFR variant III (EGFRvIII), are also presented on tumour cell surfaces independent of MHC class I, and these tumour-associated antigens are being exploited as specific targets of genetically modified chimeric antigen receptor (CAR) T cell therapies. Genetic engineering is also used in oncolytic viral therapy to create viruses that selectively infect or replicate in tumour cells. The resulting tumour cell lysis not only kills the infected tumour cells directly but can also activate immunogenic tumour cell death pathways that can stimulate antigen presentation and an adaptive antitumour immune response. From [106]

Immune-checkpoint blockades

Immune checkpoints (IC) are surface molecules expressed on activated T lymphocytes able to negatively regulate host immunity through their interaction with ligands/receptors expressed on other cells, mostly myeloid derived cells. As these effector T cells, both CD4+ T helper (TH) and CD8+ cytolytic T (CTL) cells can be found in tumors, and they are at least in part specific for tumor derived antigens, their incapacity to overcome tumor growth has been associated to their functional inhibition via the binding to ligands/receptors that can also be expressed on tumor cells. Blocking the inhibitors is thus a way to maintain the activation status of effector T cells. Checkpoint inhibition has revolutionized treatment of several advanced malignancies providing hope for cancer treatment. GBM is characterized by a restricted number of somatic mutations and by consequence by a limited repertoire of tumor specific neo-antigens, and by a limited T-cell infiltration compared with other tumor types, limiting the availability of IC blockade. Still, immune checkpoint inhibitors (ICI) gathered considerable interest in GBM therapy, considering the unique immunologically properties of CNS. The most widely investigated IC molecules are Cytotoxic T-Lymphocyte Antigen 4 (CTLA-4), involved in early T-cell activation, and programmed cell death protein 1 (PD-1), which inhibits T-cells at later stage ([108]). Recent clinical trials, however, demonstrated poor result in terms of overall survival or disease-free survival in GBM patients treated with ICI ([109–112]). Although preclinical studies suggested that the combinatorial action of CTLA-4 and IL-12 blockade can elicit the T cell-mediated glioma rejection in GBM syngeneic mice ([113]). Although, several positive results were found in translational studies, however a restricted number of hypothetical treatments will be translated into clinical trials in patients with GBM ([114]).

CAR-T therapy

In this therapeutical approach T cells are engineered to express chimeric antigen receptors (CARs), consisting of the antigen recognition domains of antibodies linked to T cell activation domains derived from the T cell receptor CD3 ζ- chain (CD3ζ) and co--stimulatory receptors (such as CD28 and/or TNFRSF9 (commonly known as 4-1BB)) ([115]). Since CAR recognition is not dependent from MHC-presentation pathway, this therapy has the advantage to arm directly the T cells for recognition of tumor cells expressing the relevant antigen bypassing the MHC antigen presentation subsequential development of adaptive immune response ([116]). Several clinical and pre-clinical trials are currently under way, for GBM, some of which have been recently completed, such as CAR-T cells targeted with various tumor antigens like EGFRvIII, HER2, IL13R α2 and B7-H3, an immune checkpoint overexpressed in GBM ([117–120]). In 2017, it was published the results of a first-in-human clinical trial (NCT02209376) of CAR T-EGFRvIII in 10 patients with recurrent GBM. The results revealed the safety and feasibility of this treatment, although no survival benefits were observed ([117]).

Additionally, a IL-8 receptor-modified CD70-CAR T cells was constructed to specifically migrate into GBM and induce an enhanced antitumor- response ([121]). Recently, bispecific T cell engagers (BiTEs) have been proposed as a solution against tumor antigen escape, that limit the durability of responses to CAR T therapy ([122]). The collective results from these early clinical investigations suggest that glioblastomas possess the ability to trigger different adaptive reactions in order to subvert anticancer immune responses and restore an immunosuppressive environment. Overcoming these escape mechanisms will be crucial in enhancing the efficacy of immunotherapy in GBM. Together, the findings of these early clinical studies suggest that glioblastomas can activate various adaptive responses to subvert anticancer immune responses and reinstate an immunosuppressive milieu; these escape mechanisms will need to be overcome if we are to improve the effectiveness of immunotherapy for this disease.

Vaccine Therapy

Differently from prophylactic vaccines, cancer vaccines are administered to cancer patients and are designed to eradicate tumor by boosting the patient immune response. The cancer vaccines have the ability to activate the immune system to specifically attack cancer cells and saving the others. Cancer vaccines have provided important insights on immune responses of GBM and are continuously investigated, especially in conjunction with multimodal treatment regimens. Vaccines are mainly divided into peptide-based vaccines and cell-based vaccines. The most studied peptide-based vaccine is rindopepimut (CDX-110) that targets the EGFRvIII variant. This truncated protein, present in approximatively 20-30% of GBMs, leads to constitutive EGF pathway activation. Actually, rindopepimut in combination with bevacizumab is in phase II trial ([123]).

ICT107 is a synthetic peptide able to stimulate DC cells and specifically designed for GBM, which has reached the phase III of clinical trials. A phase I study demonstrated the safety of ICT-107 in GBM patients HLA-A2 positive ([124]). Vaccine therapies for GBM treatment include the ex-vivo modification of glioma cell lines and the use of these cells as vaccine against the parent tumor. An example is the SMA-560 glioma cell lines engineered to express MICA, a receptor on NK and T-cells which stimulates the immune response ([125,126]). Among cell-based vaccines, the DCVax is possibly the most prominent. Basically, dendritic cells derived from patients are pulsed with different tumor-associated antigens (TAAs), antigen peptides and autologous tumor lysate ([127]). Although there is the potential risk to develop an autologous response, multiple early clinical trials were able to identify GBM patients for safe DCVax application, culminating in a phase III study. Although the study has yet to be formally completed, median overall survival has been reported at 23.1 months ([128]). A very recent phase I/II clinical trial treatment in GBM is UCPVax, a therapeutic anti-cancer vaccine based on the telomerase-derived helper peptides designed to induce strong TH1 CD4 T cell responses in cancer patients (NCT02818426).

GVAX is a cancer vaccine prepared by genetic modification of the prostate cancer cell lines genetically transduced with a retroviral vector containing the cDNA encoding the human granulocyte macrophage colony stimulating factor (GM-CSF) gene. An important advantage of GVAX resides in the fact that is a polyvalent source of tumor antigens to the immune system; the combination with the GM-CSF secretion highly increases the immune response. These vaccines have been shown to be more effective when in combination with checkpoint inhibitors, such as with PD-1 blockade or anti CTLA-4 ([129]).

Heat shock protein (HSPs) vaccines have been employed in the treatment of glioma, constituting a distinct category of vaccines. HSPs play a crucial role in protein folding and chaperoning. The efficacy of HSPs vaccines lies in their ability to exploit the interaction between antigen presenting cells and heat shock proteins. Antigen presenting cells recognize HSPs as they would any other antigen, internalize them, and subsequently display these HSP proteins on MHC complexes. Some HSPs vaccines are actually in clinical trials ([130]).

Oncolytic therapy

Clinical trials for the treatment of GBM have progressively integrated immunotherapeutic approaches, such as replication competent oncolytic viruses (OVs). Ovs are selectively anticancer and immunotherapeutic agents that are specifically able to infect, replicate, and destroy tumor cells by multiple mechanisms and without damaging normal tissue.

OVs generate a host systemic antitumoral immunity through multiple mechanisms, such as direct cytotoxicity

and also an immunotherapeutic effect. Indeed, after viral infection, the presence of OV in the immunosuppressive tumor microenvironment (TME) determines a strong immunogenic effect leading to the release of viral pathogen-associated molecular pattern (PAMPs) molecules and additional Immunogenic Cell Death (ICD) – hallmarks, such as death-associated molecular pattern (DAMPs) molecules, heat shock proteins, HMGB1, CRT, ATP and uric acid and cytokines (TNFα, IFNγ and IL.12) which stimulate the innate immune responses. Furthermore, the release of soluble TAAs can induce, after cell lysis, the activation of the adaptive immune response ([131]). Indeed, the relevance of available neo-antigens can develop an immune response and generate new T-cell clones able to circulate and kill antigen-expressing cancer cells, including the ones not infected ([132]).

Virotherapy is currently considered a promising tool of GBM immunotherapy. To date, nine different viruses families, including both DNA and RNA base viruses, have successfully moved from preclinical to early clinical trials, with more than 570 ongoing clinical trials testing OVs ([133]). Recently, preclinical studies using a retroviral-replicating vector (TOCA 511) that encodes a prodrug activator enzyme, cytosine deaminase, resulted in an efficient combinatorial therapeutical action mediated by suicide gene therapy and antitumor immunity. These promising results led to several clinical trials in patients with GBM tumors, including the ongoing phase III trials (NCT02414165). ([134])

Based on limitation of other delivery modes (i.e. intravenous treatment correlated with viral antibody neutralization ([135])), intratumoral injection is currently become the method of choice for OV delivery.

Early clinical trials showed that OVs replication after infection in tumor mass was generally transient and occurred in localized areas, resulting in suboptimal therapeutical efficacy. ([136]) Indeed, preclinical studies demonstrated that the main physical barrier to OVs were the extracellular matrix (ECM) proteins, polysaccharides, tumor-associated fibroblasts, inflammatory cells, and high interstitial fluid pressure in the tumor mass ([137,138]). Hyaluronic acid (HA) and collagen are major components of ECM, and previous preclinical studies have shown that degradation of HA by a proteolytic enzyme, hyaluronidase, reduces interstitial fluid pressure, permitting anticancer agents to reach breast cancer cells. Since Hyaluronic acid (HA) and collagen are major components of ECM, an armed oncolytic adenovirus expressing hyaluronidase PH20 (ICOVIR17), has been produced. Results revealed that ICOVIR17 degrades the HA in glioblastoma (GBM) tumors, leading to an enhanced distribution of OV within the tumor mass and a subsequent significant increase in tumor cell death in mouse tumor models of GBM ([139]).

Several virus families have been tested in clinical trials for GBM treatment. However, herpes simplex virus type 1 (HSV-1) is considered the most promising one, thanks to its own specific characteristics, such as its potent lytic ability, the broad spectrum of infected cells, ease of genomic modification, induction of long-term cellular immune responses, and availability of drugs for control of its proliferation ([140]).

The HSV genome comprises several essential and non-essential genes that can be modified to selectively replicate in cancer cells. γ34.5 is the HSV-1 gene mainly involved in viral neuropathogenicity. Its deletion results in no viral replication in healthy cells. HSV1716 (Seprehvir) was derived from wild type HSV-1 only removing neurovirulence-related gene. The safety of this OV strain has been assessed in phase I and IIa trials for high-grade glioma (HGG) ([141]).

The second generation of oncolytic HSV was engineered with the diploid deletion of γ34.5 and inactivation of ICP6, relevant for viral DNA replication. Since this gene is required to replicate in non-dividing cells, its functional deletion prevent viral damage of healthy tissue adjacent to the tumor. Clinical studies have been conducted in GBM therapy, revealing an excellent safety profile with none of the patients developing HSV encephalitis following intratumoral injections. Results obtained exhibited potential for clinical response in patients with progressive, recurrent, malignant glioma ([142,143]).

A third generation OV, G47Δ was obtained from G207 after deletion of ICP47, a gene involved in the downregulation of MHC-I, resulting in enhanced antitumor immune response. Surprisingly, this OV exhibited

strong antitumor efficacy in patients with glioblastoma when used in phase II trial (UMIN000015995) ([144]). Another phase I/II study recurrent/progressive GBM indicated a median overall survival of 7.3 months with 38.5% having a 1-year survival rate ([145]). Now it is pending approval for GBM treatment in Japan ([146]).

Another oncolytic HSV variant is rQNestin34.5v.2, obtained after restoring one copy of γ34.5 under the transcriptional control of the nestin promoter/enhancer element. This resulted in an increased oHSV-1 replication, but again limited on GBM cells, due to their higher level of nestin expression compared to healthy cells. Upon treatment with rQNestin34.5v.2, around 80% of athymic mice bearing intracerebral human U87dEGFR glioma tumors survived >90 days, compared to control group injected only with GBM ([147]). To further reduce the neurovirulence, Nakashima and collaborators generated a new oHSV-1 strain by substituting γ34.5 with GADD34. This new OV (NG34), demonstrated greater tolerability compared to rQNestin34.5 in mouse models, representing a new tool for subsequent preclinical trials ([145]). Cheema et al. constructed an oncolytic HSV based on G47Δ structure, with the additional insertion of IL-12 cDNA in the ICP6 region ([148]). Significantly, G47Δ-IL12 drastically inhibited GBM angiogenesis and extended mice survival, compared to unarmed oncolytic HSV. Particularly, data revealed a significant reduction in FOXP3+ cells and inhibition of angiogenesis ([149]). Other cytokines were inserted in G47Δ backbone, like FMS-like tyrosine kinase 3 ligand (Flt3L) or tumor necrosis factor-related apoptosis-inducing ligand (TRAIL), resulting in efficient against GBM ([150–152]).

Actually, one of the most promising strategies able to revolutionize tumor immunotherapy is the combination of OVs with immune checkpoint inhibitors. Recent studies have confirmed that a triple combination of anti–CTLA-4, anti–PD-1, and oncolytic HSV–IL-12 resulted in long-term durable survival in the majority of GBM-bearing mice as a consequence of a prominent increase in T cell population ([153]).

Recently, new therapeutical approaches have been tested, increasing the viral selectivity toward GBM. Since HER2 is frequently expressed in GBMs, R-LM113, a recombinant HSV strain generated by insertion of a single chain specific for HER2, is fully retargeted to this overexpressed protein. A study demonstrated that mice injected with HER2-engineered GBM cells infected with R-LM113 can survive twice as long as mice injected with uninfected cells ([154]).

Noteworthy, cell-based carriers are promising methods also within oHSV therapy. Particularly, Reale and colleagues disclosed a newly approach based on using monocytes as oHSV-1 carriers in vivo ([155]). Thus, more clinical and preclinical trials are needed to determine the best combination strategy. Several challenges are still required to improve the efficacy of oncolytic HSV therapy in GBM treatment.

Tumor microenvironment in GBM: mechanism of immunoediting

The TME is defined as the complex and rich multicellular environment in which a tumor develops. There is a dynamic relationship between immune surveillance, tumor-induced immunosuppression and cancer development. This highly immunoediting process is divided into 3 phases: immunosurveillance, equilibrium/editing phase between immune action and tumor growth and escape phase with uncontrolled tumor growth. TME niche in GBM is comprised of various components, including the original cancer cell with genetic alterations and other cells like astrocytes, pericytes, endothelial cells, GSCs, blood vessels, glioma-associated stromal cells, immune cells including myeloid-derived suppressor cells (MDSCs), glioma-associated microglia/macrophages (GAMs), tumour-infiltrating T-cells (TILs), NK cells, and extracellular matrix (ECM) ([156–158]) (Figure 8).

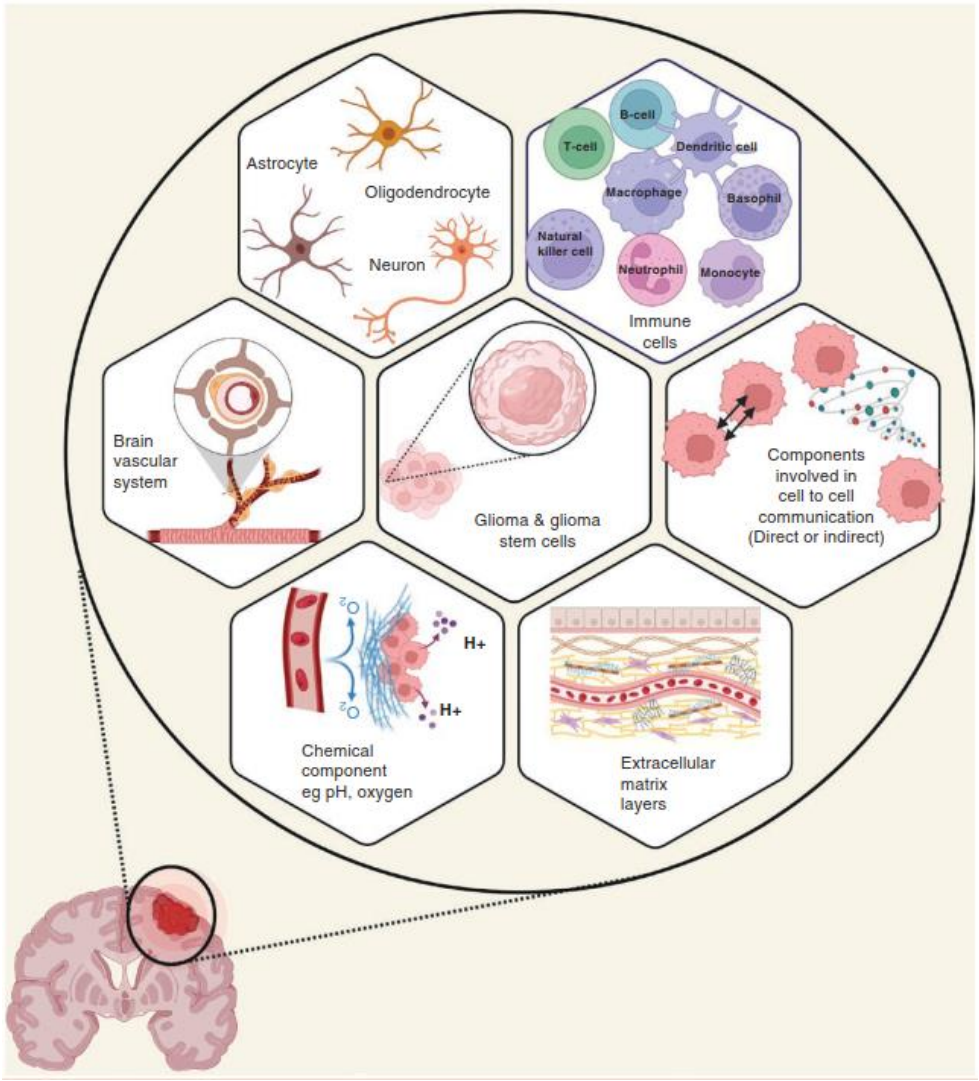

Figure 8 | Schematic representation of the glioma tumor microenvironment components. The glioma tumor microenvironment is a complex, heterogeneous, and interactive system that is consisted of glioma and glioma stem cells, immune cells, nervous system, brain vascular system, and extracellular matrix layers. The factors involved in direct and indirect cell communication and chemical tumor microenvironment such as pH and oxygen also play a significant role in modulating glioma tumor microenvironment. From [159]

The powerful immunosuppressive effect in the TME of gliomas is caused by several mechanisms, including the = presence of immunosuppressive cells M2 glioma associated macrophages (GAMs), Tregs, and myeloid derived suppressor cells (MDSCs)) and immunosuppressive cytokines (TGF-b, IL-10), limited presence of effector tumor infiltrating lymphocytes (TILs), and the high expression of inhibitory immune checkpoint molecules such as PD-1, TIM-3, and LAG-3 ([160,161]). The most abundant cells in GBM are GAMs, which are divided into two different subtypes, based on their polarization: the M1 phenotype (proinflammatory) and the M2 phenotype (immunosuppressive). M2 GAMs contribute to induce an immunosuppressive environment producing IL-10, TGF- β, arginase 1 (ARG1) and promote tumor heterogeneity and progression through secretion of vascular endothelial growth factor (VEGF) and matrix metalloproteases (MP) and promotion of GSCs proliferation. Conversely, M1 GAMs counteract tumor growth secreting pro-inflammatory molecules (IL-1β, TNF-α, IL-6, and IL-12), promoting T helper 1 (Th1)-mediated immune responses ([162–164]). = Cancer-associated fibroblast (CAFs) can also promote tumor progression through the expression of CXCL12. Consequently, CAFs induce angiogenesis by recruiting marrow-derived precursors that contribute to vessel development ([165]). MDSCs are defined as immature myeloid cells able to strongly suppress T-cell response ([166]). Their action in contributing to tumor immune escape is involved in NK cell inhibition ([167]) and reduction

of adaptive immune response. To do so, MDSCs promote FOXP3+ regulatory T cells response and inhibit T-cell function and proliferation through production of ARG1 and inducible nitric oxide (NO) synthase 2 (iNOS2) or, via reactive oxygen species (ROS) and TGF-β production, cysteine depletion, and L-selectin (CD62L) downregulation ([168,169]). Recently, it has been discovered that MDSCs upregulate PDL-1 expression on tumor cells, inducing a more T-cell exhaustion effect ([170]).The immune checkpoint expression (PD-L1 and TIGIT) by GBM cells and the low mutational load associated with the downregulation of MHC-I strongly hampers their recognition by tumor infiltrating lymphocytes (TILs) ([171–173]). Tumor Immune Microenvironment (TIME) is composed of immune cells, with restricted CTL compartment, mainly circumscribed along the invasive margin and characterized by low expression of the activation markers GZMB (GRZB) and IFNG. Prolonged immune activation and ambiguous stimulation, as consequence of uncontrolled released of cytokines, alter the CD8+ lymphocyte action, resulting in a loss of their cytotoxic pattern, also referred as T cell exhaustion ([174,175]). The release of immunosuppressive cytokines including TGF- β and IL-10 by GBM cells, together with M2 GAMs induce Treg stimulation and inhibit the activation of antigen presenting cells (APCs) and effector immune response ([176,177]). In the context of TME, neutrophils can promote tumor progression by the release of vascular endothelial growth factor A (VEGFA), after activation of CXCR2 receptor pathway. As consequence, a cascade of events including neutrophil recruitment is followed by VEGF and matrix metalloproteinase 9 (MMP9) release, leading to endothelial cell invasion and vessel formation ([178,179]). Glioma cells take a central role in regulating the functions of cellular and noncellular components of the TME via complex signaling networks which enables them to regulate processes such as biomass synthesis, maintenance of cellular processes and resistance to therapies that facilitates their survival ([180]).
GSCs can regulate cell metabolism in the TME of gliomas to increase resistance to challenging conditions in addition to reprogramming associated cells to promote tissue remodelling. The intimate interaction between GSCs and glioma TME is a critical factor to the resistance of immunotherapy, and targeting both GSCs and TME can enhance the immunotherapeutic effect.

CIITA, the master transcriptional regulator of MHC class II genes and its key role in adaptive immunity

The tight regulation of both MHC class I and class II molecules, the cell surface structures deputed to present antigenic substances to T cells, CD8+ cytolytic (CTL) and CD4+ helper (TH), respectively, are crucial for eliciting an appropriate adaptive immune response. The regulation of these genes is controlled by multiple conserved cis-regulatory elements at their proximal promoters that comprises a W/SXY module, which encompasses W/S, X1, X2 and Y boxes.
The transcription of MHC II locus is finely controlled by a multi-protein complex, involving regulatory factor X (RFX), cyclic AMP-responsive-element-binding protein (CREB), nuclear transcription factor Y (NF-Y) and CIITA, forming the enhanceosome (Figure 10) ([181,182]). Therefore, CIITA is considered the master transcriptional regulator of MHC II expression, because in its absence the transcription doesn't take place. It was identified in our laboratory through a genetic complementation approach using the HLA-II-negative cell line RJ2.2.5 ([183–185]).

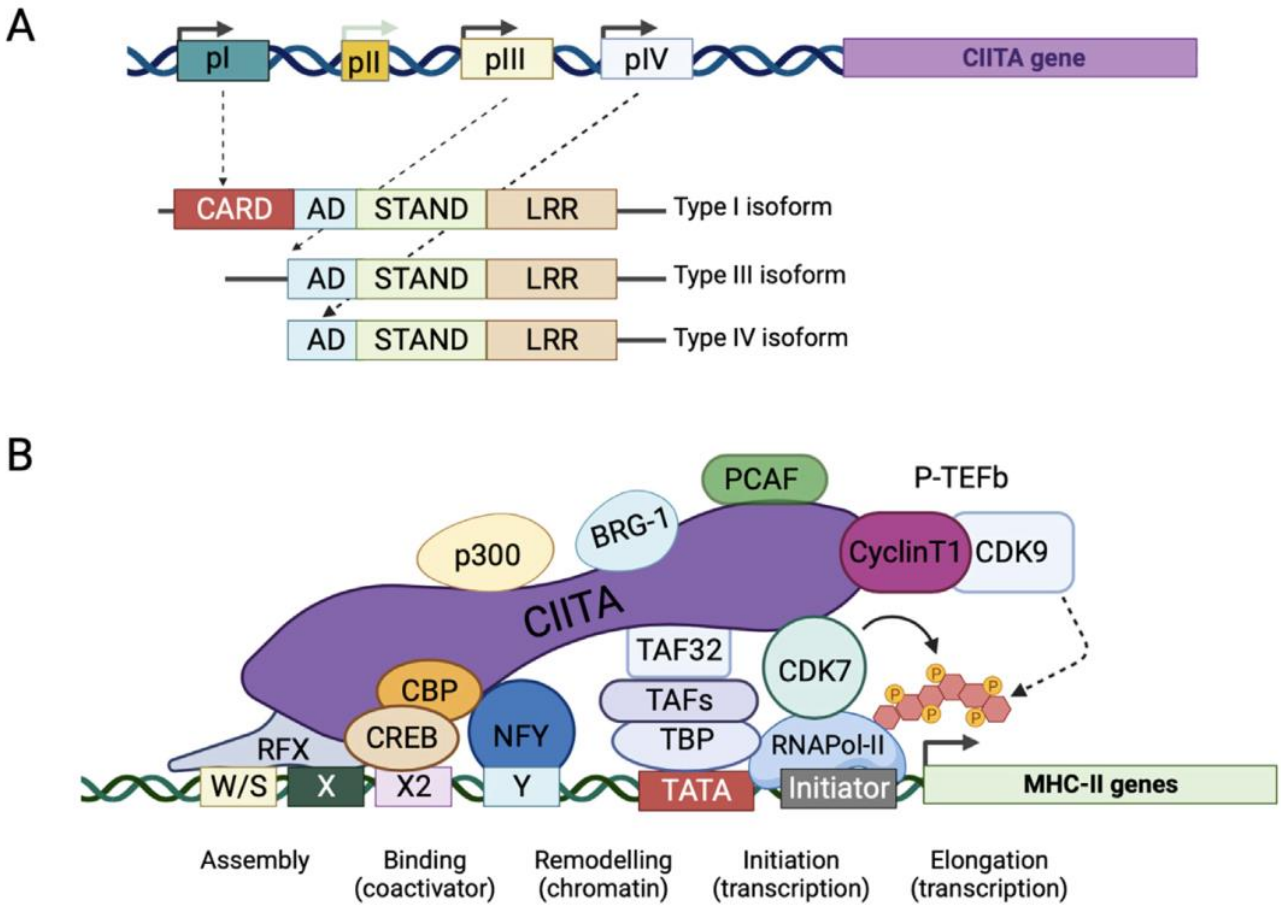

Figure 10 | The MHC class II transactivator CIITA: schematic structure of the gene and function of the protein. (A) Expression of the CIITA gene is controlled by three independent promoters (pI, pIII and pIV) having different functions and expressed in specific cell types. pII is not associated to any transcript. The three types of mRNA encoding CIITA are derived from pI, pIII and pIV, and they encode three different protein isoforms (Type I, Type II and Type III), which differ only at their N-terminal ends. The region shared by all three isoforms contains an acidic activation domain (AD), a core signal transduction ATPase with numerous domains (STAND) and a leucin rich domain (LRR). The N-terminal region of the Type I isoform encodes an additional caspase-like activation and recruiting domain (CARD), not present in the Type II and III protein isoforms. (b) CIITA leads to the assembly of the MHC-II enhanceosome by interacting with CREB/CBP and the NF-Y and RFX transcription factors associated with W/SXY module. In addition, CIITA binds to chromatin modifying enzymes, as BRG1 and many transcriptional co-activators including histone deacetylases (HDACs), histone methyltransferases (HMTs) and histone acetyltransferases (HATs), as p300 and PCAF, thus contributing to chromatin remodeling and transcription activation. Furthermore, CIITA regulates the initiation of MHC-II transcription by recruiting several components of the canonical TFIID complex, as TAFs proteins and TBP. By interacting with Cyclin T1 and CDK9 of positive transcription elongation factor-b (P-TEFb) complex and CDK7, CIITA also controls the elongation of primary transcripts. From [186].

Recently Forlani and collaborators widely described the genetic and molecular characterization of its expression. CIITA is a member of human nucleotide-binding oligomerization domain (NOD)-like receptors (NLR), a large protein family involved in inflammation, cell death and regulation of transcription of key molecules for the homeostasis of the immune system ([186]).

CIITA present a tripartite domain structure similar to that of other NLR proteins with an N-terminal caspase-like activation and recruiting domain (CARD)-like and an acidic activation domain (AD), a core signal transduction ATPase with numerous domains (STAND) and a leucin rich domain (LRR) ([187]). In general CARD domains allow interaction with proteins containing similar CARD domains. The leucin rich repeat (LRR) found in all NLR family members is thought to be important in heterologous protein-protein interactions which is a distinctive characteristic of this family. The nucleotide binding domain (NBD) which is a component of the more structured STAND module drives the self-oligomerization of the protein and is important for cellular defence across species from prokaryotes to eukaryotes ([187–189]) (Figure 10).

CIITA contains both nuclear localization signals (NLS) and nuclear export signals (NES). Indeed, unlike other NLR proteins that are mostly localized in the cytoplasm, or associated with mitochondria or the plasma membrane, CIITA can shuttle between nucleus and cytoplasm ([190]). CIITA gene expression is regulated by four independent promoters, named promoter I, II, III and IV, that can be individually activated in a cell type- and stimulus-specific manner. Three of these promoters are highly conserved between the human and mouse gene (pI, pIII and pIV). In contrast, pII has only been found in the human gene where it has been shown to display only very low transcriptional activity ([191,192]). Lack or defective expression of CIITA leads to a rare but extremely severe form of immunodeficiency, the Bare Lymphocyte syndrome (BLS), characterized by impaired adaptive immune response during the first years of life and often incompatible with life ([193]).

CIITA is constitutively expressed in APCs, but it is also induced in non-antigen presenting cells in response to IFN-γ stimulation ([194]). It acts also as a master regulator of not only polymorphic MHC-II genes but also accessory genes including invariant chain, HLA-DM and HLA-DO, involved in antigen processing and presentation ([195]). CIITA is involved in transcription initiation ad elongation through multiple mechanisms. Indeed, it recruits components of the transcriptional machinery, induces phosphorylation of RNA polymerase II, interacts with P-TEFb and with the 19S proteasomal subunit. In addition, CIITA binds to, and acts as a platform for the recruitment of many transcriptional co-activators including histone acetyltransferases (HATs), histone deacetylases (HDACs), histone methyltransferases (HMTs), chromatin remodelling factors as well as factors of the general transcription complex ([196]), which modulate the activity of enhanceosome and alter chromatin accessibility, further regulating the transcription of MHC-II genes ([197,198]). Furthermore, the interaction of CIITA with the positive transcription elongation factor-b (P-TEFb), composed of Cyclin T1 and CDK9, endows the MHC class II transactivator with a role also in the elongation of primary transcripts ([199–201]). Under defined conditions of signalling and chromatin modifications, CIITA and MHC class II molecules can be expressed in non-immune cells, often in response to infections or inflammation.

Our previous work and aim of the thesis

It is well known that the immune response against tumor starts with the cell-to-cell contact between professional antigen presenting cells (APC), and CD4+ T helper cells. This is mainly attributable to the interaction between the T cell receptor (TCR), present on CD4+ T helper (TH) cells and the tumor-associated antigens (TAAs), expressed on MHC-II surface ([202–204]). TH cells are fundamental for optimal induction of both humoral and cellular effector mechanisms ([205]). In particular for the maturation of MHC class I-restricted CD8+ naive T cells, their clonal expansions and acquisition of cytolytic function ([206]), becoming CD8+ cytolytic T cells (CTL), the real effectors against cancer cells ([207]).

However, in most cancers including GBM, MHC II molecules are rarely expressed on the surface of the cancerous cells ([208]). In addition, the GBM immunosuppressive tumor microenvironment downregulates the MHC expression, and consequently the antigen presentation is compromised ([205]). For these reasons, antigen discovery studies aiming to identify GBM-associated class II antigens resulted in a limited repertoire ([206]). Considering the importance of the $CD4^+$ T helper cells activation in the adaptive immune response against tumor, our laboratory has under-taken, an approach whereby tumor cells are genetically modified to express MHC-II molecules with the idea that they may act as surrogate APCs for self-antigen presentation ([209,210]). To do so, the constitutive MHC-II expression on MHC-II-negative tumor cells was induced by transfection with the transcriptional activator CIITA, the master transcriptional regulator of the MHC II genes expression, discovered in our laboratory ([211]).

Previous results obtained in our laboratory demonstrated that CIITA-driven MHC-II-expressing tumor cells have a potential to induce a strong TH immune response and consequently, to transform the tumor microenvironment from a pro-tumor to an antitumor milieu, associated with the infiltration of both $CD4^+$ and $CD8^+$ T cells ([212,213]). Once transformed with CIITA, tumor cells express MHC class II molecules and thus may act as surrogate APCs for their own tumor antigens for optimal presentation to tumor-specific Th cells ([214,215]). Whitin this frame, my PhD program has been mainly focused on demonstrating the efficacy of CIITA-based vaccination strategy, thus translating our experimental approach also in GBM.

Relevant to the GBM, our recent published studies, which are part of my thesis, and I will refer to, have established the following points relevant to the murine GL261 glioblastoma model:

1. CIITA-transfected GL261 cells, stably expressing MHC class II cell surface molecules after transfection of CIITA are rejected or strongly delayed in their growth when orthotopically injected into the brain of an immunocompetent syngeneic mouse.
2. GL261-CIITA rejecting mice develop an immunological memory that render them resistant to challenge with GL261 parental tumor cells when injected in the opposite hemisphere.
3. Immunohistological studies demonstrated the presence of an immunological infiltrate with preponderance of TH and CTL cells in the brain of mice injected with GL261-CIITA tumor cells

On the basis of the obtained results ([216]), it was fundamental to verify whether the above results were generalizable to other GBM murine models. To this end, an approach similar to the one performed with GL261 has been applied in my PhD thesis to the CT-2A murine GBM cells that share the same MHC genotype with GL261.

Furthermore, and of relevance, in case of positive results, it was crucial to demonstrate whether or not a cross-protection of tumor take from animals vaccinated and protected after GL261-CIITA injection could be generated after injection of CT-2A tumor cells.

Subsequently, I investigated whether oncolytic HSV could be used *in vivo* in our murine GBM tumor models

to reduce tumor growth, as a preliminary step to construct HSV viral vectors containing also CIITA to synergize the immunogenic potential of optimal tumor peptide generation and presentation to tumor specific TH cells. Finally, as future development of my thesis work, in collaboration with Dr. Michal Bassani-Sternberg of the Ludwig Institute for Cancer Research in Lausanne, Switzerland, I initiated a biochemical analysis to characterize the immunopeptidome, and particularly the MHC-II-bound peptide repertoire, expressed in GL261-CIITA tumor cells, with the aim to detect putative tumor-specific peptides that could be used as a vaccine cocktail for future studies of immune vaccination against GBM. Within this frame I have also initiated to set up a cellular model of CIITA and ZBTB18 double transfected GBM cells to assess in future biochemical studies the modification of the MHC-II immunopeptidome in a situation of synergistic modification of the tumor microenvironment. Implicit in this approach is also the question of the distinctive MHC-II immunopeptidome that could be observed in case of suppression of relevant oncogenes mediated by the ZBTB18 tumor suppressor. The above two aspects are briefly described in the section “Future Persectives” of this thesis.

Materials & methods

Animal models

C57BL/6 (H-2b genotype) mice aged 7–8 weeks were purchased from Charles River (Charles River Laboratories Italia SRL, Calco, Italy). Each experiment was repeated at least twice using five to eight mice per group. All animal experiments were conducted according to relevant national and international guidelines and were approved by the University of Insubria Internal Ethics Committee CESA and by the Italian Ministry of Health (Authorization number: 812/2020_PR).

Generation of GL261 and CT-2A cells stably expressing CIITA

The GL261 and CT-2A murine GBM cell lines were cultured in Dulbecco's Modified Eag le Medium (DMEM) (Lonza BioWhittaker™, Durham, NC, USA) supplemented with 10% heat-inactivated fetal calf serum (FCS). Tumor cells were transfected with 5 mg of FLAG-tagged full-length (amino acids 1 to 1130) CIITA (pc-fCIITA) expression vector ([217,218]) using Fugene HD (Promega, Madison, WI, USA), as previously described ([219]). MHC-II-positive cells were enriched by fluorescence-activated cell sorting with a BD FACS ARIA II cell sorter (Becton-Dickinson, Franklin Lakes, NJ, USA) and further subjected to limiting dilution cloning. In detail, CT-2A-CIITA and GL261-CIITA cells sorted for MHC-II-positive expression were diluted to 5–10 cells/ml, and 100 ml/well was dispensed into two 96-well plates. At least 50 clones were analysed and further selected for high MHC-II cell surface expression. GL261-CIITA cells were previously described ([216]).

Measurement of in vitro growth rate

CT-2A GBM tumors with their respective CIITA transfected tumor lines (5 × 104 cells per well), were seeded in 48-well plates, and cell proliferation was measured at 24, 48, and 72 h by counting the cells using trypan blue exclusion assay. Each point in the growth curve was obtained from three independent experiments performed in triplicate wells. GL261-CIITA cells were previously described ([216]).

Neurospheres Culture

For neurosphere formation, 200.000 GL261 / Gl261-CIITA cells were cultured in Dulbecco's Modified Eagle Medium: Nutrient Mixture F-12 (DMEM F12, Sigma-Aldrich, Saint Louis, MO, USA) supplemented with B27 (GIBCO), 20 ng/ml basic fibroblast growth factor (bFGF) (Peprotech), 20 ng/mL epidermal growth factor (EGF) (Peprotech), 1% penicillin/streptomycin (Invitrogen) and GlutaMAX Supplement (GIBCO). Cells were maintained at 37 ◦C in a humidified atmosphere containing 5% CO2. After neurospheres formation, cluster of cells were collected in a 50 mL tube. Washing step with DMEM/F12 medium was required to recover all the remained neurospheres in the T25 flask. Free-floating cells were washed by centrifugation at 500 RPM at RT for 5-7 minutes, resuspended in 200-500 uL growth medium and mechanically dissociated to obtain single-cell suspension. Cells were ready to be counted under light microscope and subsequently used for in vivo experiments. The remained cells were centrifugated, resuspended into DMEM/F12 fresh media and plated at a density of 200.000 cells/flask pending further neurospheres formation. Mycoplasma tests were routinely

performed on the cultured cells using the MycoAlert Mycoplasma Detection Kit (Lonza, Switzerland). Neurospheres were observed under a BX61 fluorescence microscope (Olympus, Tokyo, Japan).

Fluorescence-activated cell sorting analysis

Cell surface expression of both MHC-I and MHC-II molecules was assessed by immunofluorescence and flow cytometry (BD FACSAria™II Cell Sorter, BD Biosciences, San Jose, CA, USA) using an anti-H-2 K/D class I monoclonal antibody (clone M1/42, BioLegend, San Diego, CA, USA) and anti-IA/IE class II monoclonal antibody (clone M5/114.15.2, BioLegend), respectively. Negative controls were obtained by staining the cells with specific isotype-matched antibodies. FlowJo v. 9.5.2 software (Tree Star Inc., Ashland, OR, USA) was used to analyse the data.

Viral vector

EGFP-oHSV1 is based on strain 17+ HSV-1 and its construction and production have been previously described ([155]).

Intracranial injection

In order to verify the tumorigenicity of CIITA-transduced GBM cell lines, compared to the GBM parental controls, tumor cells were orthotopically injected in the brain of syngeneic C57BL/6. Cells were harvested by trypsinization, washed, and resuspended in PBS. Mice were anesthetized using ketamine [100 mg/kg] and xylazine [15 mg/kg], preceded by a tramadol injection [5 mg/kg] for pain relief. The head was shaved with clippers and the mouse's eyes were protected by coating with sterile ocular lubricant. The animal was then fit into a stereotactic table by placing properly the ear bars. The skull was cleaned with a sterile cotton swab soaked in ethanol and a sagittal scalp incision of 1 cm was performed from the front to the back.
A small burr hole was done 2 mm dorsal to and 1.5 mm right to the bregma with a microdrill (RWD Life Science). 30,000 GBM parental or GBM-CIITA tumor cells were then re-suspended in 3 µl of medium without serum and injected with a Hamilton syringe through a 27-gauge needle: over 1 mm into the right striatum, at 3 mm depth below the dura mater (Figure 11). Cells were implanted slowly (1 µl/min flow rate) to avoid elevation of the intracranial pressure, and the syringe was left for 3 minutes to prevent inoculated cells from ascending through the track of the needle. The cut was carefully cleaned with sterile swab soaked with sterile PBS and the skin edges were sutured. Mice were then monitored in their cages during recovery from anaesthesia on a daily basis.
Without any sign of considerable tumor burden (e.g., gait or balance difficulties as neurological sign), at day 21 after tumor injection, mice were sacrificed, their brains were harvested and checked for the presence or absence of tumors by immune-histological analysis.
As far as oHSV-1 treatment, a total of 3×10^4 GL261 cells in 3 µl of serum-free medium were intracranially injected 3 mm deep from the dura using a 26-gauge needle targeting the right striatum as indicated above. Seven days post-GL261 tumor injection, two groups of mice were injected in the same brain hemisphere with 107 EGFP-oHSV1 (oHSV-1) or vehicle (PBS). Mice were monitored daily for signs of brain tumor growth, such as seizures, ataxia, or weight loss, and were euthanized if the tumor burden became symptomatic. After 43 days from the injection of the tumor cells, long-term survivor mice (GL261+ oHSV-1) were injected in the left striatum with 3×10^4 GL261 parental tumor cells. Subsequently, all mice were euthanized after an additional

3 weeks, and their brains were prepared for histological analysis as described below.

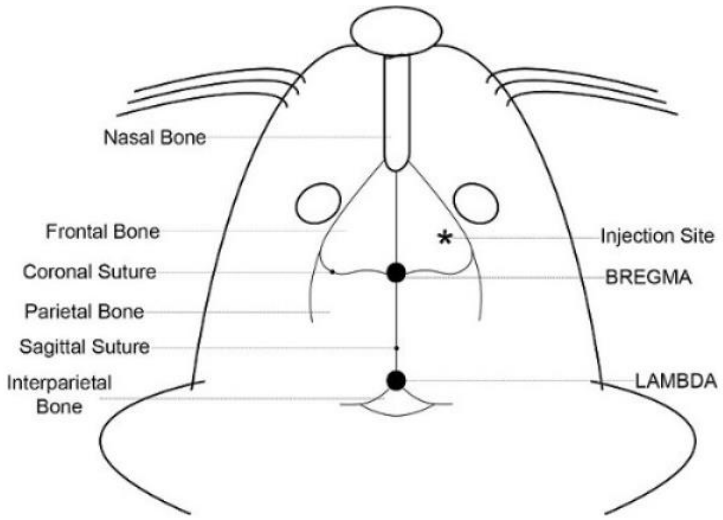

Figure 11 | Stereotaxical coordinates for IC tumor injection. The anatomical features of the mouse head and skull are illustrated. The bregma, which is on the midline axis between the eyes and the ears at the intersection of the coronal and sagittal sutures, is used to reproducibly locate the injection coordinates. From [220].

Morphological and immunohistochemical study

All the brains were sectioned coronally from most anterior to posterior, formalin-fixed and paraffin-embedded. From each paraffin blocks serial sections of 3 µm thickness were cut, equipped on positively charged slides and stained in haematoxylin-eosin (HE) for morphological evaluation or used for the immunohistochemical stains.

Immunohistochemistry

Brain sections were deparaffinised, re-hydrated and treated with hydrogen peroxide 3% for 20 minutes to inhibit endogenous peroxidases. After washing steps using TBS with 0.25% triton X-100 (Sigma) antigen retrieval was performed using citrate buffer pH 6 or EDTA buffer pH 8 based on the experimental protocols detailed in Table 1, The sections were then incubated overnight at 4 °C with the specific primary antibody at the working dilution detailed in table 1.
The day after, the tissue sections were washed in TBS with 0.25% triton X-100 and incubated for 45’ at RT with the specific biotinylated secondary antibody (Vector, Newark, CA, USA) and, subsequently, for 30’ at RT with ABC peroxidase complex (ABC Elite, Vector, Newark, CA, USA). The immunoreaction was developed with 3,3’-diaminobenzidine tetrahydrochloride (DAB) (Sigma Aldrich, St. Louis, MO, USA) as chromogen. After nuclear haematoxylin counterstaining the tissue sections were dehydrated through alcohol scale and mounted with a covering slide using Canada balm. The immunostained brain tissue is ready to be evaluated and photographed under a light microscope (Olympus, Tokyo, Japan).

Table 1: Antibodies used for histopathological characterization of GL261 wt and CIITA tumor sections.

Antibody specificity	Target cell	Source	(*Clone*)[a]	Antigen Retrieval[b]	Working dilution
CD3	T cells	Thermofisher (MA5-14524)	Rb (*SP7*)	E (20 min)	1/150
CD4	T-helper cells	Abcam (Ab183685)	Rb (*EPR19514*)	TC (20 min)	1/1000
CD8	Cytotoxic T-cells	Abcam (Ab209775)	Rb (*EPR20305*)	E (20 min)	1/1000
CD11b	Macrophages, granulocytes, dendritic cells	Abcam (Ab133357)	Rb (*EPR1344*)	E (10 min)	1/20000
CD19	B-cells	Thermofisher (14-0194-80)	Rat (*6OMP31*)	E (20 min)	1/1000
CD161	NK-cells	Abcam (Ab234107)	Rb (*EPR21236*)	TC (20 min)	1/10000
FOXP3	Regulatory T-cells	Thermofisher (14-5773-82)	Rat (*FJK-165*)	TC (20 min)	1/100
GFAP	Glia cells	Genetex (GTX108711)	Rb	TC (20 min)	1/2000
Ki67	Proliferating cells	Abcam (Ab16667)	Rb (*SP6*)	TC (20 min)	1/100
MHC-II	Antigen presenting cells	Thermofisher (14-5321-82)	Rat (*M5/114.15.2*)	E (10 min)	1/100
Nestin	Cancer stem cells	Abcam (Ab221660)	Rb (*EPR22023*)	TC (20 min)	1/4000
Synaptophysin	Neurons	Abcam (Ab32127)	Rb (*YE269*)	TC (20 min)	1/6000
TMEM119	Resident microglia	Abcam (Ab209064)	Rb (*28-3*)	E (20 min)	1/250
IBA1	Pan microglia & macrophages	Abcam (Ab178847)	Rb (*EPR16589*)	E (10 min)	1/200
CD68	Macrophages and monocytes	Abcam (Ab283654)	Rb (*EPR23917-164*)	E (10 min)	1/200
OLIG2	oligodendrocyte-lineage cells	Cell Marque (760-5050)	Rb (*EP112*)	TC (20 min)	pure
TIM3	Exhausted T-cells, tumor cells	Abcam (Ab241332)	Rb (*EPR22241*)	E (10 min)	1/300
PD1	Exhausted T-cells, tumor cells	Abcam (Ab214421)	Rb (*EPR20665*)	E (10 min)	1/300
HSV-1	HSV-1 infected cells	Abcam (Ab9533)	Rb	TC (20 min)	1/100

[a]Rb, rabbit.

[b]E, EDTA buffer pH 8.0; TC, citrate buffer pH 6.0; in parenthesis, incubation time.

Tumor size measurement

For each case, the tumor size was identified as the largest area occupied by tumor cells measured on all the consecutive sections stained in both H&E and immunohistochemistry using a computer image analysis system (Olympus Software cell Sens Entry Version 4.1). The tumor bed (TB) is defined as the tissue encompassing the original tumor site ([221]); microscopically, TB is characterized by an area of hyalinized, oedematous reactive stroma with a plethora of inflammatory infiltrating cells ([222,223]).

Statistical analysis

Mean and standard deviation of each group were determined using Microsoft Excel program. The statistical analysis was performed using GraphPad Prism 6 (GraphPad Software, http://www. graphpad.com) and Student's t-test was conducted to determine the significance. Comparisons were considered statistically significant when the corresponding p-value was <0.05. All data were expressed as the mean ± SD.

Results

Protective anti-tumor vaccination against glioblastoma expressing the MHC class II transactivator CIITA

Our recent published data ([216]) reported unprecedented results regarding the effective anti-tumor action through *in vivo* vaccination with GBM murine cell model (GL261) expressing MHC-II. Indeed, CIITA-based anti-GBM treatment could restore antigen presentation on MHC-II molecules at the surface of GL261 cells. The expression of MHC-II rendered tumor cells highly immunogenic and was instrumental in changing the tumor microenvironment. This was evidenced by intense and rapid infiltration of lymphocytes and particularly CD4+ T cells, responsible for a drastic tumor growth retardation and, in some cases, complete tumor remission; conversely a large tumor emerged after similar injections of GL261-wt cells. Notably, tumor vaccination through orthotopic injection of GL261-CIITA (n=5) revealed a remarkable protective anamnestic response following injection with parental GL261 cells in the opposite brain hemisphere. As suggested by histological data, following vaccination, parental tumors were completely rejected or greatly reduced in size. Conversely, this was not observed in non-vaccinated mice (n=5), where abundant tumor growth was associated with a restricted lymphocytic compartment (Figure 12).

A

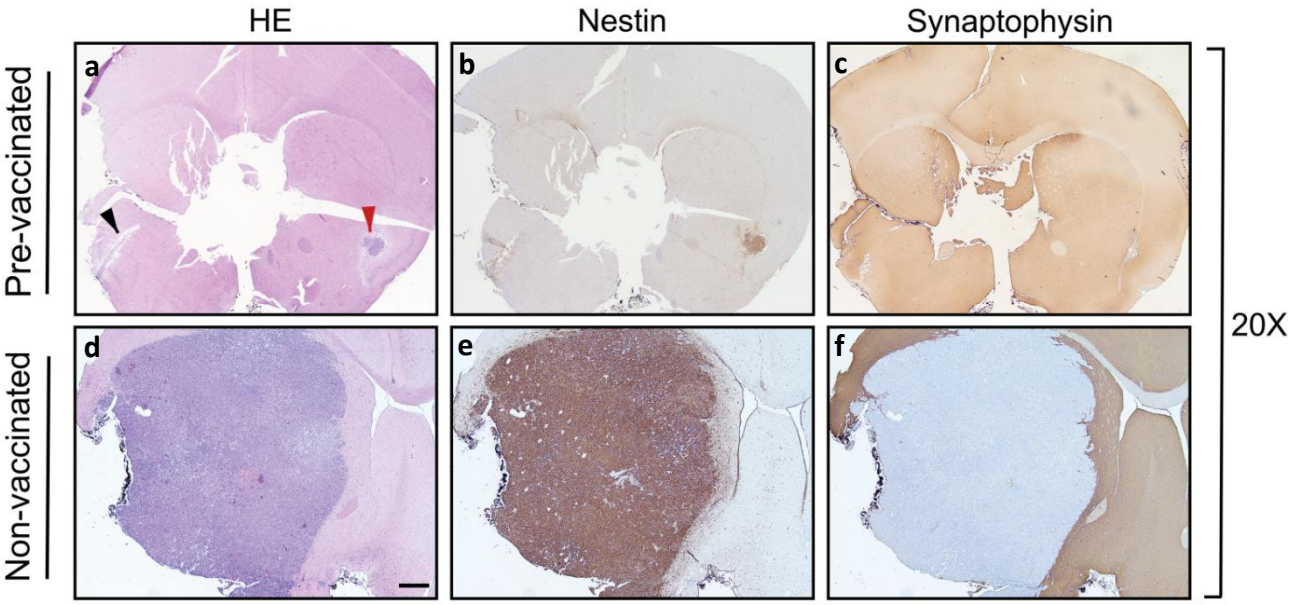

B

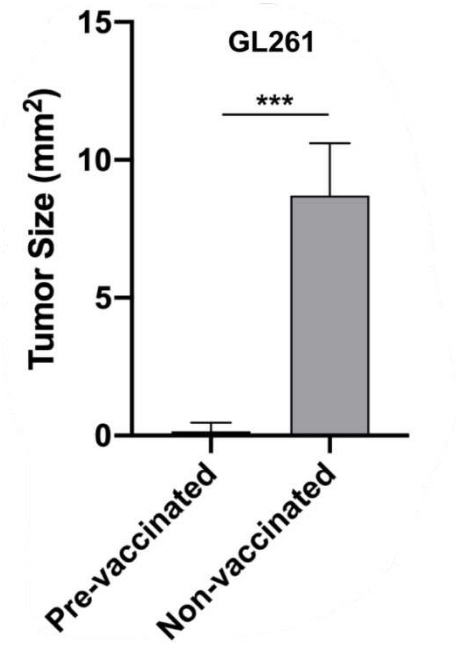

Figure 12 | **Preventive vaccination with GL261-CIITA tumor cells protects the animal against challenge with GL261 parental tumor cells**. C57BL/6 mice were intracranially (i.c.) injected with GL261-CIITA cells (n=5) into the right striatum and after 21 days challenged with parental GL261 tumor cells (n=5) in the left striatum (pre-vaccinated group). After three additional weeks, animals were sacrificed, and their brains were analyzed histologically for presence and size of tumors. As a control, another group of mice were i.c. injected with GL261 cells (non-vaccinated group), and their brains were analyzed after 3 weeks. (A) Representative histological sections of the brains harvested from pre-vaccinated (panels a – c) and non-vaccinated (panels d – f) mice, at ×20 magnification; scale bar corresponds to 500 mM. Sections were stained with HE or by IHC with nestin- and synaptophysin-specific antibodies to better identify tumoral and non-tumoral tissue, respectively. Arrowheads in the HE-stained section indicate the GL261 parental tumor site (black) and the GL261-CIITA tumor site (red). HE, hematoxylin and eosin. (B) Average size of GL261 tumors in pre-vaccinated and non-vaccinated mice. Bars represent mean values, and error bars indicate the SD of each group, n = 5. p-Values were determined via unpaired t-test; ***$p < 0.001$.

These results demonstrated the acquisition of a potent anti-tumor immune memory with protective characteristics against parental injection. Remarkably, these data also confirmed the recruitment of lymphocyte into the brain despite the existence of BBB. It is presently under scrutiny also the possibility that intratumor lymphocyte infiltration could in part or totally deriving from the recently described lymphatic nervous system. From these initial studies I could conclude that GL261-CIITA cells can be considered a potent anti-GBM vaccine stimulating a protective adaptive anti-tumor immune activation *in vivo* as a consequence of CIITA-driven MHC-II expression and consequent acquisition of surrogate antigen-presenting function toward tumor-specific CD4+ Th cells.

Long-term protection and overall survival assessment of GL261-CIITA vaccinated mice

To evaluate the efficacy of our vaccination strategy with GL261-CIITA in eliciting a long-lasting protection, an Overall Survival (OS) study has been performed. To this purpose, GL261-CIITA or GL261 parental tumors (30.000 cells) were intra-cranially injected into syngeneic C57BL/6 mice as described (Figure 21). Mice were monitored daily to assess their health status taking into consideration the following parameters: weight change, exhibition of abnormal behaviour, hunched position, ocular-nasal discharge, gait, food consumption. Mice were euthanized upon reaching humane endpoints and their brains were harvested for immunohistochemical assessment. The Kaplan-Meier survival analysis revealed a notable difference in overall survival between the two groups of mice. The group that received GL261-CIITA tumor cells (n=15) exhibited a significantly prolonged overall survival compared to the group of mice injected with the GL261 parental tumor (n=5). The median OS of parental GL261 injected mice was 26 days, compared to a median OS of 60 days in the GL261-CIITA injected mice. Statistical data revealed a survival rate at day 110 corresponding to 33.33% (Figure 13).

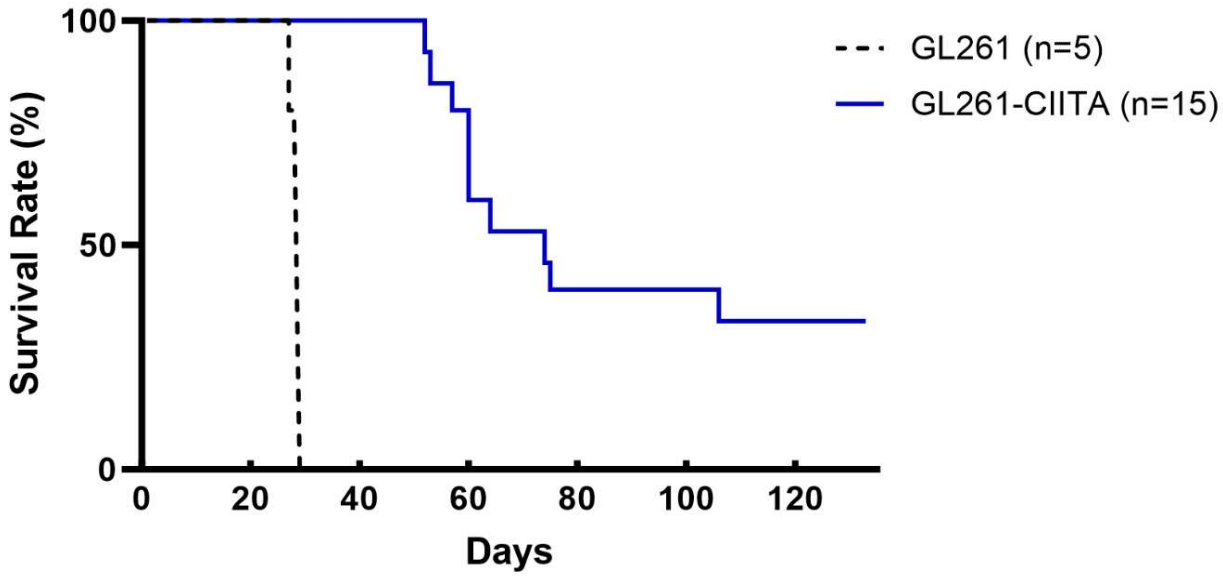

Figure 13 | Kaplan–Meier survival curves of C57/BL6 mice bearing GL261 or GL261-CIITA tumors. OS was significantly longer in the GL261-CIITA group (median, 60 days – green line) compared with the GL261 (median, 26 days – red dotted line). Surprisingly, GL261-CIITA mice were survived at day 131, showing a health status predictive of complete healing.

Furthermore, we also assessed the health status of both experimental groups. The data revealed an overall state of neoplastic cachexia in mice injected with parental GL261. Particularly, in these mice, the loss of body mass (with an average of 13,8 g corresponding to a 23% loss), was associated with negative prognostic indicators including matted fur, hunched posture, ataxia, conjunctivitis and general dullness. In contrast, in the CIITA group, an increasing body mass (with an average of 19,3 g corresponding to a 6,5% gain) was associated with positive prognostic indicators of the health status of the animal: smooth-glossy fur, clear eyes, no behavioural changes (Figure 14).

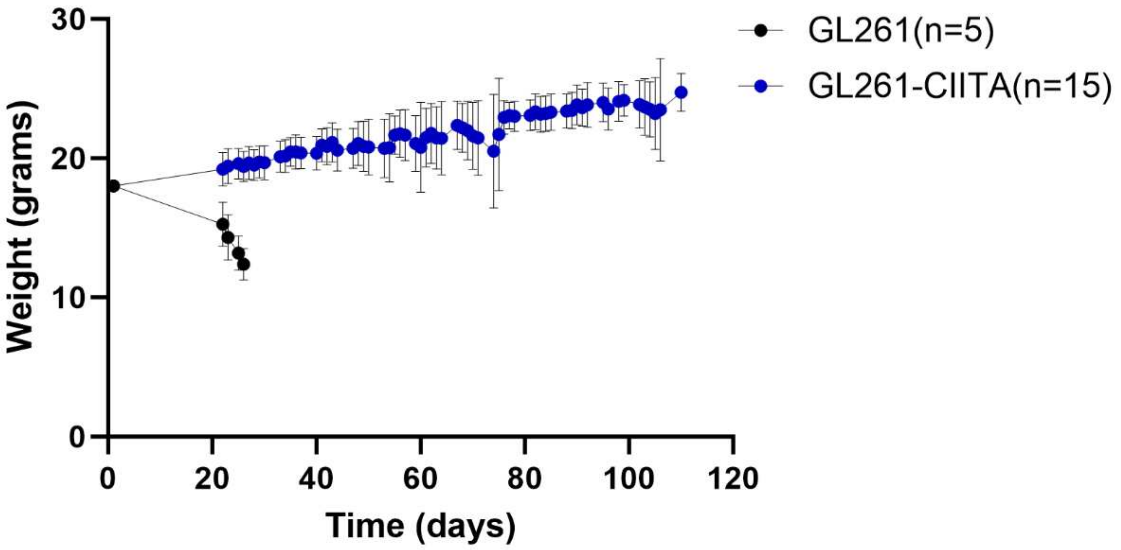

Figure 14 | Body-weight changes in mice injected with GL261 compared to GL261-CIITA. Mean bodyweight of GL261 (black circles) and GL261-CIITA (white circles) injected mice were measured over time (days). Significant differences were observed comparing the body weight among the two groups of mice.

After confirming the long-lasting memory through the expression of MHC-II molecules on GBM cell surface, the survived mice at day 110 (n=5) were grouped and intracranially challenged with the parental tumor in the opposite brain hemisphere. Mice were monitored daily for signs of illness or distress and their weight was recorded. Mice were euthanized at day 21 after challenge and their brains were harvested for immunohistochemical assessment. A control group (n=5) was intracranially injected with GL261 cells only. The experimental scheme is shown in figure 15.

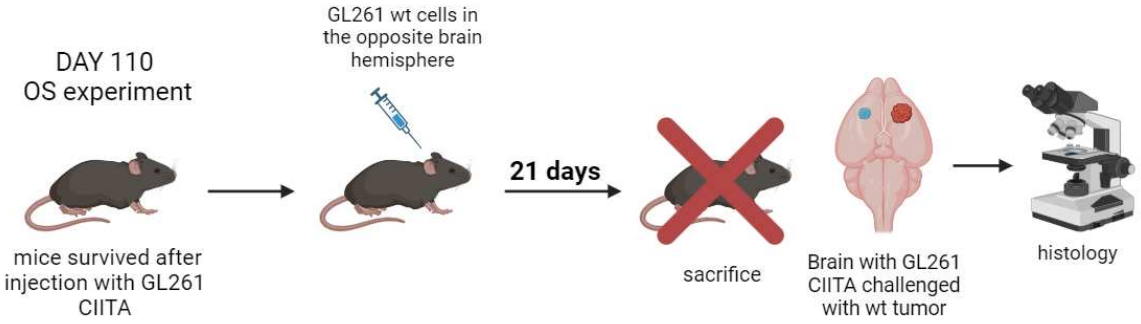

Figure 15 | **Experimental scheme.** At 110 post-GL261-CIITA vaccination all surviving mice were challenged with parental $3x10^4$ GL261 tumor cells in the opposite brain hemisphere, and after additional 3 weeks mice were sacrificed, and their brains were harvested and analysed histologically. Adapted from *BioRender.com*

Importantly, challenge with GL261 parental tumor cells in the opposite hemisphere, resulted in a complete tumor regression in both hemispheres in 80% of cases. Indeed, neither tumor nor haemorrhage was macroscopically detected in 80% of vaccinated mice, only revealing the sites of injection. The cut surface did not provide evidence of any tissue alterations within the brain parenchyma. In particular, IHC analysis conducted on both hemispheres, shown evidence of full tumor regression, characterized by a residual fibrotic distortion immersed in a rich lymphocyte cellular infiltrate (Figure 16B, panels a and e, red and black

arrowheads respectively). Abundant dystrophic calcifications together with hemosiderin-laden and mucin lakes may also be visible. Of note, as consequence of complete tumor remission, 60% of mice were characterized by absence of inflammatory response, showing a state of complete healing. The control Gl261, possessed the same characteristics of the below and previously described GL261 line ([216]) such as high tumorigenicity, restricted lymphoid and myeloid infiltrate, epithelioid phenotype and high proliferation rate. Notably, the average parental GL261 tumor area was 8.04 mm^2 in non-vaccinated control group (Figure 16A).

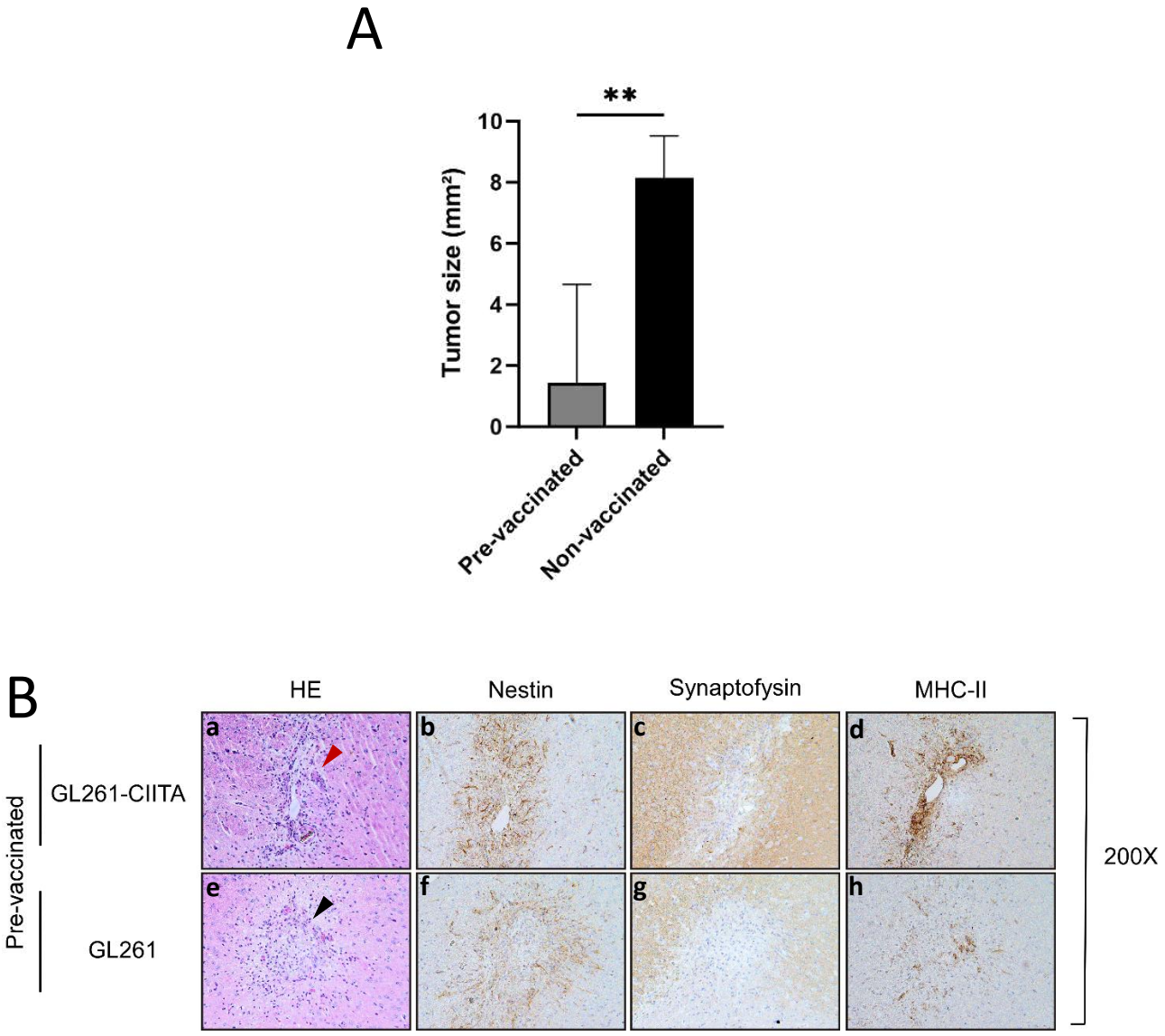

Figure 16 | Preventive vaccination with GL261-CIITA tumor cells protects the animal against challenge with GL261 parental tumor cells also after 110 days post vaccination, revealing a strong memory response. C57BL/6 mice were intracranially (i.c.) injected with GL261-CIITA cells into the right striatum. The survived mice at day 110 (n=5) were challenged with parental GL261 tumor cells in the left striatum (pre-vaccinated group). After three additional weeks, animals were sacrificed, and their brains were analyzed histologically for presence and size of tumors. As a control, another group of mice (n=5) were i.c. injected with GL261 cells (non-vaccinated group), and their brains were analyzed after 3 weeks. (A) Average size of GL261 tumors in pre-vaccinated and non-vaccinated mice. Bars represent mean values, and error bars indicate the SD of each group, n = 5. p-Values were determined via unpaired t-test; **p < 0.01. (B) Representative histological sections of the brains harvested from pre-vaccinated mice injected with GL261-CIITA (panels: a – d) and with GL261 (panels: e – h), at ×200 magnification. Sections were stained with HE or by IHC with nestin, synaptophysin and MHC-II specific antibodies. Arrowheads in the HE-stained section indicate the challenged GL261 (black) and the GL261-CIITA (red) residual tumor beds. HE, hematoxylin and eosin.

Both GL261-CIITA and GL261 parental tumor injected sites displayed intense membranous Nestin expression of reactive astroglia, surrounding the residual fibrotic architecture (Figure 16B, panels b and f). Nestin is an intermediate filament protein (class Type VI) expressed during the development and used as a marker for neural stem cells differentiating into astrocyte progenitors ([224]). Quantification of Ki67 staining revealed a complete absence of proliferating cells of non tumor origin.
A diffuse and finely granular synaptophysin-positive signal was observed in the grey matter of both the cerebrum and cerebellum, whereas was negative in all GBM regressed tumors (Figure 16B, panels c and g). Activated microglia and macrophages are the main cell type in the brain that are supposed to present antigens to the adaptive immune system (i.e., lymphocytes) via MHC-I and MHC-II cell surface molecules. Antigen presentation is a critical element for inducing an effective anti-tumor immune response. For this reason, MHC-II expression has been evaluated not only in CIITA-transduced-MHC-II-expressing tumor cells, but also in the microglial-dendritic compartment.
Immunostaining revealed a strong and intense MHC-II expression in residual fibrotic tissues of both GL261 challenged GL261-CIITA pre-vaccinated mice and their GL261-CIITA positive controls. A prominent MHC-II + infiltrate was observed, lining the desmoplastic region and widely distributed in the surrounding healthy parenchyma. MHC-II staining disclosed a higher dendritic population in GL261-CIITA (90%) injected mice compared to the challenged regressed tumours (25%) (Figure 16B, panels d and h). Glioblastoma is frequently considered as an "immunologically cold" tumor, due to its scarce infiltration of lymphocytes and to a immunosuppressive microenvironment possibly correlated to Glioma-Associated Microglia/Macrophages ([225]). Cell morphology alone does not fully indicate microglial function and it is therefore important to examine a range of microglial and macrophage markers to gain a better understanding of these cells in the context of tumor microenvironment. For this reason, the immunoreactive profile of additional markers such as CD11b, IBA1, CD68, GFAP and TMEM119 was assessed (Figure 17).
CD11b belongs to the β2-integrin family of adhesion molecules ([226]). Similarly to CD11c, CD11b is present on monocytes, neutrophils, a specific subset of B cells and dendritic cells ([227]). Its roles encompass cellular adhesion, phagocytosis, extravasation, and potentially participation in chemotaxis ([226,228]). Significant changes in dendritic CD11b expression by immunohistochemistry was detected between GL261-CIITA (in the right hemisphere) and challenged GL261 in the opposite cerebral hemisphere. Although both lines share the same cell distribution pattern, CD11b was highly expressed (95-100%) in the right striatum, compared to the challenged GL261 (35%) (Figure 17, panels a and f, yellow arrowhead). The higher marker positivity was consequence of an intense glial overexpression, where a well-organized GFAP+ microglia was found in both hemispheres surrounding the tumor bed and throughout the fibrotic stroma (100%) (Figure 17, panels d and i, blue arrowhead).
Ionized calcium binding adaptor molecule 1 (IBA1) is a 17 kDa protein expressed on microglia/macrophages and its up-regulation occurs in several brain diseases ([229]). IBA1 expression was significantly increased in both hemispheres, appearing with a more ameboid shape inside the residual architectural distortion (Figure 17, panels c and h). Branched IBA1+ cells adjacent to the fibrotic margin appeared elongated in morphology and hypertrophic, showing gradient-like morphology with normalization of their features as the distance from the tumor bed increased (Figure 17, panels c and h, black and red arrowheads respectively).
CD68, also referred to as GP110, LAMP4, or SCARD1, is a transmembrane protein expressed in various monocyte cell types, including macrophages, microglia, and osteoclasts ([230]). CD68 plays a crucial role in numerous physiological and pathological processes, including tumor progression ([231,232]). Within the tumor microenvironment (TME), bone marrow-derived macrophages are the most prevalent tumor-infiltrating immune cells and are vital mediators of the antitumor immune response ([233–235]). CD68+ cells and IBA1+ cells shared the same distribution pattern. Particularly, CD68 stained sections revealed that the majority of macrophages were mainly focused into the neoplastic bed (Figure 17, panels b and g, green arrowhead). Conversely, a more CD68+ branched subpopulation was partially present in the surrounding area (85% CIITA, 55% wt).

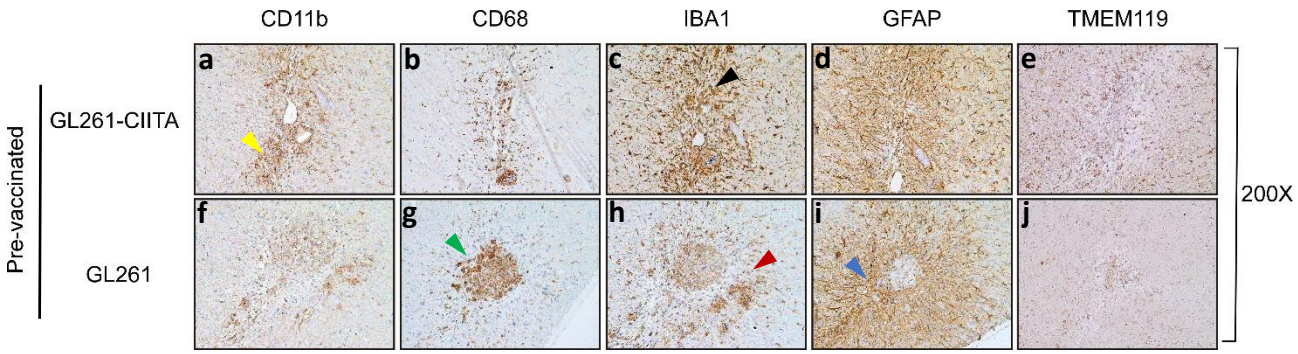

Figure 17 | Intracranial implantation of MHC-II positive GL261-CIITA tumor cells completely reject GL261 tumor *in vivo*. Immunostaining of serial brain sections. Representative histological sections of the brains harvested from pre-vaccinated (n=5) (panels: a – e) and non-vaccinated (n=5) (panel: f – j) mice, at ×200 magnification. HE, haematoxylin and eosin. Slides from the brain tissues isolated from challenged GL261 or GL261-CIITA tumor bearing mice were subjected to immunohistochemical staining with anti-CD11b, anti-CD68, anti-IBA1, anti-GFAP and anti-TMEM119 antibodies. CD11b+ dendritic cells were predominantly spread over the tumor bed and in the surrounding areas (yellow arrowhead). Green arrowhead points CD68+ cells that were concentrated within the fibrotic tissue. Black and red arrowheads indicate IBA1+ branched cells adjacent to the fibrotic margin, displaying elongated morphology and hypertrophy that is gradually reduced by increasing the distance. Blue arrowhead indicates a pronounced overexpression of glial cells, surrounding the tumor bed.

Microglia together with the macrophage-dendritic population are capable of expressing a variety of cytokines and chemokines that are responsible for the lymphocytic cell recruitment. For this reason, they have an essential role in the anti-tumor response. Results clearly suggest that the myeloid cell overexpression reflects the effective anti-tumor immune response against both GBM lines.

TMEM119 is a specific type I transmembrane protein exclusively expressed in homeostatic human and murine microglia, but not in activated microglia or in infiltrating blood-derived macrophages. For this reason, TMEM119 staining allows to investigate the role and function of microglia in various neurological processes ([236–238]). TMEM119+ resident microglia exhibited, in both hemispheres a comparable level of marker expression in healthy parenchyma. Notably, a tight halo of TMEM119 negative staining was observed surrounding the neoplastic bed, mainly in challenged GL261. As previously noticed, the halo of negativity was a direct consequence of the fibrotic nature at the regressed tumor site (Figure 17, panels e and j).

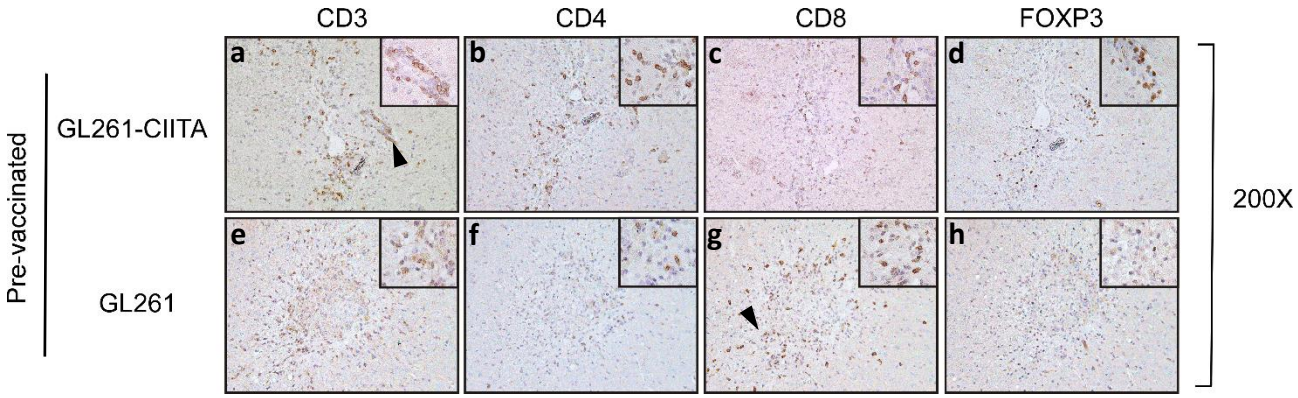

Figure 18 | Rejected GL261 parental tumors in pre-vaccinated mice are strongly infiltrated by anti-tumor T cell cells. Representative immunohistology images of tumor sections. The upper series of horizontal panels (a – d) depict GL261-CIITA tumors in pre-vaccinated mice 121 days after inoculum (pre-vaccinated, GL261-CIITA), stained for the specific markers listed at the top. The lower series of panels (e – h) depict challenged GL261 parental tumors in GL261-CIITA pre-vaccinated mice (pre-vaccinated, GL261). Slides from the brain tissues were subjected to immunohistochemical staining with anti-CD3, anti-CD4, anti-CD8 and anti-FOXP3 antibodies. Small square boxes are the areas represented in the corresponding large square boxes of each IHC image. Images were taken at ×200

magnification. Large square boxes were taken at ×400 magnification. Black arrowheads point significant T-cell infiltration in both hemispheres.

It is interesting to note the relevant infiltration of lymphocytes in both hemispheres of GL261-CIITA vaccinated and further GL261 challenged mice. These cells were CD8+ T cells and CD4+ T cells (Figure 18, panels c and g, b and f respectively). T cells spread along the fibrous stands and within the peritumoral vessels (Figure 18, black arrowheads). Conversely, among the inhibitory T cell compartment, some rare FOXP3+ cells were observed (Figure 18, panels d and h), but not TIM3+/PD1+ cells. Altogether, these findings suggest a long term driven protection against the parental tumor, elicited by a long memory adaptive immune response. The improvement in overall survival in the GL261-CIITA and the long term driven protection against GL261 suggests the potential therapeutic benefits of CIITA-based immunotherapy in GBM.

Evaluating the Applicability of Experimental Methods on Different GBM Lines: Characterization of the CT-2A Tumor Cell Line

The CT-2A GBM cell line was chemically induced by Seyfried et al. in 1992 by injecting methylcholanthrene in C57BL/6 mice ([239]). This cell line effectively replicates various characteristics of human GBM, including the high cellular heterogeneity and the proliferative and metabolic profiles ([240]). Genetically, CT-2A tumors exhibit wild-type p53 and PTEN deficiency, which is also observed in certain human GBMs ([241]). It is worth noting that CT-2A cells can be utilized to study glioma stem cells. When cultured as monolayer cells (ML/CT-2A) *in vitro,* CT-2A cells express different stem cell markers such as CD133, nestin, and Oct4 ([242]). These features are conserved *in vivo,* indicating that these cells stably maintain their stemness phenotype during tumor growth ([350]). Another characteristic of CT-2A cells consists in their high tumorigenicity, as mice injected with as few as $1x10^4$ cells intracranially have a median survival of 20 days, making CT-2A cells suitable for in vivo experiments with shorter durations ([153]). In contrast to the GL261 model, CT-2A cells do not exhibit enrichment of any immune response-related pathway. Overall, CT-2A is a versatile model characterized by an immune suppressive tumor microenvironment and high tumorigenicity ([243]).
Upon stable CIITA transfection, the MHC-II-negative CT-2A cell lines displayed a stable MHC-II IA-positive phenotype, as assessed by flow cytometry and immunofluorescence (Figure 19). Moreover, CIITA transfection was also able to partially promote a more homogenous expression of MHC-I molecules on CT-2A cell surface. CT-2A-CIITA and CT-2A parental cells displayed a similar in vitro proliferative rate (Figure 20).

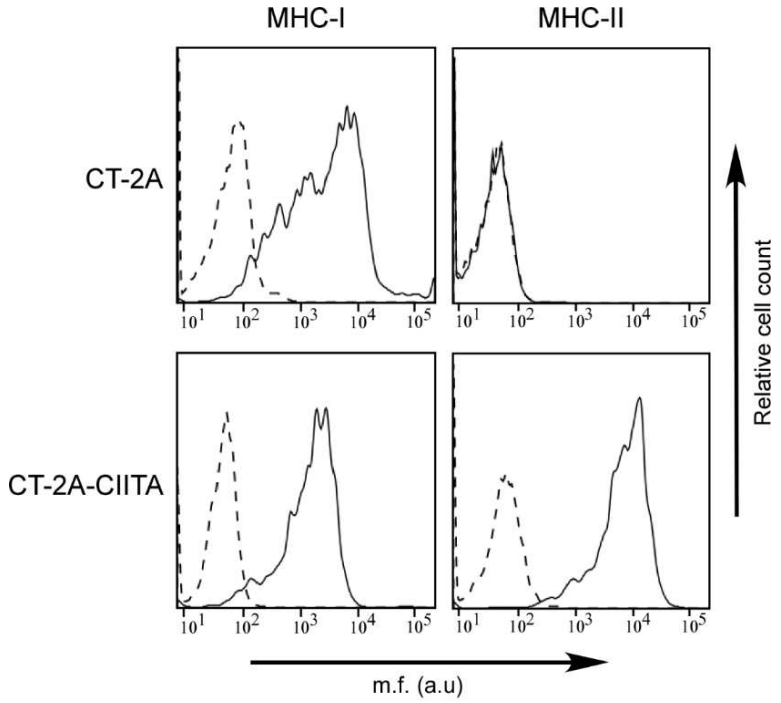

Figure 19. Expression of MHC-I and MHC-II cell surface molecules in CT-2A glioma cells after stable expression of CIITA. The stable expression of CIITA in CT-2A GBM cells induces MHC-II expression (CT-2A-CIITA). MHC-I and MHC-II cell surface expression was assessed by immunofluorescence and FACS analysis. Histograms represent fluorescence profiles of the cells indicated on the left incubated with specific anti-MHC-I or MHC-II mAbs (solid line). Controls (dashed line) are cells incubated with the specific isotype matched control. Mean fluorescence (m.f.) values are expressed in the abscissa as arbitrary units (a.u.). A representative experiment out of three independent experiments is shown.

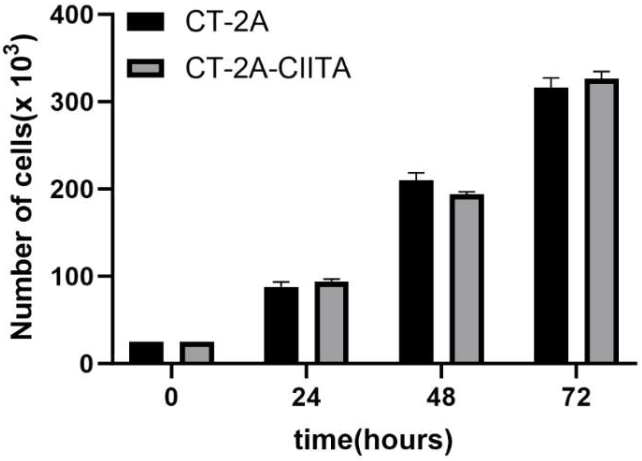

Figure 20 | The expression of CIITA in CT-2A GBM cells does not affect their proliferation rate in vitro. Bar graphs represent the number of alive CT-2A and CT-2A-CIITA cells counted at the specific time points listed in the abscissa, as assessed by trypan blue exclusion assay. Bars represent the mean ± S.D. from three independent experiments. p-Values were determined via unpaired t-test (not significant at the different time points).

A pilot study was performed before conducting a full-scale research experiment.
Mice were intracranially injected with 300, 3.000, 10.000 or 30.000 CT-2A–CIITA or CT-2A parental cells into the right cerebral hemisphere. Mice were monitored daily for neurological symptoms, lethargy, and hunched posture that would qualify as signs of tumor burden. After 21 days, the mice were sacrificed, and their brains were harvested and analysed histologically.
Histological analysis conducted on the pilot group revealed that injection of 30.000 cells was partially in line with the results obtained in the GL261 tumor model. This number of cells was then used in subsequent experiments.
The following in vivo experiments are based on this general experimental scheme (Figure 21).

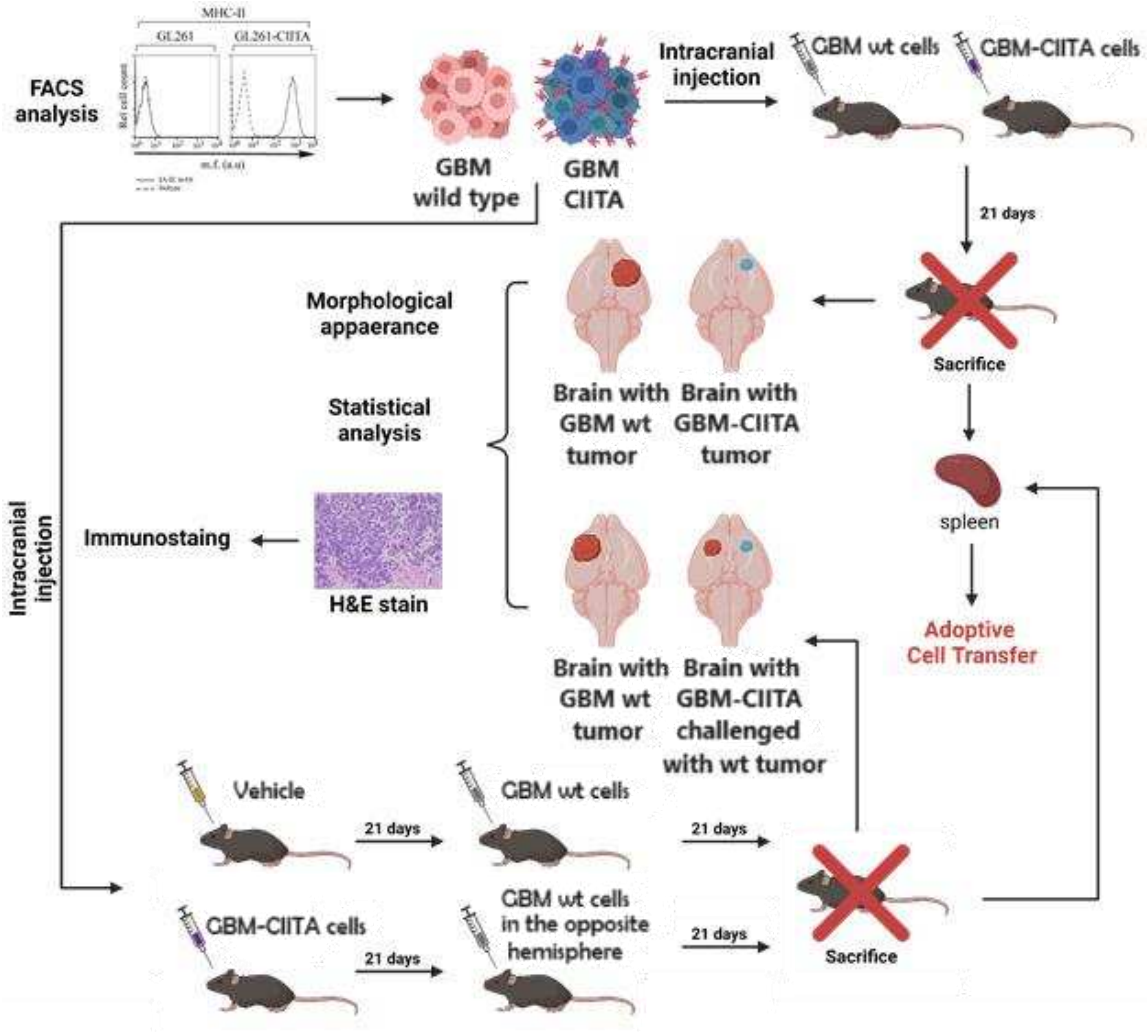

Figure 21 | **Experimental scheme.** Murine glioma cells were stably transfected with flag-tagged CIITA expressing vector. MHC-II+ cells were enriched by FACS analysis and further subjected to limited dilution cloning. The MHC-II expression was confirmed by immunofluorescence and flowcytometry. GBM cells or GBM-CIITA transfected cells were intracranially injected in C57BL/6 murine model and after 21 days mice were sacrificed, their brains were harvested for histological analysis. Additionally, to assess the efficacy of CIITA, mice that were previously vaccinated with CIITA transfected cells were challenged with parental GBM tumor cells in the opposite brain hemisphere. Their brains were harvested for further immunohistochemical studies. Adapted from *BioRender.com*

Macroscopic observation of brains from all animals injected with CT-2A parental cells revealed a dramatic tumor development along the sagittal plane, involving approximately 3/4 of the hemisphere. High leptomeningeal invasive pattern was also observed (75%), together with a greater tendency toward sublateral-intracerebral development. Cortical infiltration tended to develop in a thickened tan cortex overlying a necrotic zone in the white matter. Notably, these infiltrating tumors produced abnormalities in the surface vasculature, which are usually identified as thrombosed vessels. The cut surface was variable in colour, with peripheral greyish to pink masses and central areas of yellowish necrosis usually associated with haemorrhagic areas.

Histological analysis of CT-2A parental tumors (n=5) revealed high cellularity, with a strong tendency to invade the normal brain parenchyma. Moreover, due to the high invasiveness, CT-2A tumors tended to spread along compact fibre pathways, such as the corpus callosum, fornix and subependymal zones. Histological analysis confirmed the high tendency for exophytic development (i.e. indicated as *EXTRA tum* in the figure below), associated with leptomeningeal infiltration. Specifically, leptomeningeal invasion may incur, up to infiltrate the bone tissue of the cranial theca, reaching the profound soft tissues of the mouse galea aponeuronica (Figure 22B and 23, panels i, green arrowhead). These results contradicted the reported studies by Shelton et al. in which a low invasive pattern has been observed ([244]). In addition to intrinsic tumor growth and

invasiveness, CT-2A were prone to tumor budding where isolated single cancer cells or clusters are located at the invasive tumour front. This feature reflects the high tumorigenicity of this tumor line. Palisading necrosis or large ischemic necrotic zones were observed together with microvascular proliferation characterized by a glomeruloid pattern (Figure 23, panel e). Vascular proliferations tended to accumulate in the peripheral region of high cellularity, even if they may originate outside the infiltrative edge and inside the neoplastic mass. Pseudo-palisading cells usually exhibited higher rates of apoptosis due to hypoxic conditions. A central vascular lumen may occur inside the palisades, together with intravascular thrombosis (Figure 23, panel e, yellow arrowhead).

Several atypical mitotic figures were present, especially along the invasive margin, but also spread throughout the mass. Cellular pleomorphism was common and included the formation of small and primitive appearing cells with round hyperchromatic nuclei, undifferentiated epithelioid cells and a predominance of spindle and fusiform cells that form intersecting bundles and fascicles resembling a more sarcomatous pattern. This fascicular growth rearrangement resembles areas of mesenchymal transformation named oncostreams. Based on literature data, the presence of oncostreams is associated with a more aggressive GBM phenotype ([245,246]). Small cells with little cytoplasm can appear so monomorphous to mimic anaplastic oligodendrogliomas. Perinuclear halos may also be observed. These phenotypic changes may reflect the clonal evolution of tumors. Neoplastic core may undergo oncocytic differentiation. Histology confirmed the weakly immunogenic phenotype of this tumor cell line, revealing a limited number of infiltrating T cells. In contrast, an abundant granulocytic population was present, which typically spreads throughout the mass, with prevalence in necrotic areas, where eosinophils are intermingled with karyorrhexis tumor cells (Figure 23, panel e). Similar results were observed in those mice in which CT-2A-CIITA tumors were growing. The fact that a proportion of CT-2A-CIITA injected mice were not protected from tumor growth was likely due to the down-modulation of MHC-II expression *in vivo* in CIITA transfected cells (see below) as previously observed in other tumor models of distinct histological origin ([212]).

Of particular relevance, instead, sixty percent of animal injected with CT-2A-CIITA show no macroscopical sign of tumor growth neither of haemorrhage (Figure 22B, panel a, black arrowhead). Tumor rejection was accompanied by significant regressive changes, associated with profound fibrotic replacement and by an abundant inflammatory infiltrate distributed along an oedematous desmoplastic tissue (Figure 23, panel a). The presence of mucin lakes, hemosiderin-laden and foamy macrophages are signs of resorption and of a pathologically complete response. Similarly, to the GL261-CIITA tumor model in which a drastic reduction of the tumor area is observed (at day 21) as a result of an effective anti-tumor immune response, the CT-2A-CIITA injected mice exhibits a resolving anti-tumor response, leading to complete remission (Figure 22B, panel A). In contrast, CT-2A parental injected mice were characterized by an extensive intra/extra-cerebral tumor area (i.e. *EXTRA tum* and *INTRA tum*) corresponding to 27.48 mm^2 (Figure 22A and 22B, panels e and i).

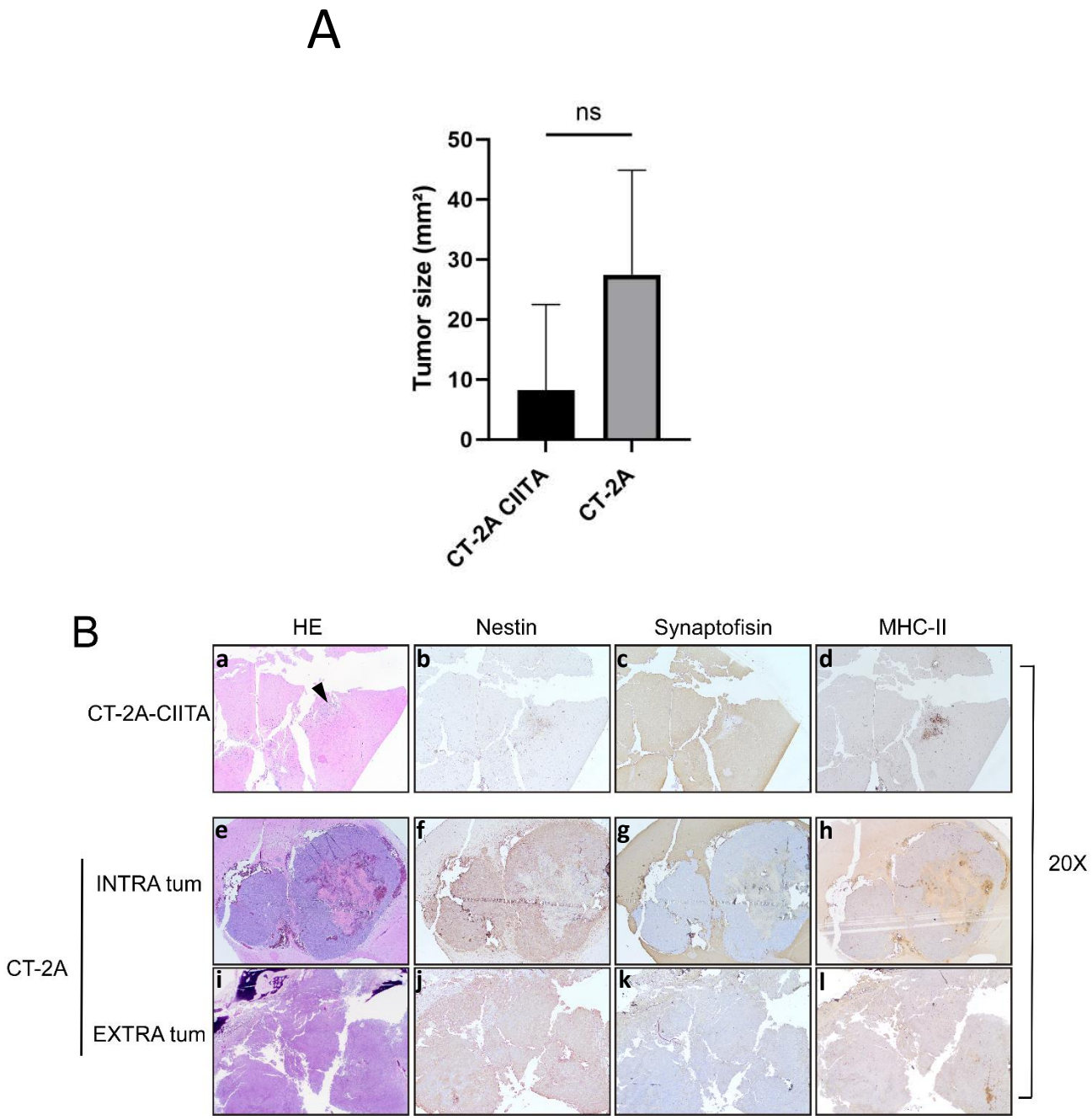

Figure 22 | Intracranial implantation of MHC-II positive CT-2A-CIITA tumor cells results in tumor rejection in *vivo*. C57BL/6 mice received intracranial injection of 3×10^4 CT-2A or CT-2A-CIITA glioma cells. On day 21 after injection, mice were sacrificed, brains were removed, and serial sections of the brain were carried out to measure tumor size and for staining. (A) Average tumor size of CT-2A and CT-2A-CIITA tumors. Data are represented as mean values, and error bars indicate the standard deviation (SD) within each group. p-Values were determined via unpaired t-test (ns). (B) HE and IHC staining of serial brain sections. Representative histological sections of the brains harvested from mice injected with CT-2A-CIITA (panels: a – d) and with CT-2A (panels: e – l), at ×20 magnification. HE, haematoxylin and eosin. Slides from the brain tissues isolated from CT-2A or CT-2A-CIITA tumor bearing mice were subjected to immunohistochemical staining with anti-nestin, anti-synaptophysin and anti-MHC-II antibodies. INTRA tum refers to tumor development inside the brain, EXTRA tum refers to extra brain development. Black arrowhead in the HE-stained section indicates the CT-2A-CIITA tumor site of injection.

Higher magnification of histological section staining (Figure 23) showed highly Nestin stem-cell marker expression (95-100%) in CT-2A tumors and the absence of peritumoral microglia (Figure 23, panel f). Notably, Nestin positivity provided evidence not only of mesenchymal oncostreams, but also of the presence of tumor budding, reflecting the extremely invasiveness of CT-2A tumor cells. Of note, Nestin+ cells were interspersed with necrotic areas (negative for marker) (Figure 23, panels f and j, black arrowheads). Surprisingly, in CT-2A-

CIITA tumor tissue, Nestin+ reactive astrocytes were widely distributed along the fibrotic stands and in the surrounding healthy parenchyma (Figure 23, panel b). Quantification of Ki67 staining showed high cell proliferation within the tumor microenvironment in CT-2A group. Particularly, a regional heterogeneity in Ki67 staining was observed, with higher levels at the peripheral/leading edge of the tumor and lower levels in the intermediate zone and avascular tumor center and regions of geographic necrosis. Notably, homogenous distribution in Ki67 staining was observed in the extracerebral masses (Figure 24, panels l and r, black arrowheads). Remarkably, immunostaining on CT-2A-CIITA revealed the complete absence of Ki67+ tumor cells (Figure 24, panel f).

Immunoreactivity for synaptophysin that could indicate neuronal aberrant differentiation of CT-2A tumors, focally spread into the extracerebral neoplastic mass (Figure 23, panel k, brown arrowhead). Conversely, no positivity was observed in CT-2A-CIITA tissues, with the exception of rare, trapped neurons into the fibrotic matrix (Figure 23, panel c, red arrowhead).

MHC-II expression on CT-2A-CIITA was evaluated by immunohistochemical analysis. As expected, diffuse and intense MHC-II expression was observed in CT-2A-CIITA, in approximatively 95-100% of the neoplastic bed, accurately defining the fibrotic margins (Figure 23, panel d). Additional dendritic/macrophage cells were also present in the surrounding area. Conversely, MHC-II expression in CT-2A tumors revealed rare dendritic/ macrophage cells zonally distributed within the neoplastic mass and absent peritoumorally (Figure 23, panels h and l, blue arrowhead).

Microglia and macrophages represent the first-line defence against pathogens and traumatic injuries. However, their functionality is influenced by GBM, which manipulates the microglia-gene expression to support its own growth ([247]). In order to investigate the impact of tumor progression on microglia and macrophages, we examined their recruitment and possible morphological changes through the immunostaining of specific markers such as GFAP (specific for microglia), CD68 (specific for macrophages), and IBA1, expressed by both the cell types, and compared to CD11b+ marker widely expressed in myelomonocytic cell lineage.

Restricted CD11b+ dendritic compartment was observed in CT-2A tumors, zonally distributed inside the neoplastic region and partially along the tumor margin. A rich granulocyte-CD11b+ infiltrate was also present, mainly distributed into the necrotic areas (5%) (Figure 24, panels g and m, black arrowhead). In CT-2A-CIITA group, immunohistochemistry revealed a higher number of CD11b+ dendritic cells with infiltrative features, widely spread along the fibrotic tissue and in the surrounding area (100%) (Figure 24, panel a, red arrowhead). Similarly, expression of Glial fibrillary acidic protein (GFAP), a type III intermediate filament protein localized intracellularly, specifically expressed by astrocytes ([248,249]), in CT-2A-CIITA injected mice revealed a prominent and diffuse astrogliosis distributed throughout the dysplastic tissue and along its margins (100%). The abundant GFAP+ population reflects a compact and well-organized glial matrix architecture. A gradient of morphological modifications was observed in the surrounding healthy parenchyma with a gradual increase in terminal arborizations approaching the altered tissue site (Figure 24, panel d, blue arrowhead). Conversely, a restricted microglial component was spread along the tumor margin, resulting in a rare and thinned glial matrix architecture (20%) (Figure 24, panel j).

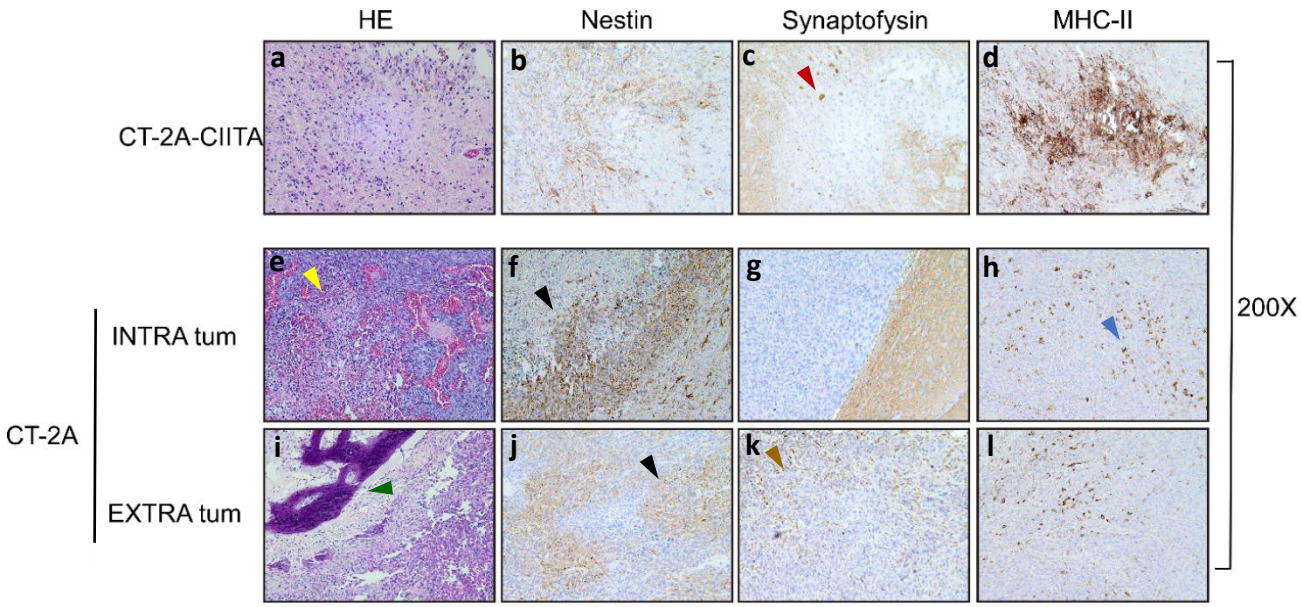

Figure 23 | Intracranial implantation of MHC-II positive CT-2A-CIITA tumor cells reject the tumor *in vivo*. HE and immunostaining of serial brain sections. Representative histological sections of the brains harvested from mice injected with CT-2A-CIITA (panels: a – d) and with CT-2A (panels: e – l), at ×200 magnification. HE, haematoxylin and eosin. Slides from the brain tissues isolated from CT-2A or CT-2A-CIITA tumor bearing mice were subjected to immunohistochemical staining with anti-nestin, anti-synaptophysin and anti-MHC-II antibodies. INTRA tum refers to tumor development inside the brain, EXTRA tum refers to extra brain development. High cellularity, intravascular thrombosis and pseudo-palisading cells are common features in CT-2A tumors (yellow arrowhead). Red arrowhead points rare occurrences of trapped neurons with the fibrotic matrix in CT-2A-CIITA. Conversely, neuronal aberrant differentiation was observed in parental tumors (brown arrowhead). Black arrowheads indicate the nestin staining, revealing the presence of nestin+ cells interspersed within necrotic areas which are negative for marker. In parental tumor cells, revealed occasional zones of dendritic/macrophage distribution within neoplastic mass (blue arrowhead).

IBA1 expression was significantly increased in CT-2A-CIITA tumor tissue (100%) in comparison to the parental tumors (25-30%). Notably, in CIITA tumors hypertrophic IBA1+ cells appeared to have an ameboid shape, with a similar distribution pattern of GFAP+ microglia. Indeed, a rich IBA1+ compartment completely invaded the neoplastic bed and the surrounding parenchyma (Figure 24 panel c). These cells showed a gradient-like morphology with normalization of their features as the distance from the altered tissue site increased. In contrast, a poor cellular IBA1 positivity was detected in CT-2A tumors, where IBA1+ cells with a dendritic/ramified phenotype were uniformly distributed throughout the mass with the exception of necrotic areas (Figure 24, panels i and o, yellow arrowheads).

A significant change in CD68 expression was found between CT-2A parental and CT-2A-CIITA tumor tissues. In parental tumors, most of the macrophages were zonally distributed in the neoplastic area, with high infiltrative tendency toward the necrotic regions (5-10%) (Figure 24, panels h and n, orange arrowhead). The central tumor hypoxia and necrosis in turn might potentially induce a more infiltration pattern of bone marrow–derived cells, like CD11b+ and CD68+ cells. Instead, in CIITA tumors, an increased number of CD68+ cells were observed, surrounding peripheral vessels and infiltrating the tumor bed (75-80%). Notably, both ramified and amoeboid phenotype was observed, consistent with a dynamic range of activation states along the neoplastic bed and the surrounding area (Figure 24, panel b).

Resident microglia in the surroundings of the CT-2A tumor area, appeared to be downregulated in their TMEM119 expression forming a TMEM119-negative halos around the neoplasia. Surprisingly, in CT-2A-CIITA, a comparable TMEM119 expression was observed. However, the circumscribed halo of negativity around the tumor bed was a consequence of the fibrous nature at the site of tumor remission. This resulted in a decreased marker expression at the desmoplastic surface (Figure 24, panels e and k, green arrowheads).

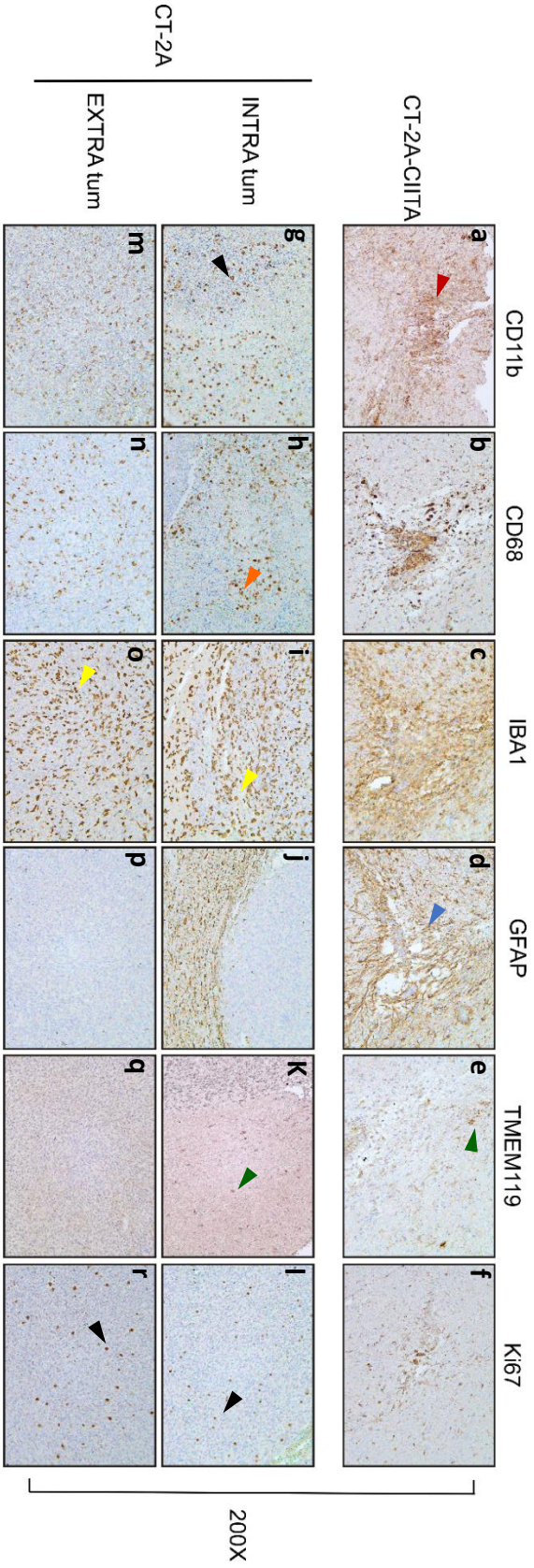

Figure 24 | Immunohistological characterization of CT-2A-CIITA tumors compared to CT-2A control group. Representative histological brain sections harvested from mice injected with CT-2A-CIITA (panels: a – f) or with CT-2A (panels: g – r), at ×200 magnification. Slides from the brain tissues isolated from CT-2A or CT-2A-CIITA tumor bearing mice were subjected to immunostaining with anti-CD11b, anti-CD68, anti-IBA1, anti-GFAP, anti-TMEM119 and anti-Ki67 antibodies. INTRA tum refers to tumor development inside the brain, EXTRA tum refers to extra brain development. Black arrowhead points rich CD11b+ granulocyte infiltration in CT-2A tumor necrotic areas, whereas red arrowhead indicates CD11b+ dendritic cells were abundantly spread along the fibrotic tissue and

in the surrounding area respectively. In CT-2A tumors, the majority of macrophages were distributed in zones within necrotic regions (orange arrowhead). A low IBA1 positivity was present in parental tumors, whereas IBA1+ cells where uniformly distributed throughout the tissue with the exception of necrotic areas (yellow arrowheads). Blue arrowhead indicates a progressive increase in GFAP+ terminal arborizations as it approaches the adjacent tissue site. TMEM119 immunoreactivity indicate the presence of resident microglia, forming a halo of a negative population surrounding the neoplastic region and the tumor bed in CT-2A and CT-2A-CIITA (green arrowheads). Black arrowhead points the high mitotic index in CT-2A tumors.

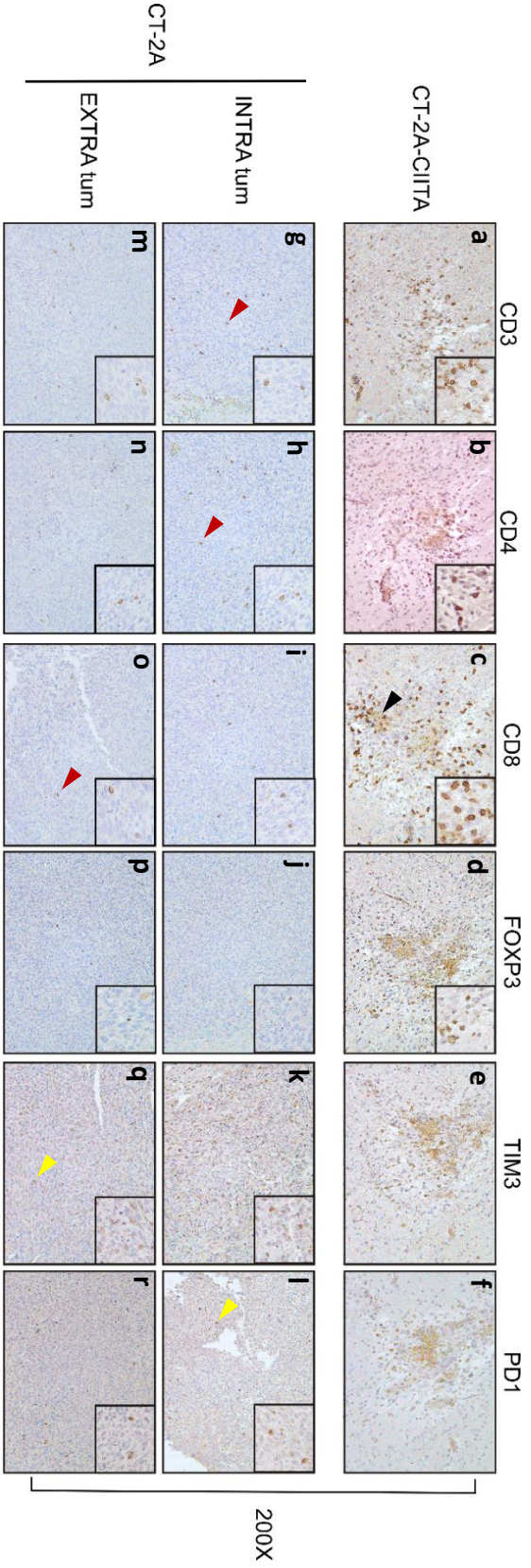

Figure 25 | CT-2A-CIITA tumors are strongly infiltrated by anti-tumor T cells: Immunostaining for CD3, CD4, CD8, FOXP3, PD1 and TIM3 in CT-2A (EXTRA and INTRA tum) (panels: g – r) and CT-2A-CIITA (panels: a – f) at x200 magnification. Small square boxes are the areas represented in the corresponding large square boxes of each IHC image. Large square boxes were taken at ×400 magnification. Note that selected areas in IHC images of CT-2A parental tumors were taken in the rare zones in which positive cells for the selective marker were present. IHC, immunohistochemistry. INTRA tum refers to tumor development inside the brain, EXTRA tum refers to extra brain development. T-cells were uniformly dispersed throughout the neoplastic region in CT-2A tumors (red arrowheads). Black arrowhead points numerous TILs inside and along the neoplastic bed in CT-2A-CIITA tumors. Some rare TIM3+ and PD1+ cells were observed in parental tumors (yellow arrowhead).

IHC studies were then performed to characterize the lymphocyte content in CT-2A and CT-2A-CIITA tumors. In brains of CT-2A-CIITA injected mice, staining revealed an abundant lymphocytic infiltrate, diffusely distributed throughout the tumor bed and partially in the surrounding tissue (Figure 25, panel a). Notably, a large number of TILs were observed inside and along afferent vessels, specifically migrating toward the inflammatory and fibrotic neoplastic bed (Figure 25, panel c, black arrowhead). As a consequence of an effective anti-tumor immune response, a prominent CD8+ T cell infiltration cell was present, together with a less pronounced presence of CD4+ T-helper cells (Figure 25, panels c and b respectively).
Programmed death 1 (PD-1) together with T cell immunoglobulin and mucin domain-containing protein 3 (TIM3) are co-inhibitory receptors expressed on the surface of CD3+/CD8+ T-cells following their activation. These receptors play a role in limiting the immune response, leading to the functional T-cell exhaustion ([250]). Regulatory T cells, also known as Tregs (FOXP3), are crucial for maintaining self-tolerance and ensuring the proper functioning of a healthy immune system ([251]). However, in the context of cancer, Tregs can have a negative impact on anti-tumor immune responses, contributing to an immunosuppressive tumor microenvironment (TME) ([252]). A limited amount of T-reg FOXP3+ cells was distributed inside the fibrotic stands. PD1+ and TIM3+ cells were not present. Conversely, a very scarce T-cell infiltration was observed in parental tumors, with cells homogeneously spread into the neoplastic region (Figure 25, panels g – i, m – o, red arrowheads). No T cells were detected peritoumorally. FOXP3+ Treg cells were weakly detected, and a restricted number of TIM3+ and PD1+ tumor cells were observed (Figure 25, panels j – l, p – r, yellow arrowheads).
Of note, the 40% of CT-2A-CIITA injected mice that developed tumors showed an immunosuppressive phenotype similar to the one found in CT-2A injected mice. Indeed, immunohistochemistry revealed a poor lymphocyte infiltration distributed within the lesion and a restricted myeloid repertoire. Particularly, a limited amount of CD68+ (10%) and CD11b+ cells (5%) was observed, together with a massive reduction in IBA1/GFAP expression (25% and 20% respectively).
Importantly, the immunosuppressive properties of this group reflected the breakdown in the cell-mediated adaptive immune response. Indeed, MHC-II immunostaining revealed a severe 75% reduction of MHC-II cell surface expression with a very limited and zonally MHC-II-positive cells (Figure 26, panel c, black arrowhead).

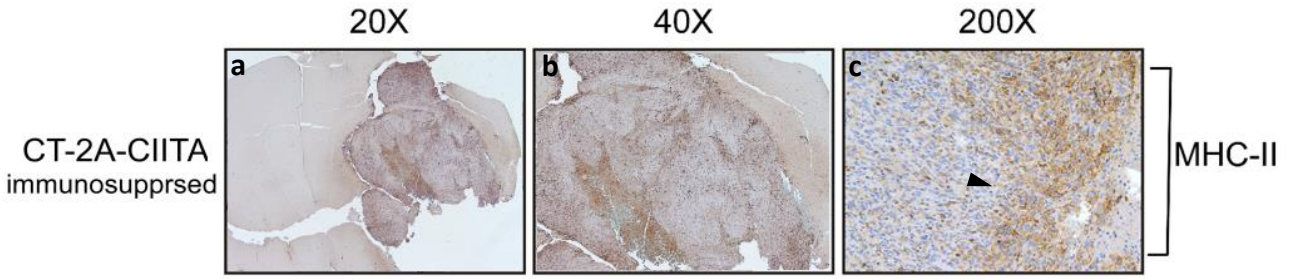

Figure 26|*In vivo* downmodulation of MHC-II expression reflects the immunosuppressive properties of some CT-2A-CIITA tumors. MHC-II staining of serial brain sections reveal the loose of marker expression in some CT-2A-CIITA tumors. The panels (a – c) were taken at ×20, x40 and x200 magnification respectively. Notably, the staining observed in x20 and x40 magnification are results of diamino benzidine precipitation in correspondence of necrotic areas. Black arrowhead indicates MHC-II+ cells, localized limitedly in zonal pattern.

Dysfunction in the anti-tumor immune response reflects on a marked increase in cellularity and stemness. This results in high tumor growth with a high invasive nature corresponding to a 20.59 mm^2 surface, consistent with the CT-2A tumor size. Conversely, an efficient MHC-II antigen expression was strongly correlated with tumor remission. Overall, these data underline the critical association between MHC-II expression in CT-2A and induction of a protective antitumor adaptive immunity.

Preventive GL261-CIITA vaccination in one brain hemisphere determines an effective tumor remission against CT-2A challenge in the other hemisphere

As previously observed, the vaccination with GL261-CIITA tumors induced a long-lasting immune response able to protect against GL261 parental tumor cell challenge. In order to extend and translate the efficacy of our vaccination strategy, I evaluated whether the vaccination with one specific CIITA-positive GBM tumor in one brain hemisphere could prevent the tumor growth of another GBM tumor line in the opposite brain hemisphere. To this purpose C57BL/6 mice (n=6) were injected with $3x10^4$ GL261-CIITA cells into the right striatum and after 21 days challenged with parental CT-2A tumor cells in the left striatum. After additional 3 weeks, animals were sacrificed, and their brains analysed histologically. As control, another group of mice (n=5) was i.c. injected with $3x10^4$ CT-2A cells and their brains were analysed after 3 weeks as above. Mice were monitored daily for neurological symptoms, lethargy, and hunched posture that would qualify as signs of tumor burden. As previously described, the gross appearance on the control group injected with CT-2A GBM line revealed a strong tumor development along the sagittal plane, involving approximately 4/5 of the hemisphere (Figure 27B, panel g). Conversely, pre-vaccinated mice challenged with CT-2A tumor cells, disclosed a significant regressive pattern that resulted in complete tumor rejection (Figure 27B, panel d, black arrowhead). The residual architectural distortion was associated with profound fibrosis-tumor replacement and by an abundant inflammatory infiltrate spread along an oedematous desmoplastic tissue (Figure 28, panel f, yellow arrowhead). Signs of resorption, like hemosiderin-laden and foamy macrophages, as well as mucin lakes and dystrophic calcifications could be observed. Notably, some pre-vaccinated mice, revealed a residual small CT-2A tumor mass, characterized by an abundant inflammatory T cell compartment, distributed throughout the tumor mass as well as in the peritumoral area, favouring the neoplastic perimeter. Vascular involvement was evident around the invasive margin and along the peritumoral area, required for the lymphocytic recruitment to the neoplastic site. The low mitotic rate associated with the high lymphocytic infiltration suggest an effective anti-tumor action directing toward a subsequent complete tumor remission. Consistently, data resulted in a complete tumor remission in 67% of vaccinated mice whereas the remaining mice revealed a significant suppression of tumor growth of CT-2A tumor cells. Histopathological analysis of control CT-2A was described above (see page 43) (Figure 27B, panel g; figure 28, panel k).
Notably, the average parental CT-2A tumor area was 0,35 mm^2 in GL261-CIITA vaccinated mice compared to 22,71 mm^2 in non-vaccinated control group, corresponding to a 65-fold reduction in tumor mass (Unpaired Student's T test, $p < 0.05$) (Figure 27A). As a parallel important confirmation of my previous studies, 80% of GL261-CIITA tumors in pre-vaccinated mice revealed a complete GL261-CIITA tumor remission after 42 days post injection, confirming the existence of a potent protective antitumor state (Figure 27B, panel a, red arrowhead; figure 28, panel a). Consistent with previous data, immunohistochemistry revealed 100% Nestin expression in control CT-2A tumors, accompanied with the total absence of peritumoral reactive microglia. Notably, tumor budding and mesenchymal oncostreams were visible after Nestin immunostaining (Figure 27B, panel h; figure 28 panel l, black arrowhead). Conversely, in GL261-CITA and in challenged mice, a Nestin+ residual tumor mass was surrounded by well-organized microglial cells (Figure 28, panel b, blue arrowhead).

Moreover, Nestin+ reactive astrocytes were also clearly visible along the fibrotic stands of a fully regressed CT-2A tumor (Figure 28, panel g).

Ki67 staining revealed a high mitotic index in control CT-2A tumors, spread along the invasive margin and inside the neoplastic region (Figure 28, panel o, brown arrowhead). Notably, marker positivity was observed in challenged group, although quantitatively reduced in comparison with the non-vaccinated mice. Remarkably, immunostaining on reverted CT-2A tumor (and on reverted GL261-CIITA) revealed the complete absence of Ki67+ cells.

To explore the distribution of synaptophysin, a marker of neuronal synaptic vesicles, immunohistochemical staining in the CNS was conducted. A diffuse and finely granular synaptophysin-positive signal was observed in the grey matter of both the cerebrum and cerebellum, whereas was negative in all GBM tumors (Figures 27B panels c, f and i, figure 28, panels c, h and m). Notably, rare and focal immunopositivity was present only in parental tumors, that could indicate neuronal aberrant differentiation.

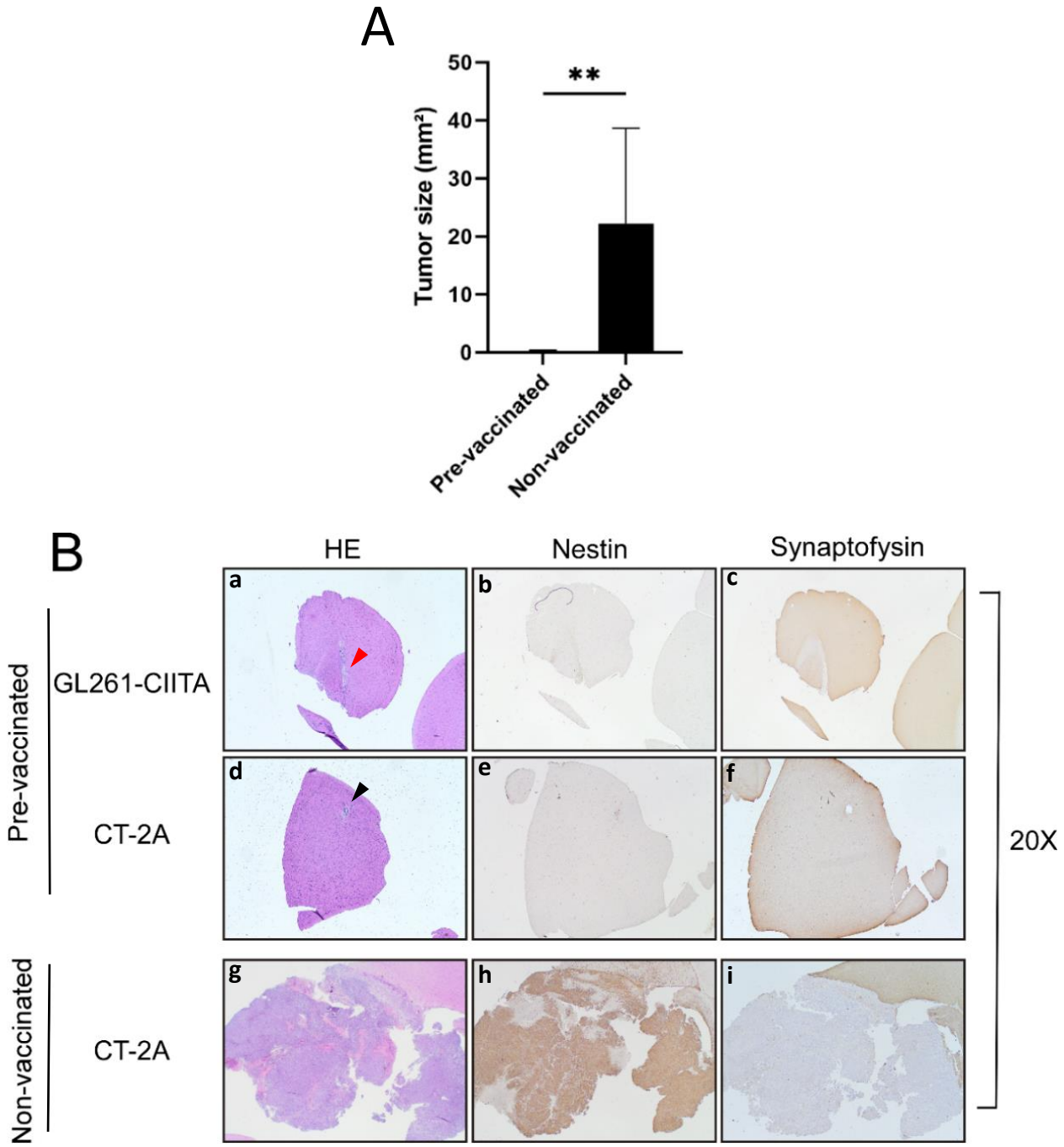

Figure 27 | Preventive vaccination with GL261-CIITA tumor cells protects the animal against challenge with CT-2A parental tumor cells. C57BL/6 mice were intracranially (i.c.) injected with GL261-CIITA cells into the right striatum and after 21 days challenged with parental CT-2A tumor cells in the left striatum (pre-vaccinated group). After three additional weeks, animals were sacrificed, and their brains were analyzed histologically for presence and size of tumors. As a control, another group of mice were i.c. injected with CT-2A cells (non-vaccinated group), and their brains were analyzed after 3 weeks. (A) Average size of GL261 tumors in pre-vaccinated and non-vaccinated mice. Bars represent mean values, and error bars indicate the SD of each group, n = 5. p-Values were determined via unpaired t-test; **p < 0.01. (B) Representative histological brain sections harvested from pre-vaccinated mice injected with GL261-CIITA (panels: a – c) and with CT-2A (panels: d – f), and from non-vaccinated mice injected with CT-2A only (panels: g – i) at ×20 magnification. Sections were stained with HE or by IHC with nestin- and synaptophysin-specific antibodies to better identify tumoral and non-tumoral tissue, respectively. Arrowheads in the HE-stained section indicate the CT-2A parental tumor site (black) and the GL261-CIITA tumor site (red). HE, hematoxylin and eosin.

An abundant MHC-II+ compartment was present, including dendritic cells predominantly spread along the fibrotic stands and partially in the surrounding brain zone (50%) (Figure 28, panels d and i, red arrowheads). MHC-II expressing cells were also observed within peritumoral vessels, attracted to the tumor site by leukocyte diapedesis. Conversely, non-vaccinated control mice showed weak dendritic-macrophage presence, zonally distributed within the necrotic areas and absent peritoumorally (10%) (Figure 28, panel n, green arrowhead). Overall, these results strongly suggest that the relevant MHC-II expression in the contralateral hemisphere is associated to presentation of GBM shared antigens between GL261 and CT-2A instrumental to generate an adaptive immune response against GBM.

In challenged CT-2A, prominent dendritic population (80-85%) was spread throughout the mass and partially along the peritumoral brain zone. No granulocytes were observed. In fully reverted CT-2A tumors (as well as in reverted GL261-CIITA), immunohistochemistry revealed a higher number of CD11b+ dendritic cells with infiltrative features, widely spread along the fibrotic tissue and partially in the surrounding area (90%) (Figure 29, panel a and f). Conversely, a limited CD11b+ dendritic compartment was present in CT-2A control group, zonally distributed inside the neoplastic region and partially along the tumor margin. A CD11b+ granulocyte infiltrate was also present, mainly distributed into the necrotic areas (5-10%) (Figure 29, panel k, black arrowhead).

Immunohistochemistry on mice injected with CT-2A only, revealed a restricted GFAP+ microglial content, spread along the invasive margin and forming a not well-organized glial matrix architecture (20%) (Figure 29, panel n). In contrast, a compact and organized glial texture was revealed in challenged CT-2A (and in GL261-CIITA), completely surrounding the tumor mass. A gradient of morphological modifications such as cell body hypertrophy and terminals arborization occurring during the reactive astrogliosis could be appreciated in challenged-CT-2A tumors and in GL261-CIITA, where GFAP+ cells were distributed along the neoplastic bed (90%) (Figure 29, panels d and i, blue arrowheads). The involvement of a complex and well-organized astroglial matrix architecture resulted in an effective physical hindrance to neoplastic growth. Conversely, in case of non-inhibited tumor growth, the microglial lining component was quantitatively reduced.

IBA1 staining illustrated a limited myeloid cell presence in CT-2A tumors of non-vaccinated mice, randomly distributed inside the neoplasia (35-40%), except for areas of necrosis (Figure 29, panel m). Differently, in challenged CT-2A, a gradual phenotypic change was observed as tumor surface was widely invaded by amoeboid-like IBA1+ cells, whereas a more branched subtype was peritoumorally distributed (95%). Surprisingly, in reverted CT-2A tumors (as well as in GL261-CIITA), IBA1+ cells with macrophagic features were prominently spread throughout the desmoplastic region and along the surrounding healthy parenchyma (100%) (Figure 29, panels c and h, red arrowheads). Similarly to GFAP expression, IBA1+ cells showed a slight reduction in expression in CT-2A challenged tumors with higher tumorigenicity. These results emphasized the relevance of the microglial population in tumor confinement.

Expression of CD68, a pan-macrophage marker, was significantly increased in challenged CT-2A specimens, in comparison to the parental tumors. Immunostaining confirmed the zonal distribution pattern of these cells, with high infiltrative tendency toward the necrotic regions (5-10%) (Figure 29, panel l, brown arrowhead).

Consistent with previous data, a strong negative correlation was found between the CD68+ cell content and the tumor growth. These results underline the pivotal role of macrophages, together with microglia in an efficient tumor impediment to spread. In addition, it should be noted the fact that in rejected CT-2A tumors (and also in GL261-CIITA), the CD68+ infiltrate completely invaded the desmoplastic region (80-85%) (Figure 29, panels b and g).

Expression of TMEM119 in challenged mice was similar to that found in CT-2A parental tumors of non-previously vaccinated mice, particularly for the aspect of downregulation of the microglial response (Figure 29, panels j and o, yellow arrowheads). However, the localized halo of negativity surrounding the tumor bed was a result of the fibrous nature present at the site of tumor remission. Consequently, this led to a reduced marker expression at the desmoplastic surface.

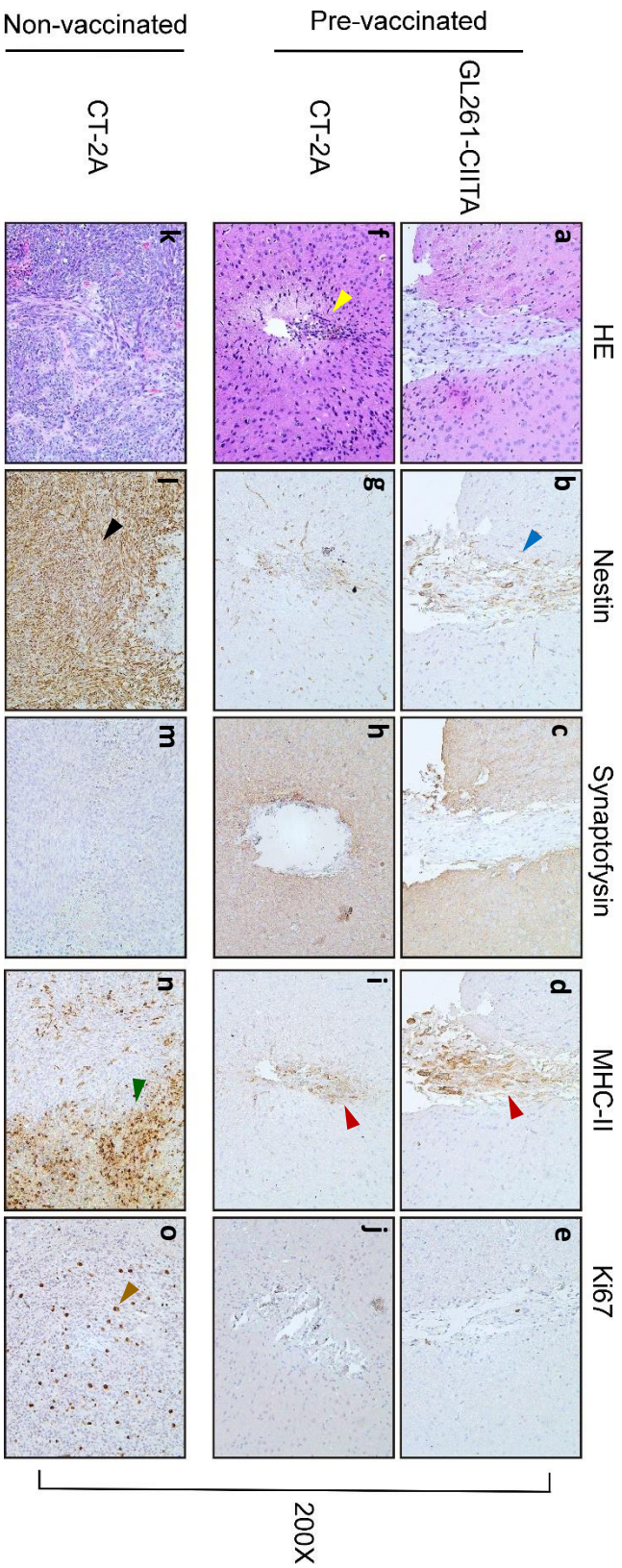

Figure 28| Immunohistological characterization of CT-2A tumor rejection in GL261-CIITA pre-vaccinated mice. Representative histological brain sections harvested from pre-vaccinated mice (n=5) injected with GL261-CIITA (panels: a – e) and with CT-2A (panels: f – j), and from non-vaccinated mice injected with CT-2A only (n=5) (panels: k – o) at ×200 magnification. Slides from the brain tissues isolated from pre-vaccinated and non-vaccinated tumor bearing mice were subjected to immunohistochemical staining with anti-nestin, anti-synaptophysin, anti-MHC-II and anti-Ki67 antibodies. Yellow arrowhead in the HE-stained section indicates the pre-vaccinated CT-2A, revealing the site of injection. Black arrowhead points the presence of mesenchymal oncostreams in CT-2A tumors. Blue arrowhead indicates Nestin+ residual tumor mass, being surrounded microglial cells in GL261-CIITA mice. An abundant MHC-II

compartment, was predominantly distributed along the fibrotic stands and partially within the surrounding brain zone (red arrowheads). In contrast, non-vaccinated control mice have shown a sparse distribution of dendritic macrophages localized within necrotic areas and absent peritoumorally (green arrowhead). Brown arrowhead points the high mitotic index in CT-2A tumors.

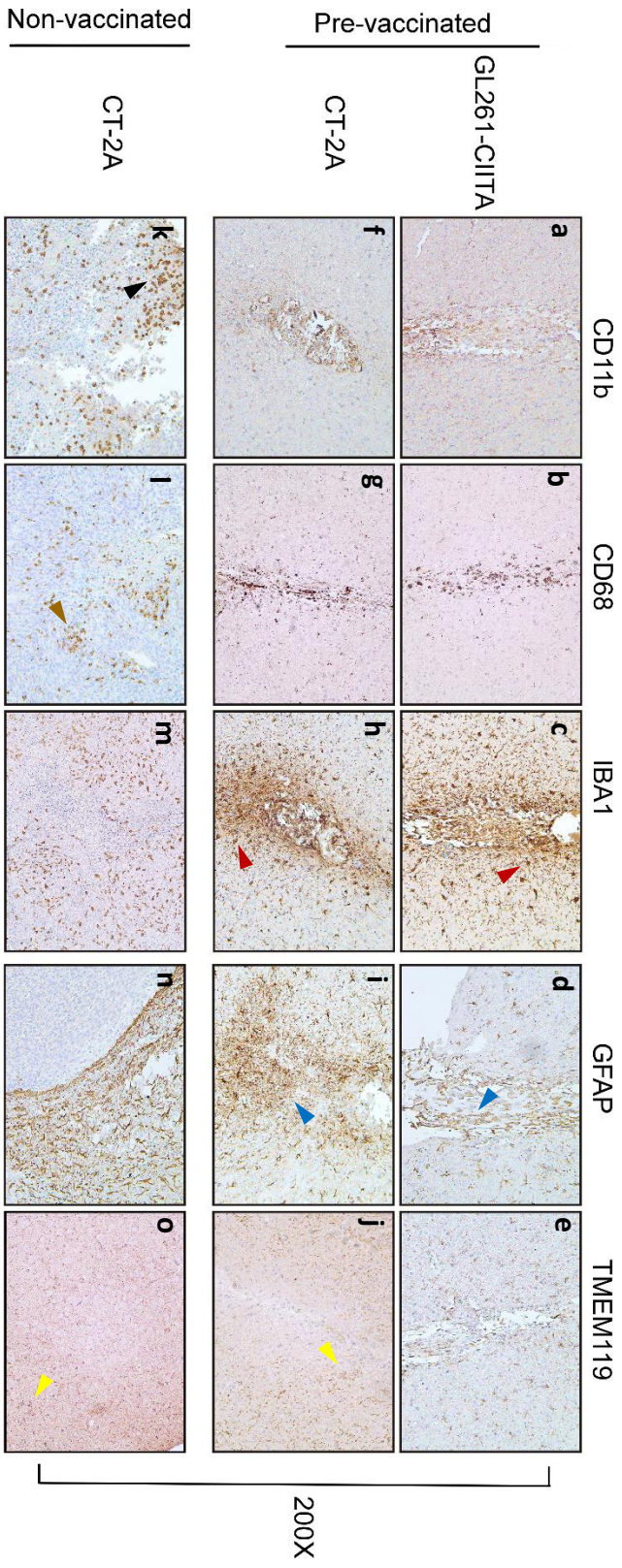

Figure 29 | Immunohistological characterization of CT-2A tumor rejection in GL261-CIITA pre-vaccinated mice. Representative histological brain sections harvested from pre-vaccinated mice (n=5) injected with GL261-CIITA (panels: a – e) and with CT-2A (panels: f – j), and from non-vaccinated mice injected with CT-2A only (n=5) (panels: k – o) at ×200 magnification. Slides from the brain tissues isolated from pre-vaccinated and non-vaccinated tumor bearing mice were subjected to immunohistochemical staining with anti-

CD11b, anti-CD68, anti-IBA1, anti-GFAP and anti-TMEM119 antibodies. Black arrowhead indicates rich infiltration of CD11b+ granulocytes which were distributed into the necrotic area (in CT-2A control group). Brown arrowhead points CD68+ cells revealing their high infiltrative tendency throughout the necrotic regions. Red arrowheads points IBA1+ cells with macrophagic features in reverted CT-2A and GL261-CIITA tumors, which were predominantly dispersed throughout the desmoplastic region and along the surrounding parenchyma. Blue arrowheads indicate the presence of a compact and organized glial texture, which was prominently seen in challenged CT-2A tumors and also in GL261-CIITA tumors, completely surrounding the tumor mass. TMEM119 immunoreactivity indicate the presence of resident microglia, forming a halo of a negative population surrounding the neoplastic region and the tumor bed in non-vaccinated and pre-vaccinated CT-2A respectively (yellow arrowheads).

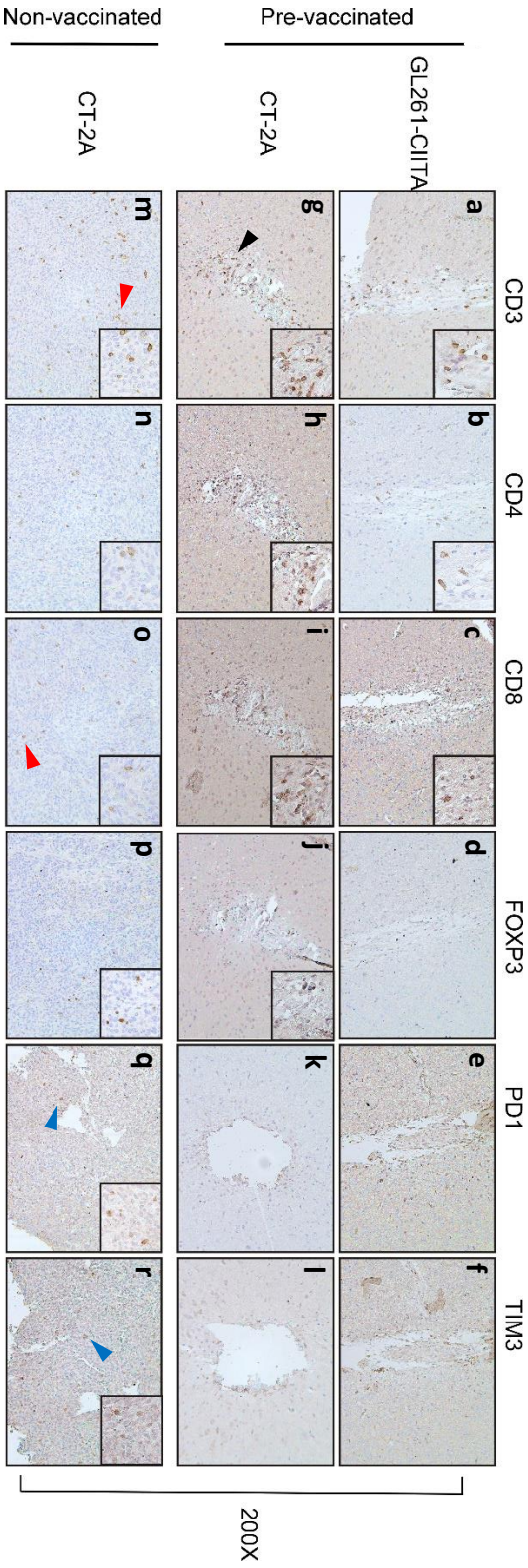

Figure 30 | Rejected CT-2A parental tumors in pre-vaccinated mice are strongly infiltrated by anti-tumor T cell cells. Representative immunohistology images of tumor sections. The upper panels (a – f) depict GL261-CIITA in pre-vaccinated mice at 42 days after inoculum stained for the specific markers listed at the top. The middle panels (g – l) depict CT-2A parental tumors in GL261-CIITA pre-vaccinated mice (pre-vaccinated, CT-2A). The lower panels (m – r) depict CT-2A parental tumors in non-vaccinated mice (non-vaccinated, CT-2A). Slides from the brain tissues were subjected to immunohistochemical staining with anti-CD3, anti-CD4, anti-CD8, anti-FOXP3, anti-PD1 and anti- TIM3 antibodies. Small square boxes are the areas represented in the corresponding large square boxes of each IHC image. Images were taken at ×200 magnification. Large square boxes were taken at ×400 magnification. Note that selected areas in IHC images of CT-2A parental tumors of non-vaccinated mice are taken in the rare zones in which positive cells for the selective marker were present. The lymphocytic compartment was primarily distributed throughout challenged CT-2A tumor bed (black arrowhead). In the control non-vaccinated mice, only a scattered and a minimal presence of T-lymphocytes was observed within the tumor mass (red arrowheads). Some TIM3+ and PD1+ tumor cells were observed in CT-2A tumors (blue arrowheads).

A deeper analysis of the phenotype of tumor infiltrating cells was then caried out to better associate the tumor rejection/retardation *in vivo* observed in GL261-CIITA pre-vaccinated and CT-2A challenged mice to the presence of specific subpopulations (Figure 30). In challenged CT-2A tumors, an abundant inflammatory infiltrate was uniformly spread throughout the tumor mass as well as in the peritumoral area, promoting the neoplastic perimeter. Notably, vascular involvement was evident around the invasive margin and along the peritumoral area, required for the lymphocytic recruitment to the neoplastic site. Moreover, a discrete lymphocytic compartment, both CD4+ and CD8+ T cells, was mainly distributed throughout the tumor bed and partially in the surrounding tissue in completely rejected CT-2A samples (Figure 30, panels g – i, black arrowhead). Some regressed GL261-CIITA and CT-2A tumors disclosed a restricted number of lymphoid cells, as consequence of a complete tumor remission (Figure 30, panels a – c). Conversely, in control non-vaccinated mice, few and randomly distributed T lymphocytes were observed inside the tumor mass (Figure 30, panels m – o, red arrowheads). Nor plasma cells, neither NK+ cells were observed.
Immunohistochemistry revealed a limited amount of T-reg FOXP3+ population, restricted along the fibrotic tissue of the tumor bed and partially distributed inside the challenged CT-2A tumors (Figure 30, panel j). In control group, instead, increased number of cells with nuclear FOXP3+ cell expression was detected (Figure 30, panel p), together with the presence of exhausted TIM3+/PD1+ population. Notably, some TIM3+ and PD1+ tumor cells were observed (Figure 30, panels q and r, blue arrowheads).
Thus, vaccination with GL261-CIITA drastically reprogrammed the anti-tumor immune response against the CT-2A line reversing the immunosuppressive phenotype, toward a more immunogenic pattern able to induce a complete tumor remission in 50% of cases. Taken together, the above results demonstrate that a cross adaptive immunity can be generated against two distinct GBM tumor cell lines strongly emphasizing the existence of common tumor associated antigens that can be efficiently provided and presented to CD4+ TH cells by MHC-II antigen presentation machinery (APM), on the surface of tumor cells.

Novel approach to optimize similarities between *in vitro* cultured and *in vivo* growth of GBM: a study on the potential of neurospheres

The 2D in vitro culture models, albeit easily established and reproducible, fail to replicate the *in vivo* tissue architecture. In contrast, the development of 3D cell culture models, such as glioma spheroids or neurospheres (NS), provides a more suitable approach for glioblastoma research. These models offer a more accurate representation of gliomas *in vitro* compared to the conventional serum cultures ([253]). In order to simulate the intricate network of interactions among glioma cells in the microenvironment of brain tumors, GL261 and Gl261-CIITA murine glioblastoma lines were cultured *in vitro* to generate neurospheres (GL261-NS and GL261-NS-CIITA respectively, see material and methods). Indeed, GL261 and GL261-CIITA cells cultured *in vitro* displayed round neurospheres-like floating aggregates (Figure 31).

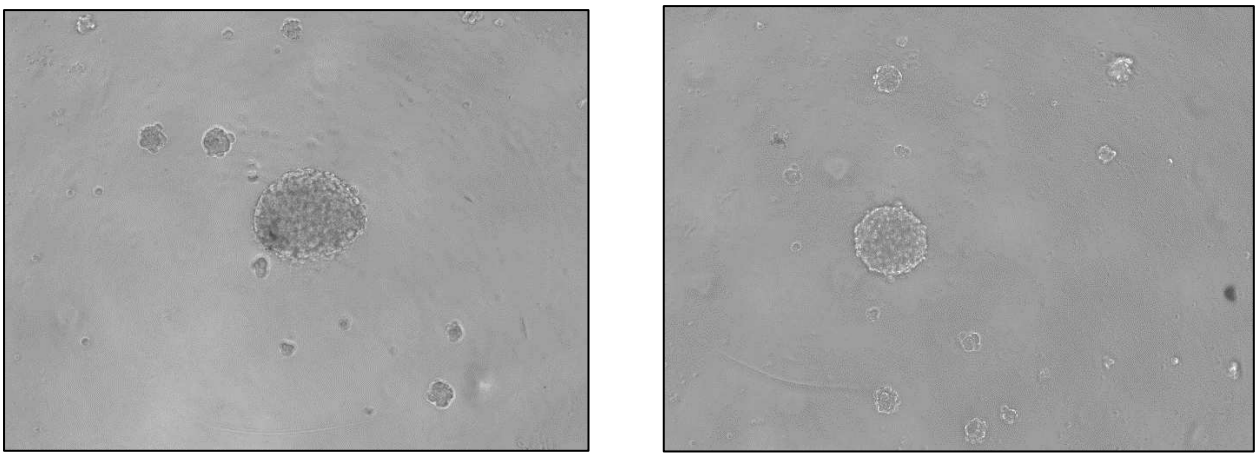

Figure 31 | Representative images of GL261-NS (left) and GL261-NS-CIITA (right) neurospheres.

After dissociation in a single-cell suspension, murine GBM cells ($3x10^4$ cells in 3 µL PBS) were stereotactically injected intracranially in anaesthetized mice as previously described ([216]). Mice were observed daily for death or neurological symptoms and were subsequently sacrificed at day 21. The brains were removed, processed, and analysed histologically.

Previous studies suggested that GL261-NS possess stronger tumorigenicity *in vivo* compared to GL261 grown as monolayer adherent cells (GL261-AC). The high lethality was also confirmed by Kaplan-Meier survival analysis, disclosing a significantly more aggressive pattern than GL261-AC in C57BL/6 mice ([254]).

Consistent with the data previously obtained from Pellegatta et al. ([255]), macroscopic appearance revealed in GL261-NS a remarkable tumor development along the sagittal plane, starting from the frontal lobe (site of injection) till the parietal-temporal lobe. Exophytic development could occur with a greater tendency toward intracerebral development. Cortical infiltration tended to develop in an inflamed and thickened cortex overlying a compact tumor zone in the white matter. Notably, these tumors may produce abnormalities in the surface vasculature, which are usually identified as thrombosed vessels. The cut surface was variable in colour, with peripheral greyish to pink masses and a distinct darker central area, suggesting the presence of a massive lesion accompanied by haemorrhage. No necrosis has been observed. On the other hand, neither tumor nor haemorrhage was macroscopically detected in GL261-NS-CIITA-bearing mice, only revealing the site of injection. With rare exceptions, the cut surface did not provide evidence of tissue alterations within the brain parenchyma.

Both GL261-NS and GL261-NS-CIITA tumors revealed an epithelioid pattern, defined by a loosely cohesive aggregate of cells with a distinct cell membrane, an abundant eosinophilic cytoplasm and eccentric or

centrally located nuclei (Figure 32B, panels i and m). Cellular pleomorphism may occur, characterized by numerous, multinucleated, and bizarre giant cells usually focused along the invasive margin. Histological analysis of GL261-NS tumors revealed high cellularity, with a strong tendency to invade the normal brain parenchyma but, with greater tendency for circumscribed development (Figure 32B, panel e). Indeed, a sharp boundary between a solid neoplastic mass and healthy brain parenchyma may occurs. Occasionally, the margins between tumor and normal brain tissue were unclear, showing intraparenchymal invasion pattern of the tumors. Microvascular proliferation could be present, whereas zonal necrosis was rarely found. Several atypical and bizarre mitotic figures could occur, especially along the invasive margin. Haematoxylin and Eosin-stained sections of GL261-NS revealed a limited number of infiltrating T cells. In contrast, an abundant granulocytic population was present, which typically spread throughout the mass (Figure 32B, panel m). Conversely, GL261-NS-CIITA were characterized by a loose structure, in which cells with irregular margins were arranged in nests and rows and surrounded by an oedematous matrix. The mitotic rate was remarkably low. An abundant inflammatory infiltrate was uniformly spread throughout the tumor mass as well as in the peritumoral area, favouring the neoplastic perimeter. Notably, vascular involvement was evident around the invasive margin and along the peritumoral area, required for the lymphocytic recruitment to the neoplastic site (Figure 33B, panel i).

Fifty percent of the mice injected with GL261-NS-CIITA showed a strong delay in tumor growth, with a tumor size 22-fold smaller compared to the parental control (0,57 mm^2 for GL261-NS-CIITA, 12,88 mm^2 for GL261-NS) (Unpared Student T test, $p < 0.0001$), indicating that CIITA tumor spheres were also retarded in their growth in vivo (Figure 32A, 32B panel a, red arrowhead).

Immunohistochemistry revealed prominent and patchy Nestin expression in GL261-NS and GL261-NS-CIITA tumor tissues and the complete absence of expression in the adjacent normal brain parenchyma (Figure 32B, panels b, f, j, n). Nevertheless, Nestin+ reactive astrocytes were clearly visible along the tumor margin, especially in CIITA tumors, where well-organized microglia surround the neoplastic mass (Figure 32B, panel j, black arrowhead).

Ki67 staining has been conducted to quantify the cellular proliferation rate. Brisk mitotic index characterized GL261-NS tumors, with Ki67+ tumor cells mainly distributed along the invasive margins and spread into the neoplasia and in addition in focal tumor zones inside the mass (Figure 36, panel f, black arrowhead). No Ki67+ cells were revealed in GL261-NS-CIITA tissues (Figure 36, panel d).

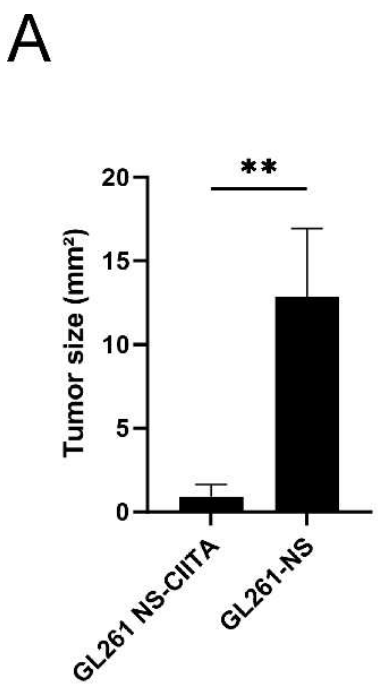

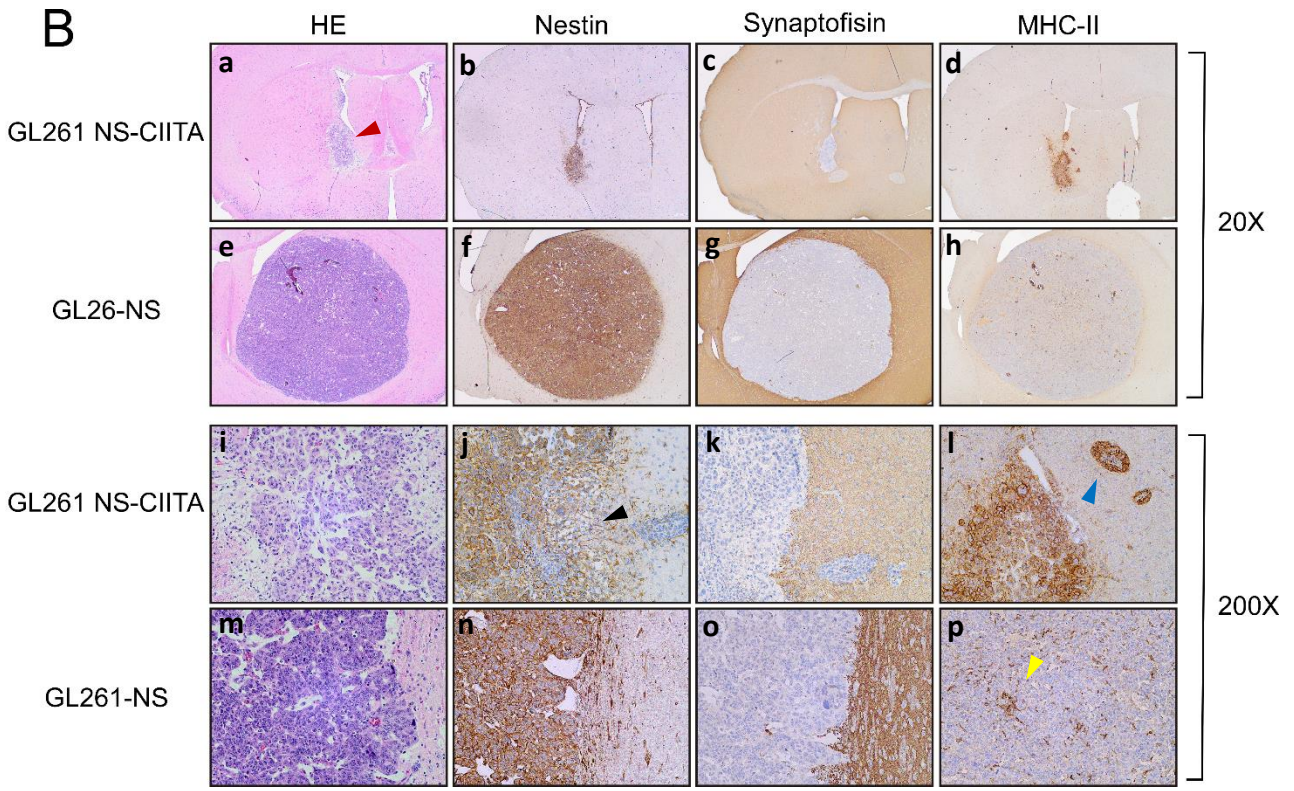

Figure 32 | Intracranial implantation of MHC-II positive GL261-NS-CIITA tumor cells dramatically retarded tumor growth *in vivo*. C57BL/6 mice received intracranial injection of 3×10^4 GL261-NS (n=7) or GL261-NS-CIITA (n=10) glioma cells. On day 21 after injection, mice were sacrificed, brains were removed, and serial sections of the brain were carried out to measure tumor size and for staining. (A) Average tumor size of GL261-NS and GL261-NS-CIITA tumors. Data are represented as mean values, and error bars indicate the standard deviation (SD) within each group. p-Values were determined via unpaired t-test; **p < 0.01. (B) Representative histological brain sections harvested from mice injected with GL261-NS-CIITA (panels: a – d and i – l) and with GL261-NS (panels: e – h and m – p) at x20 and x200 magnification respectively. HE, haematoxylin and eosin. Slides from the brain tissues isolated from GL261-NS or GL261-NS-CIITA tumor bearing mice were subjected to immunohistochemical staining with anti-nestin, anti-synaptophysin and anti-MHC-II antibodies. Red arrowhead in the HE-stained section indicates the GL261-CIITA tumor. Black arrowhead points the presence of nestin+ astrocytes along the tumor margin, particularly in GL261-NS-CIITA tumors. Blue, and yellow arrowheads point MHC-II staining in GL261-NS-CIITA and GL261-NS respectively. Prominent MHC-II expression was observed in cells, within peritumoral vessels potentially attracting leukocytes to tumor site through leukocyte diapedesis. While as in GL261-NS a uniformly dispersed dendritic population was observed.

MHC-II expression in GL261-NS-CIITA tumor cells and in both myeloid and lymphoid cells infiltrating the tumor was then analyzed. Particularly, immunostaining revealed prominent membranous and cytoplasmatic MHC-II expression on GL261-NS-CIITA cells (100%), accompanied by an abundant dendritic population predominantly distributed peritoumorally and along the neoplastic margins. MHC-II expressing cells were also observed within peritumoral vessels, possibly attracted to the tumor site by leukocyte diapedesis (Figure 32B, panel i, blue arrowhead). A restricted dendritic population was found in parental tumors, uniformly dispersed within the tumor surface (10%) (Figure 32B, panel p, yellow arrowhead).

Given the central role exerted by the TME in the neoplastic progression ([256,257]), it appeared necessary to characterize the glial-dendritic cell component in order to specifically identify their function in the immunological context.

In GL261-NS-CIITA a higher number of dendritic-CD11b+ cells were observed, predominantly surrounding the tumor margin, and widely distributed along the peritumoral area (45-50%) (Figure 33, panel a, yellow arrowhead). This pattern is shared with the GFAP+ astrocytic population, forming an organized and dense

texture around the neoplastic mass. Instead, weak CD11b+ cell accompaniment was observed in GL261-NS tumors, in which cells with a dendritic phenotype were uniformly distributed along the tumor perimeter and partially along its margin (Figure 33, panel f). A rich granulocytic infiltrate was predominantly present in the tumor core (10-15%). A strong correlation was observed between tumorigenicity and the amount in CD11b+ myeloid cell infiltration in parental tumors. Particularly, an increase in tumor growth and invasiveness, with a high Ki67 positive mitotic rate was observed, together with specific CD11b+ cells expressing granulocytic phenotype.

The immunohistochemistry analysis of the peritumoral GFAP expression revealed an increasing intensity of the signal with an increasing number of reactive astrocytes surrounding the tumor margin. A gradient of morphological modifications such as cell body hypertrophy and terminals arborization occurring during the reactive astrogliosis could be appreciated mainly in GL261-NS-CIITA tumors, revealing a compact and dense glial matrix architecture (55-60%) (Figure 33, panel d, black arrowhead). Instead, GFAP+ astrocyte processes resulted to be very restricted along the invasive margin of GL261-NS tumors (10%). Notably, some astrocytic processes were trapped inside the neoplastic mass (Figure 33, panel i, red arrowhead). Astrocytes are the CNS resident cells that may share a common origin with the GBM cells ([257]). Indeed, immunostaining revealed prominent membranous GFAP+ microglial expression and some faint diffuse or granular cytoplasmic staining in both GL261-NS and GL261-NS-CIITA cells.

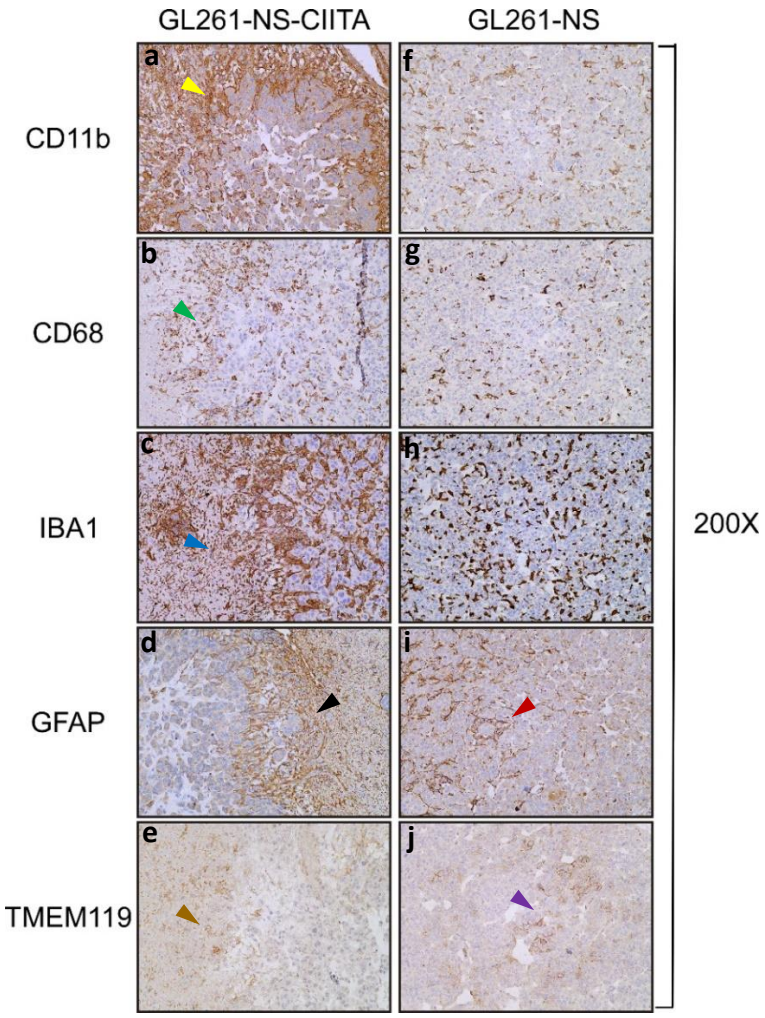

Figure 33 | Immunohistological characterization of GL261-NS-CIITA tumors compared to GL261-NS control group. HE and IHC staining of serial brain sections. Representative histological brain sections harvested from mice injected with GL261-NS-CIITA (n=10) (panels: a – e) or with GL261-NS (n=7) (panels: f – j), at x200 magnification. HE, haematoxylin and eosin. Slides from the brain tissues

isolated from GL261-NS or GL261-NS-CIITA tumor bearing mice were subjected to immunohistochemical staining with anti-CD11b, anti-CD68, anti-IBA1, anti-GFAP and anti-TMEM119 antibodies. CD11b+ cells were notably present in GL261-NS-CIITA tumors, particularly along the tumor margin (yellow arrowhead). Green arrowhead points the consistent presence of CD68+ cells within the peripheral neoplastic region of GL261-NS-CIITA. Blue arrowhead points the distinct phenotypes of IBA1+ cells within GL261-NS-CIITA tumor area. The GFAP staining revealed high signal intensity, correlating with an increased number of astrocytes, surrounding GL261-NS-CIITA tumor margin (black arrowhead). Meanwhile, the red arrowhead highlights the presence of entrapped astrocytic processes within the neoplastic mass. Brown arrowhead points predominant TMEM119 immunoreactivity in healthy brain parenchyma surrounding GL261-NS-CIITA, while it was notably absent in GL261-NS where few tumor cells has acquired TMEM119+ phenotype (violet arrowhead).

IBA1 immunostaining analysis demonstrated different phenotypes of these cells: central tumor areas predominantly exhibit an amoeboid shape, while the infiltration zones display a more ramified phenotype. Since ramified and amoeboid forms of these cells are linked to low- and high activation states, respectively ([258]), these observations support a gradual increase in activated IBA1+ towards the tumor centre. Particularly, this pattern is found in CIITA tumors, in which a gradual phenotypic shift of these cells can be detected (80%) (Figure 34, panel c, blue arrowhead). In contrast, moderate cellular population was found in GL261-NS, in which amoeboid-like IBA1+ cells are uniformly distributed in the neoplastic region (40%) (Figure 33, panel h).
The pan-macrophage marker CD68 was expressed in GL261-NS-CIITA tumor tissue, in a consistent number of cells, surrounding the peripheral neoplastic region and infiltrating the tumor mass. Notably, both ramified and amoeboid CD68+ cells were partially observed, consistent with a dynamic range of activation states throughout the tumour tissue (35-40%) (Figure 33, panel b, green arrowhead). A branched subpopulation was partially present along the invasive margin and partially distributed throughout the tumor area in GL261-NS (20-25%) (Figure 33, panel g). Notably, in the final steps of CIITA-tumor remission, a rich myeloid infiltrate characterized by CD68+ and CD11b+ cells with a dendritic phenotype was accompanied by abundant GFAP+/IBA1+ microglial component. These cells acquire a more infiltrative pattern, rearranging their distribution within the tumor region (100%).
TMEM119 immunoreactivity was mainly present in the surrounding brain parenchyma of GL261-NS-CIITA tumors but not in GL261-NS, here with the exception of some tumor cells that acquire the TMEM119+ phenotype (Figure 33, panel j, violet arrowhead). In CIITA tumors, TMEM119+ cells assumed the aspect of intense ramifications of resident microglia along the tumor margin that are maintained within the surrounding brain parenchyma (Figure 33, panel e, brown arrowhead). These findings suggest an overall inhibition of resident microglia in parental tumors. In this case, the immunosuppressive nature of the GL261-NS appeared to be associated with diminished marker expression. Reduced resident microglial phenotype is followed by a subsequent downregulation toward an activating microglial pattern (as confirmed by reduced expression of the markers IBA1 and GFAP) (Figure 33, panels h and i).
OLIG2 is a basic helix-loop-helix (bHLH) transcriptional repressor protein that plays a crucial role in the development of the central nervous system. Its main function is to maintain glial progenitor cells in a state of competent proliferation and promote their specification. OLIG2 is ubiquitously expressed in human gliomas and it is important for maintaining the stem status of glioma and activate cell proliferation machinery to promote tumorigenesis ([259,260]). Furthermore, OLIG2 can counteract the tumor suppressor protein p53 by directly repressing the transcription of p21, a cell cycle inhibitor induced by p53 ([261]).
Positive OLIG2 staining supported the differentiation toward oligodendroglial lineage. Particularly, 90-95% of GL261-NS cells demonstrated strong diffuse nuclear OLIG2 expression (Figure 36, panel e). Conversely, a patchy to focal OLIG2 expression has been observed on GL261-NS-CIITA, revealing a very limited marker expression pattern (0-5%) with the exception of the resident glia, distributed throughout the healthy parenchyma (Figure 36, panel c, red arrowhead).
Immunostaining revealed an abundant lymphocytic infiltrate, mainly distributed along the tumor margin and partially within the neoplastic surface. Of note, a large number of TILs were observed in CIITA tumors, near peritumoral vessels and extending into the adjacent neoplastic margin, suggesting a migrant path originating from vessels and heading to the tumor area. An abundant immune compartment was also detected in the peritumoral zone (Figure 34, panel a, black arrowhead). As a consequence of an effective anti-tumor immune

response, a prominent CD8+ T cell infiltration cell was present, together with a less pronounced presence of CD4+ T-helper cells (Figure 34, panels c and b respectively). Conversely, the presence of T cells was greatly decreased in the GL261-NS tumors and the few TILs were uniformly distributed throughout the tumor mass (Figure 34, panels g – i). Overall, results showed intense tissue infiltration from the adaptive immune compartment in CIITA tumors, compared to the parental GL261-NS tumors.

To better understand the critical role of the immunosuppressive compartment on GBM microenvironment, FOXP3, PD1 and TIM3 T-cell markers were also analysed (Figure 34).

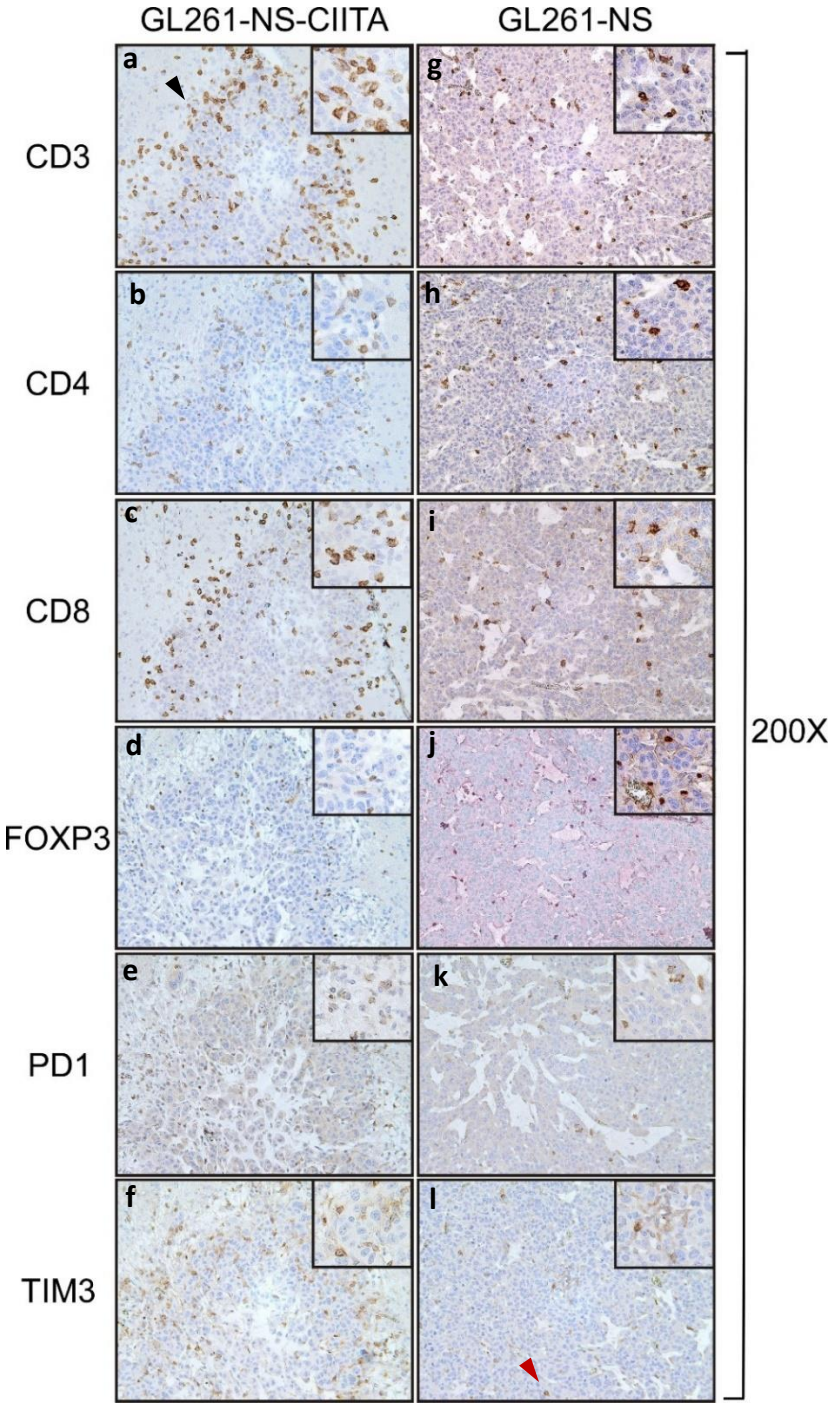

Figure 34 | GL261-NS-CIITA tumors are strongly infiltrated by T cell compartment: immunostaining for CD3, CD4, CD8, FOXP3, PD1 and TIM3 in both GL261-NS (right panels) and GL261-NS-CIITA (left panels). Small square boxes are the areas represented in the corresponding large square boxes of each IHC image. Representative histological brain sections harvested from mice injected with GL261-NS-CIITA (panels: a – f) or with GL261-NS (panels: g – l), at ×200 magnification. Large square boxes were taken at ×400

magnification. Note that selected areas in IHC images of GL261 parental tumors were taken in the rare zones in which positive cells for the selective marker were present. Black arrowhead indicates the presence of CD3+, cells within the tumor, suggesting their involvement in tumor microenvironment. Additionally, TIM3+ cells were observed within the tumor (red arrowhead).

A limited T-reg FOXP3+ population was observed in GL261-NS-CIITA tumors, together with a restricted amount of PD1+ and TIM3+ TILs (Figure 34, panels d – f). These exhausted T-cells exhibited a similar distribution pattern of CD4+ and CD8+ T-cells. Notably, the most striking feature of GL261-NS-CIITA associated CD4+ T cells was a vigorous FOXP3+ T cell commitment, although this had no negative implications on the effectiveness of the T cell-mediated response. Of note, TIM3+ and PD1+ tumor cells were observed also in GL261-NS (Figure 34, panels k and l, red arrowhead).

As previously mentioned, 50% of mice injected with GL261-NS-CIITA cells escaping tumor resistance revealed a markedly immunosuppressive phenotype, mimicking the tumorigenic hallmarks of parental tumors. Immunostaining identified a restricted myeloid repertoire, characterized by limited amounts of CD68+ (10%) and CD11b+ cells (10%), randomly distributed within the lesion (Figure 35, panels a – d). Similar to GL261-NS tumors, the microglial recruitment was quantitatively decreased (IBA1 5-10%, GFAP 10-15%), restricted along the tumor margin and not organized to form an efficient peritumoral lining (Figure 35, panel c, black arrowhead). A limited amount of TILs were present, scattered inside the tumor mass (Figure 35, panel e, red arrowhead). Notably, GL261-NS-CIITA with an immunosuppressive phenotype also shared a strong and diffuse nuclear OLIG2 expression with the parental tumor (Figure 36, panel a).

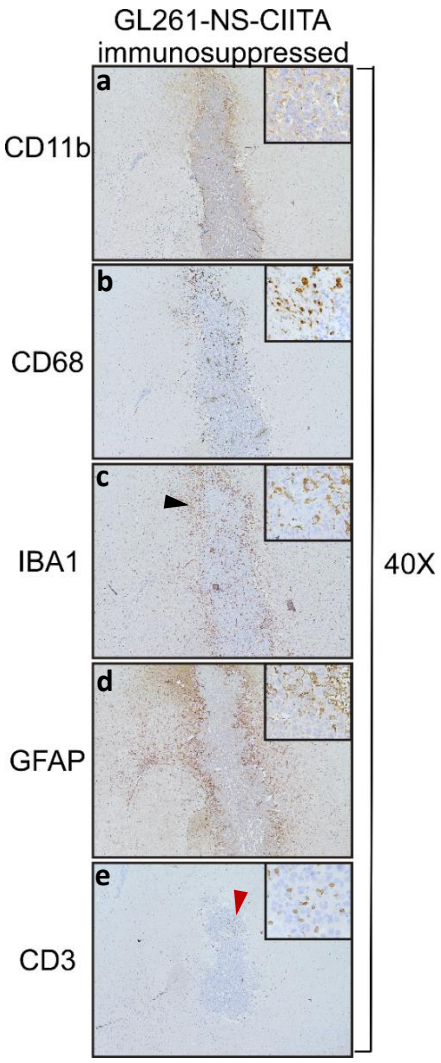

Figure 35 | GL261-NS-CIITA immunosuppressive phenotype observed in a population of GL261-NS-CIITA tumors. Immunostaining of serial brain sections. All the panels were taken at ×40 magnification. HE, haematoxylin and eosin. Slides from the brain tissues

isolated from GL261-NS-CIITA tumor bearing mice subjected to immunohistochemical staining with anti-CD11b, anti-CD68, anti-IBA1, anti-GFAP and anti-CD3 antibodies. Small square boxes are the areas represented in the corresponding large square boxes of each IHC image. Representative histological brain sections harvested from mice injected with GL261-NS-CIITA that shows an immunosuppressive phenotype (panels: a – e), at ×40 magnification. Black arrowhead indicates restricted presence of IBA1+ cells along the tumor margin. Scattered CD3+ cells were distributed inside the tumor mass (red arrowhead).

An important finding was obtained by comparing on GL261-NS and GL261-NS-CIITA the OLIG2 expression, infiltrating lymphocytes content and tumor growth.

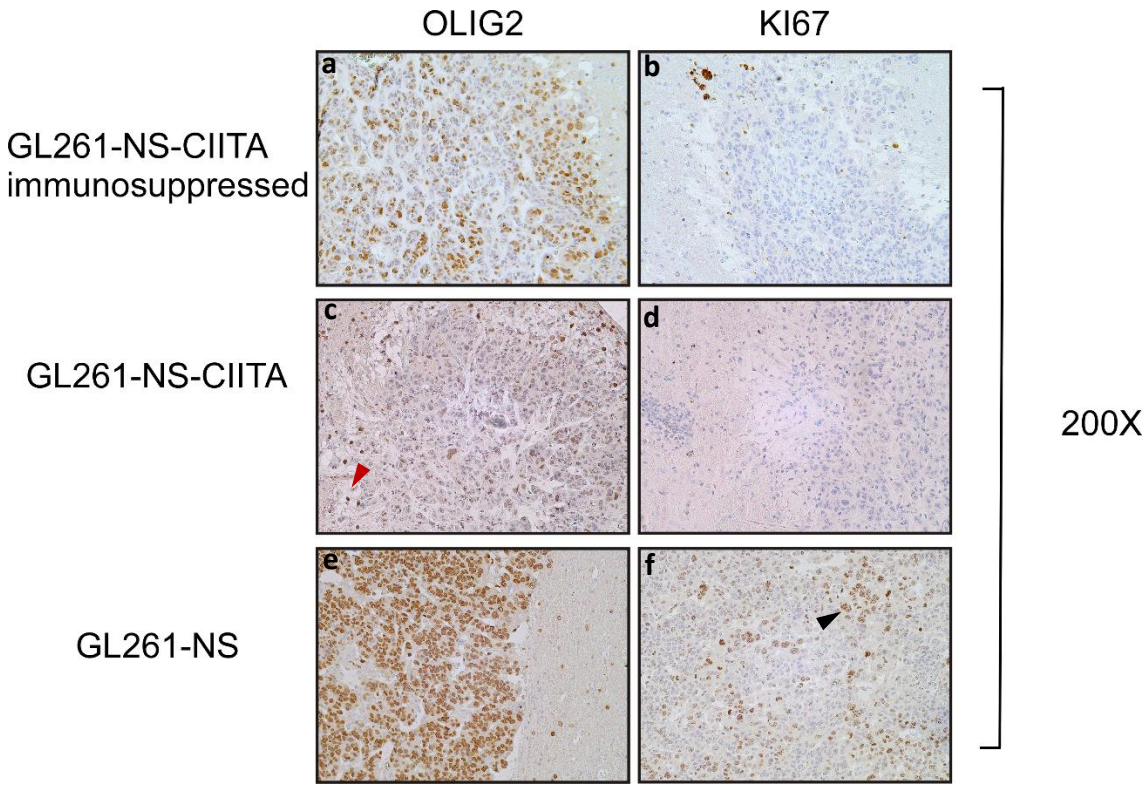

Figure 36 | OLIG2 and Ki67 expression in GL261-NS, GL261-NS-CIITA and GL261-NS-CIITA with an immunosuppressive phenotype. IHC staining of serial brain sections. Representative histological brain sections harvested from mice injected with GL261-NS-CIITA that shows an immunosuppressive phenotype (panels: a, b), or with GL261-NS-CIITA (panels: c, d) or with GL261-NS (panels e, f), at ×200 magnification. IHC, immunohistochemistry. Slides from the brain tissues isolated from GL261-NS and from GL261-NS-CIITA tumor bearing mice were subjected to immunohistochemical staining with anti-OLIG2 and anti-Ki67 antibodies. OLIG2 is expressed in immunosuppressed GL261-NS-CIITA population, but not in the other GL261-CIITA-NS, in which the positivity was limited to the oligodendrocytes surrounding tumor area. Red arrowhead points the distribution of resident glia surrounding healthy parenchyma. Ki67+ cells are abundant in tumor isolated from non-treated mice (black arrowhead).

Indeed, data suggest a strong negative correlation between the presence of TILs and the oligodendroglial marker expression. In more detail, GL261-NS-CIITA tumors exhibit higher mitotic index, higher OLIG2 expression, restricted infiltrative pattern, and 2.5-fold larger tumor area than GL261-NS-CIITA injected areas with scarce or not growing tumors which displayed immunogenic features (Figure 36).
These results reflect the critical relevance of successful MHC-II molecule expression on the tumor surface in the induction of a robust and effective strong adaptive immune response, able to induce an anti-tumor immunity, preventing or retarding tumor growth.

New GBM therapeutical approach using HSV-1 oncolytic virus

To assess the potential implications of HSV-1 oncolytic virus (oHSV-1) on GBM immunotherapy, I began to investigate, in collaboration with Dr. Reale of the University of Padova, the impact of EGFP-oHSV-1 on GBM tumors. This viral vector has been modified to expresses the reporter gene EGFP in the UL55-UL56 intergenic region. Additionally, the virus contains a double deletion in its γ34.5 neurovirulence gene and in Us12 gene and an insertion of a miRNA at the 3' of UL29 viral gene essential for the HSV-1 life cycle.
To appreciate cell responses to the oHSV-1 infection, $5x10^4$ GL261 cells were infected in vitro with EGFP-oHSV1 at MOI 10 plaque forming unit (PFU)/cell. Using immunofluorescence microscopy, cells were daily monitored. The experimental scheme is shown in figure 37. Viral replication was measured by plaque titration assay and mortality of cells with Trypan blue exclusion test. Within 24 hours, initial signs of cell lysis were observed. Within 13 days after exposure to the oncolytic vector, complete cell infection and clear signs of cytopathic effect were observed (Figure 38). These preliminary results underline the extraordinary pathogenic potency of the virus that leads to the lysis of all infected cells.

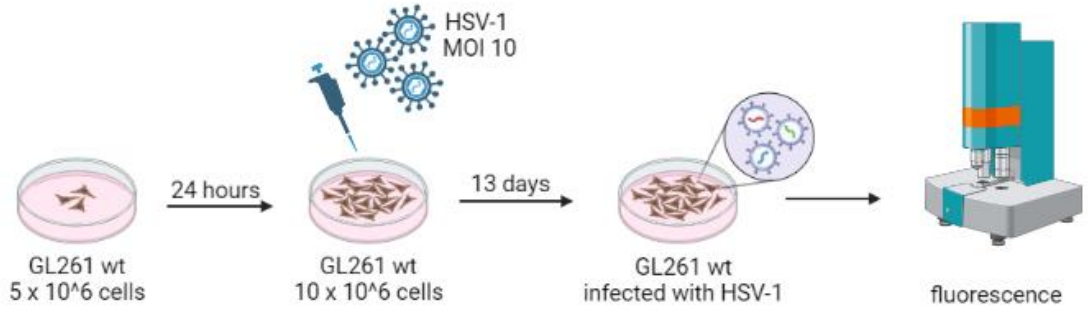

Figure 37 | Experimental scheme. $5x10^6$ GL261 cells were seeded in petri dish. 24 hours later, cells were infected with EGFP-oHSV-1. Following the infection, cells were monitored regularly under fluorescence microscope. 13 days after infection, all the infected GL261 cells die. Adapted from *BioRender.com*

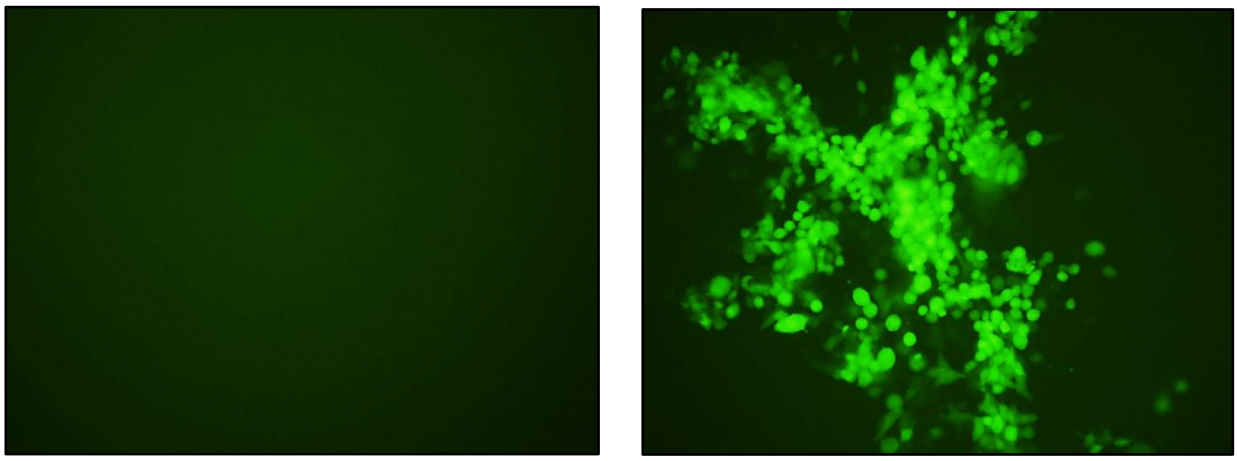

Figure 38 | Fluorescence analysis reveals the effective EGFP-oHSV1 infection on GL261 WT cells (right), compared to the negative control group (left).

To evaluate the therapeutical efficacy of EGFP-oHSV1 oncolytic virus in vivo, C57BL/6 mice were injected with 30.000 GL261 into the right striatum. 7 days after tumor implantation, mice were then injected with 10^6 pfu EGFP-oHSV1 in the same brain hemisphere. As a control, a group of mice were intracranially injected only with GL261 and after additional 7 days, they were i.c. injected with PBS (vehicle). Mice were monitored daily

for signs of illness or distress and their weight was recorded. Mice were euthanized when presenting signs of sufferance. Their brains were harvested for immunohistochemical assessment. The Kaplan-Meier survival analysis revealed a notable difference in OS between the groups. Indeed, mice receiving injection of EGFP-oHSV1 after 7 days from tumor injection exhibited a remarkable increase in OS compared to the control group, with a median survival of 64 days. These results correspond to a 146.15% increase in survival rate over the control group injected with GL261 (of note, the obtained median survival is strictly linked to their sacrifice at day 64 after challenge) (Figure 39).

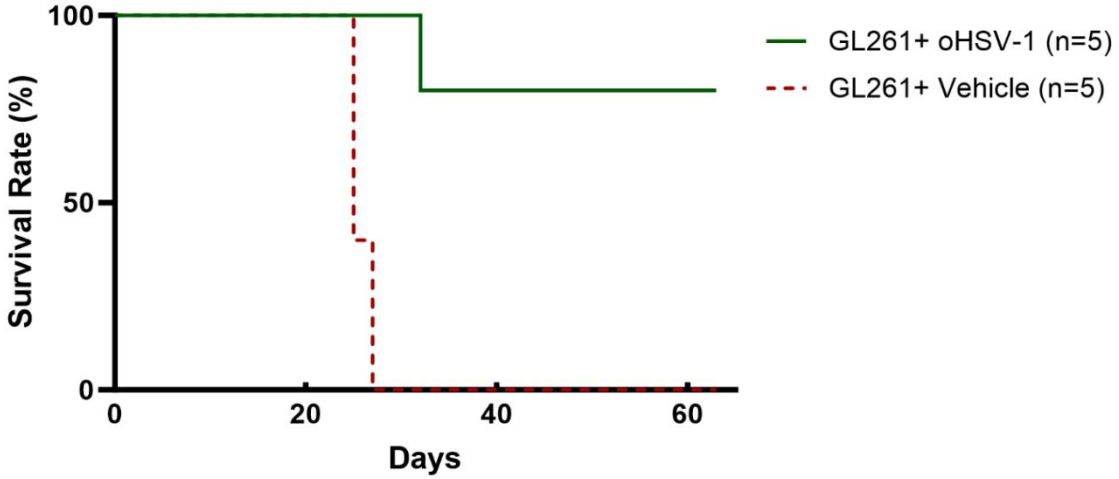

Figure 39 | Kaplan–Meier survival curves of C57BL/6 mice bearing GL261 tumor, treated with EGFP-oHSV-1 or with vehicle (PBS). OS was significantly longer in the GL261 group after OV therapy (median, 64 days – blue line) compared with the GL261 injected with PBS (median, 26 days –green line). Surprisingly, 80% of mice treated with EGFP-oHSV-1 were survived at day 64, showing a health status predictive of complete healing.

Prognostic indicators of the health status such as smooth-glossy fur, clear eyes, body weight and no behavioural changes were all in favour of mice receiving EGFP-oHSV-1 injection versus vehicle.
In order to explore the efficacy of HSV in inducing a protective immune response against the tumor, surviving mice were challenged at day 43 with 30.000 GL261 cells intracranially injected into the opposite, left brain hemisphere. Mice were monitored daily for signs of illness or distress and their weight was recorded. 21 days post challenge mice were sacrificed, their brains harvested and analysed histologically. These challenged mice were compared to GL261 control injected with vehicle (n=5) (Figure 40). Prognostic indicators of the animal health status during the challenge were again all positive.

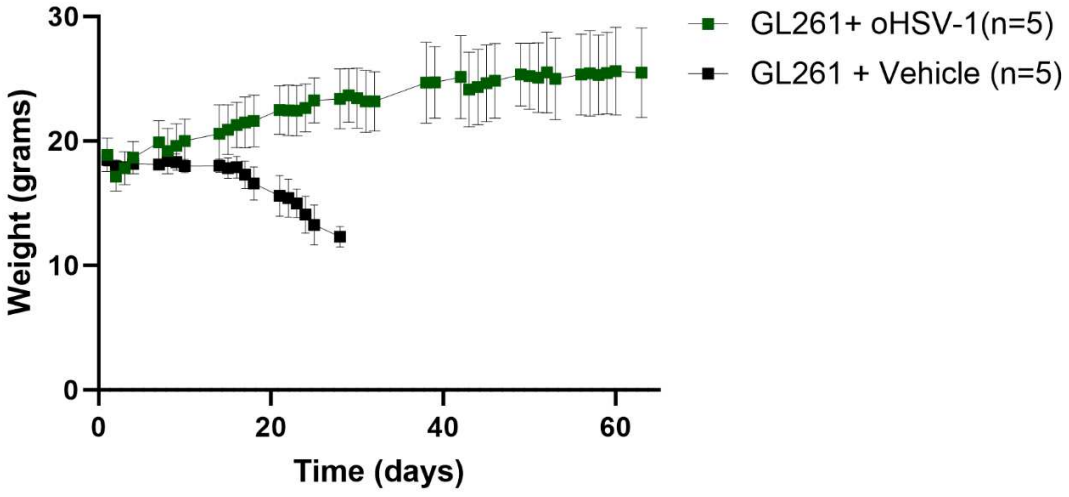

Figure 40 | Body-weight changes in mice injected with GL261 compared to GL261 treated with EGFP-oHSV-1. Mean bodyweight of mice injected GL261 treated with vehicle (black squares) or with EGFP-oHSV-1 (white squares) was measured over time (days). Significant differences were observed comparing the body weight among the two groups of mice.

Importantly, GL261 challenged mice showed a complete protection from tumor growth in 100% of the cases (Figure 41A, B). These results clearly demonstrate the therapeutical efficacy of EGFP-oHSV1 oncolytic virus on GL261 parental tumor. Neither tumor nor haemorrhage was macroscopically detected in EGFP-oHSV1-treated mice. The cut surface did not provide evidence of any tissue alterations within the brain parenchyma. Particularly, histology conducted on both hemispheres, revealed predominant desmoplastic reaction, as sign of complete tumor remission as compared to control untreated mice injected only with GL261. The residual architectural distortion was characterized by a rich leucocyte content, distributed along the fibrotic stands and accompanied by an abundant calcific deposit (Figure 41C, panels a and f, yellow arrowhead).
The control Gl261, possessed the same characteristics of the already above and previously described GL261 line ([216]) such as high tumorigenicity, restricted lymphoid and myeloid infiltrate, epithelioid phenotype and high proliferation rate (Figure 41B, panel e, figure 41C, panel k). Notably, the average parental GL261 tumor area was 5.11 mm^2 in non-vaccinated control group (Figure 41A).
Nestin+ reactive astrocytes were clearly visible along the tumor bed, especially in challenged-GL261 tumors, where well-organized microglia surround the fibrotic tissue (Figure 41C, panels b and g, red arrowhead).

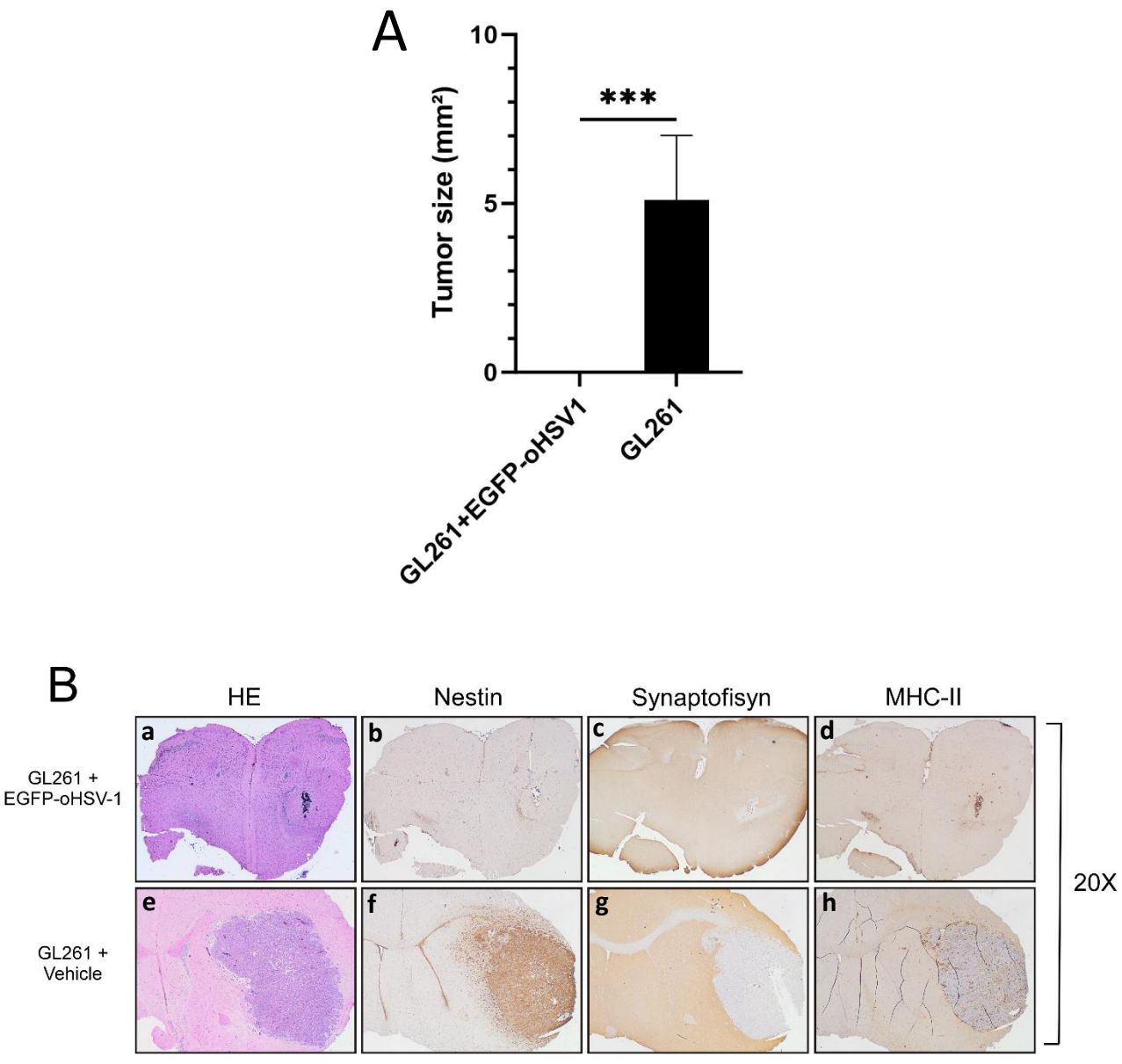

C

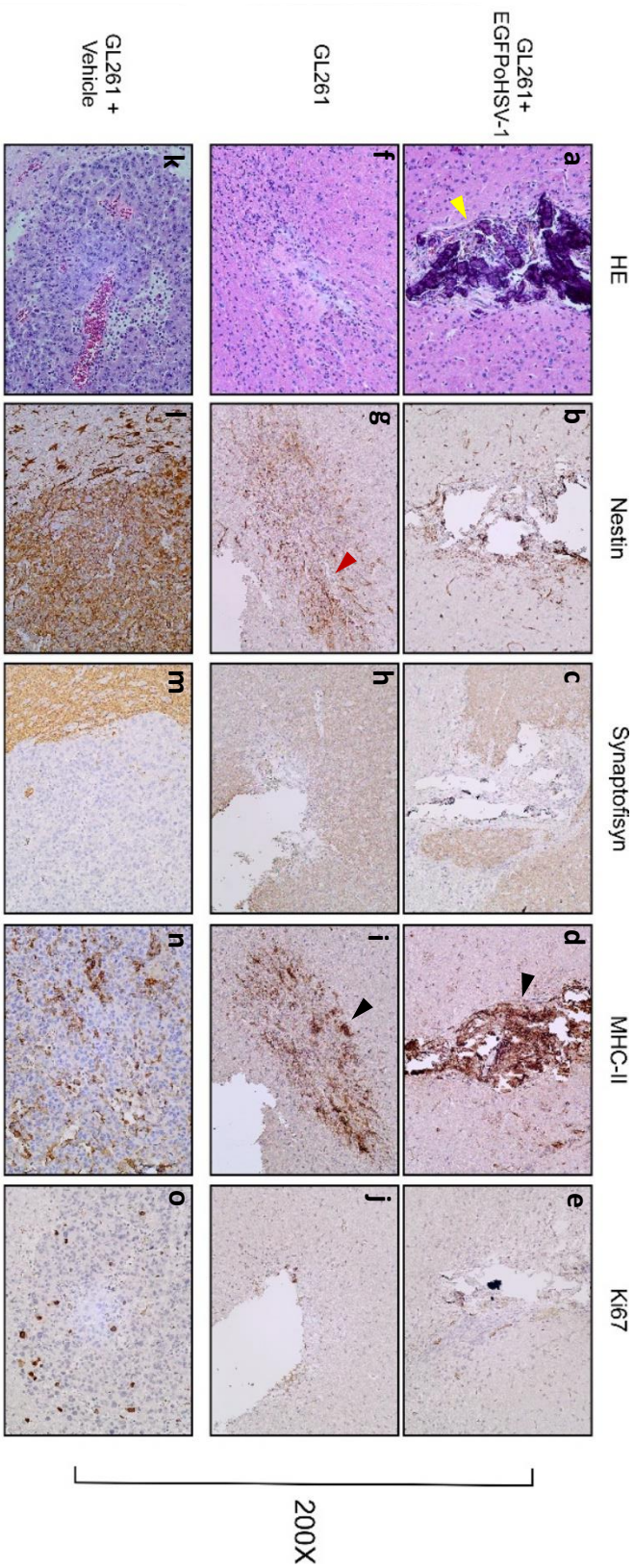

Figure 41 | EGF-oHSV-1 intratumoral injection induce a complete GL261 tumor regression (*in vivo*). C57BL/6 mice received orthotopic implantation of 3 × 10^4 GL261 GBM cells. On day 7 after tumor injection, mice were treated with 10^6 pfu EGFP-oHSV1 in the same brain hemisphere. At day 43, 80% of mice was alive, showing health general status. Then, the survived mice were challenged with another injection of GL261 in the opposite brain hemisphere. After additional 21 days, mice were sacrificed, brains were removed, and serial sections of the brain were carried out to measure tumor size and for staining. (A) Average tumor size of challenged GL261 (n=5) after OV treatment and of GL261 after injection with vehicle (PBS) (n=5). Data are represented as mean values, and error bars indicate the standard deviation (SD) within each group. p-Values were determined via unpaired t-test; ***p < 0.001. (B) HE and

IHC staining of serial brain sections. Representative histological brain sections harvested from mice firstly injected with GL261, then treated with EGFP-oHSV-1 and finally challenged with GL261 (panels: a – e). The second series of panels (e – h) represents the histological brain section of mice injected with GL261, treated with PBS 1X (vehicle). All the panels were taken at x20 magnification. HE, haematoxylin and eosin; IHC, immunohistochemistry. Slides from the brain tissues isolated from GL261 + EGFP-oHSV-1 or GL261 + vehicle were subjected to immunohistochemical staining with anti-nestin, anti-synaptophysin and anti-MHC-II antibodies. (C) HE and IHC staining of serial brain sections. Representative histological brain sections harvested from mice firstly injected with GL261, then treated with EGFP-oHSV-1 (panels: a – e) and finally challenged with GL261 (panels: f – j). The third series of panels (k – o) represents the histological brain section of mice injected with GL261, treated with PBS 1X (vehicle). All the panels were taken at x200 magnification. Slides of brain tissues isolated from GL261 + EGFP-oHSV-1 or challenged GL261 are indicated in the first- and second-line panels. Slides of brain tissues isolated from GL261 + vehicle (control group) are indicated in the third-line panels. Sections were stained with HE or by IHC with nestin-, synaptophysin-, MHC-II- and Ki67-antibodies. Yellow arrowhead in the HE-stained section points the presence of calcium residues, fibrosis and infiltrating lymphocytes. Red arrowhead in the panel g showing nestin staining of oHSV-1 treated mice point to astrocytosis-enriched area. Black arrowheads in panels d and I showing MHC-II+ myeloid cells concentrated over the tumor bed in both brain hemispheres of oHSV-1 treated mice or dispersed along the GL261 tumor (vehicle).

Synaptophysin, marker of neuronal synaptic vesicles was negative in all cases (Figures 41B and 41C, panels c and h) and the quantification of Ki67 staining revealed the complete absence of Ki67+ cells (Figure 41C, panels e and j). To evaluate the microenvironment of GL261 challenged mice after treatment with HSV, several cell markers of various cell populations were analyzed. Particularly, immunostaining revealed prominent membranous and cytoplasmatic MHC-II expression in the right hemisphere, where an abundant dendritic population was completely distributed along the neoplastic bed (100%). MHC-II expressing cells were also observed within peritumoral vessels, attracted to the tumor site by leukocyte diapedesis. In the left hemisphere, an abundant MHC-II-restricted dendritic population was distributed throughout the fibrous bed and in the tightly surrounding area (75-80%) (Figure 41C, panel i and d, black arrowheads).

Although activated microglia and macrophages share the morphological features, peripheral-derived-macrophages are abundant in the glioblastoma tissue and have different transcriptional states compared to their brain resident counterparts ([262]). In the right striatum, the site of primary tumor injection and EGFP-oHSV-1 administration, a remarkable number of dendritic-CD11b+ cells were observed. Similar to MHC-II distribution pattern, CD11b+ cells were mainly infiltrated into the fibrotic tissue (100%) (Figure 42, panel a, red arrowhead). In the challenged left hemisphere, immunostaining revealed prominent dendritic expression along the tumor bed and diffuse in the surrounding tissue (100%) (Figure 42, panel f).

In the right hemisphere, a GFAP+ astrocytic population formed an organized and dense texture around and along the tumor bed (100%) (Figure 42, panel d, black arrowhead) with a distribution similar to that of CD11b+ cells. Conversely, in the left striatum, the astrocytic processes were fully organized to generate a compact and dense cellular matrix lining the fibrous compartment (45-50%). In the surrounding area, GFAP+ staining was gradually reduced towards the healthy brain parenchyma (Figure 42, panel i, black arrowhead). IBA1 staining illustrated the different phenotypes of these cells: in the tumor bed, IBA1+ cells were mostly amoeboid in shape, whereas in the infiltration zones they displayed a more ramified phenotype. As previously described, ramified and amoeboid forms are linked to low- and high activation states, respectively. This pattern was found in both hemispheres, in which a gradual phenotypic shift of these cells can be detected (100%) (Figure 42, panels c and h, yellow arrowheads).

In the challenged GL261 tumor, an increased number of CD68+ macrophage cells were observed, infiltrating the tumor bed and invading the surrounding parenchyma (100%). Notably, both ramified and amoeboid CD68+ cells were observed, consistent with a dynamic range of activation states throughout the tumour tissue (35-40%). In the right hemisphere, a prominent CD68+ ameboid compartment was fully distributed along the neoplastic bed (100%) (Figure 42, panels b and g, green arrowheads).

In challenged GL261, TMEM119+ resident microglia appeared intensively stained, completely spread around the tumor bed and gradually decreasing in number towards the healthy brain parenchyma. Notably, in the opposite right hemisphere, TMEM119+ cells were widely distributed along the tumor bed, confirming their association with a complete tumor remission state (Figure 42, panels e and j, blue arrowhead).

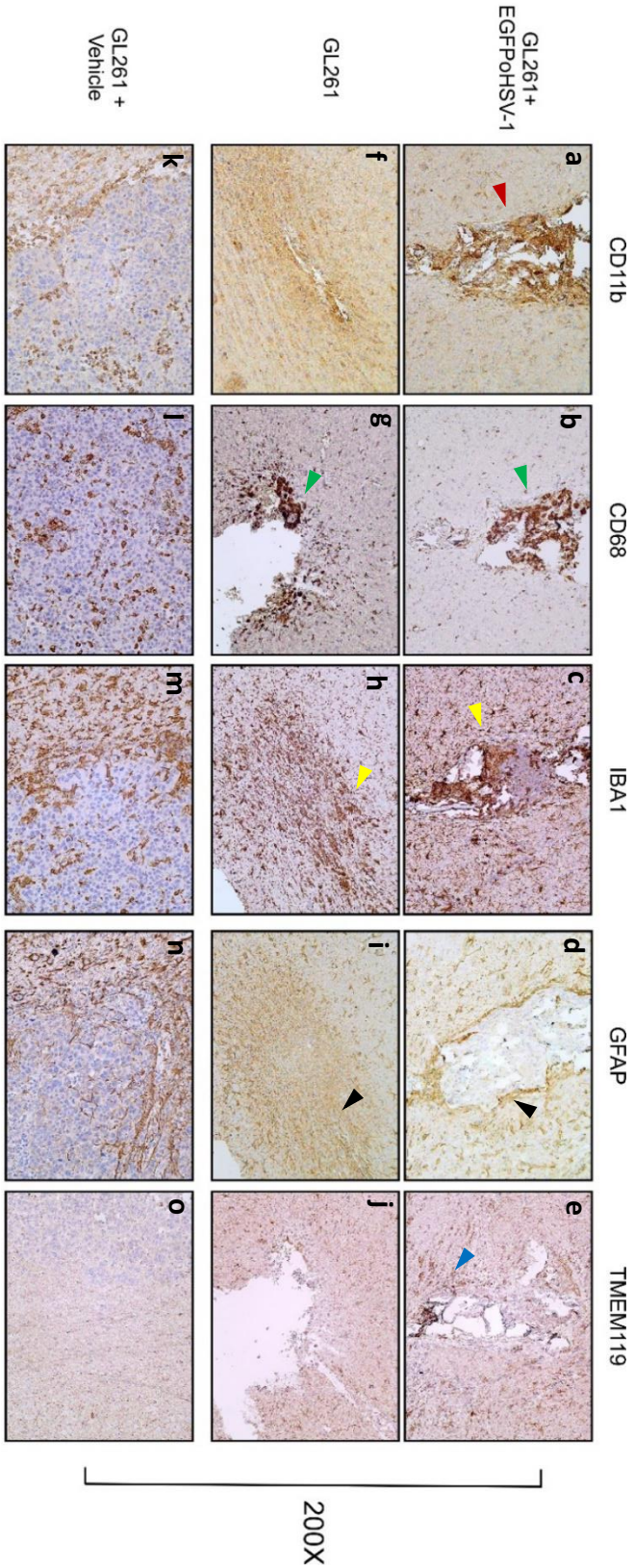

Figure 42 | Immunohistological characterization of GL261 C57BL/6 bearing mice treated with EGF-oHSV-1 or with vehicle. Immunostaining of serial brain sections. Representative histological brain sections harvested from mice firstly injected with GL261, then treated with EGFP-oHSV-1 (panels: a – e) and finally challenged with GL261 (panels: f – j). The lower panels (k – o) represents the histological brain section of mice injected with GL261, treated with PBS 1X (vehicle). All the panels were taken at x200 magnification. Slides of brain tissues isolated from GL261 + EGFP-oHSV-1 or challenged GL261 are indicated in the first- and second-line panels. Sections were stained with HE or by IHC with anti-CD11b, anti-CD68, anti-IBA1, anti-GFAP and anti-TMEM119 antibodies. Red arrowhead in the panel a showing CD11b+ cells concentrated along the tumor bed. CD68 stating revealed abundant presence of

activated macrophages in both hemispheres (green arrowheads). Yellow arrowheads in IBA1 stained panels (c and h), points to amoeboid and branched macrophages. Black arrowheads in panels d and I pointing reactive astrogliosis over both the hemispheres. Some positive TMEM119+ cells were observed (blue arrowhead).

In the right hemisphere, a GFAP+ astrocytic population formed an organized and dense texture around and along the tumor bed (100%) (Figure 42, panel d, black arrowhead) with a distribution similar to that of CD11b+ cells. Conversely, in the left striatum, the astrocytic processes were fully organized to generate a compact and dense cellular matrix lining the fibrous compartment (45-50%). In the surrounding area, GFAP+ staining was gradually reduced towards the healthy brain parenchyma (Figure 42, panel i, black arrowhead). IBA1

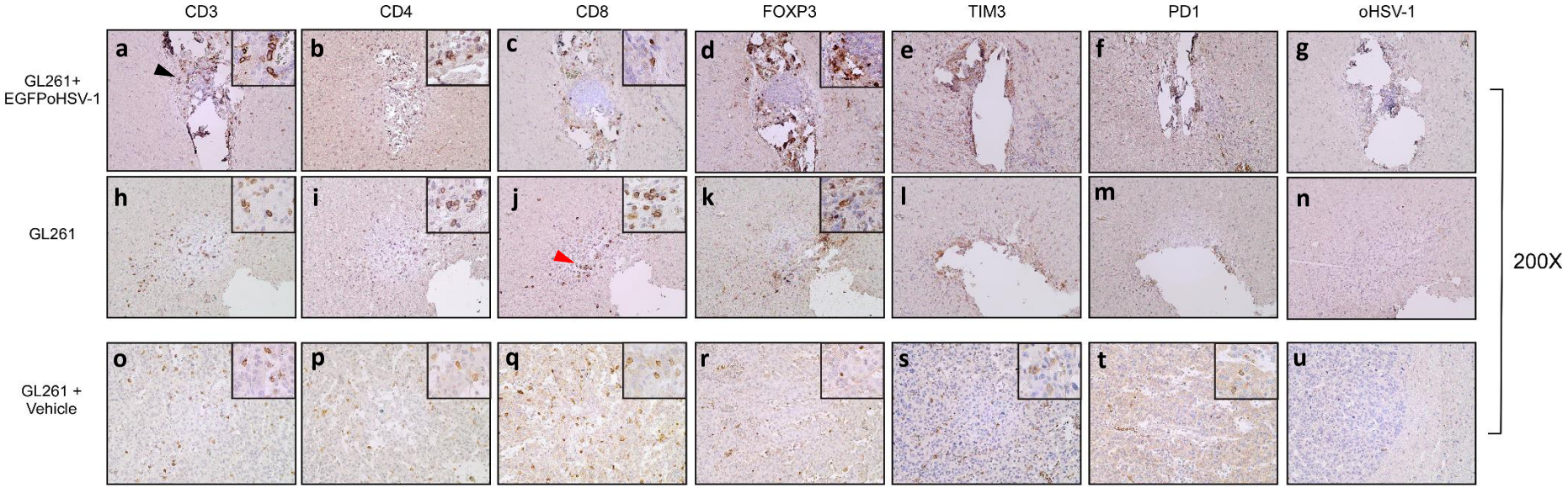
CD3
CD4
CD8
FOXP3
TIM3
PD1
oHSV-1
GL261+ EGFPoHSV-1
GL261
GL261 + Vehicle
a
b
c
d
e
f
g
h
i
j
k
l
m
n
o
p
q
r
s
t
u
200X

Figure 43 | Rejected GL261 parental tumors in mice treated with EGFP-oHSV-1 are strongly infiltrated by anti-tumor T cells. Immunostaining of serial brain sections. Representative histological brain sections harvested from mice (n=5) firstly injected with GL261, then treated with EGFP-oHSV-1 (panels: a – g) and finally challenged with GL261 (panels: h – n). The third series of panels (o – u) represents the histological brain section of mice injected with GL261, treated with PBS 1X (vehicle) (n=5). All the panels were taken at x200 magnification. Sections were stained by IHC with anti-CD3, anti-CD4, anti-CD8, anti-FOXP3, anti-TIM3, anti-PD1, and anti-HSV-1 antibodies. Small square boxes are the areas represented in the corresponding large square boxes of each IHC image. Images were taken at ×200 magnification. Large square boxes were taken at ×400 magnification. Note that selected areas in IHC images of GL261 parental tumors were taken in the rare zones in which positive cells for the selective marker were present. Black and red arrowhead pointing CD3+ and CD8+ lymphocytes, distributed over the tumor bed and in the surrounding parenchyma.

To determine whether EGFP-oHSV1 therapy was able to induce a specific antitumor T-cell response, challenged GL261 and GL261 tumor tissues were immunohistochemical stained with T-cell markers. Immunostaining revealed in both hemispheres, a rich lymphocytic infiltrate, mainly distributed along the fibrotic tissue and partially in the surrounding brain parenchyma (Figure 43, panels a – c, black arrowhead, h – j, red arrowhead). Staining restricted to the immunosuppressive compartment was also performed. A limited T-reg FOXP3+ population was observed in both hemispheres (Figure 43, panels d and k), together with the complete absence of TIM3+ and PD1+ TILs (Figure 43, panels e and l, f and m).

To correlate the tumor remission with presence of virus replication, immunohistochemistry was used to detect viral antigen and demonstrate immune cell infiltration subsequent to tumor viral infection and lysis. However, immunohistology revealed no evidence of HSV-1 antigen staining (Figure 43, panels g and n).

Our results were consistent with data obtained from Egan and collaborators, showing no viral antigen staining at day 15 post HSV-1 infection. Indeed, data revealed no viral particles after day 5 post infection ([263]). *In vivo* kinetic of EGFP-oHSV1 infection will be required to determine the time frame of viral replication, so to exactly define the molecular mechanism underlining the oHSV-1 potency.

To conclude, the results indicate that all the mice challenged with the 30.000 GL261 in the opposite brain hemisphere have completely rejected the tumor. Mice were 100% tumor free in both hemispheres. Immunizing mice with EGFP-oHSV-1 has shown considerably higher survival rates compared to the control group which succumbed to the disease no later than 26 days. This outcome possibly indicates that HSV treatment promotes durable, systemic antitumor responses. Interestingly, data revealed that EGFP-oHSV1 not only infects and lyses tumor cells but also plays a role in activating the immune memory. The presence of improved T cell response following EGFP-oHSV-1 treatment may occur as a result of alternative or improved antigen presentation and processing within GL261-primary tumor. As result, the subsequent immunogenic cell death induced by EGFP-oHSV-1, promotes the neo-antigen recognition by dendritic cell and results in efficient tumor specific cytotoxic T cell response, able to eradicate the challenged GL261 tumor in the opposite brain hemisphere. Indeed, results illustrated a prominent CD8+ cytotoxic response concurrent with a consistent but lower CD4+ T helper cells. In addition, immunostaining revealed an abundant dendritic/macrophage compartment, effectively distributed along the tumor bed surface. It is likely that the tumor microenvironment would be polarized versus a M1 macrophage phenotype and consequent pro-inflammatory/anti-tumor pattern witnessed by the presence of CD8+ T cells, which in turn are stimulated through effective antigen cross-presentation ([264]) (figure 44).

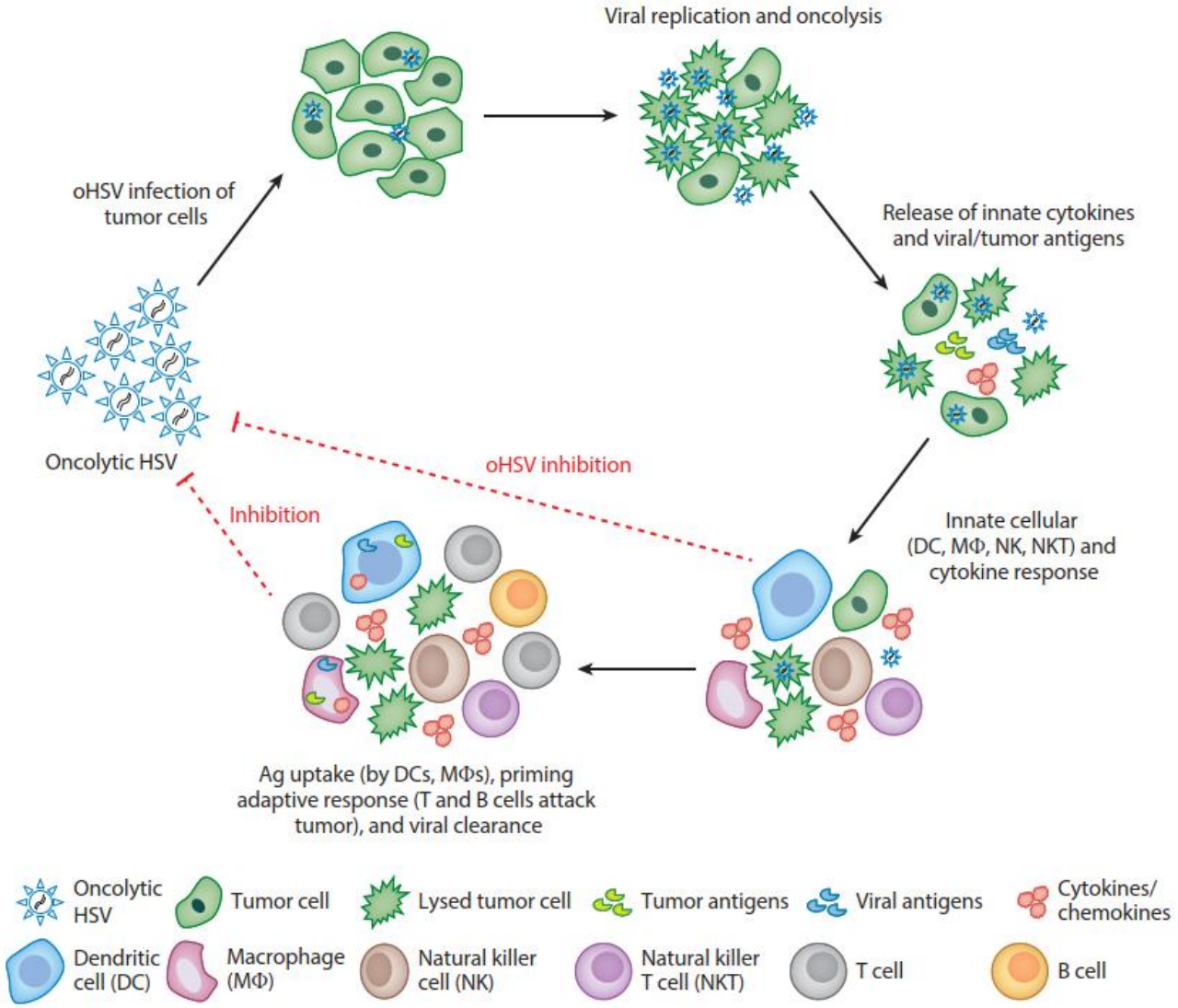

Figure 44 | Dual mechanisms of action for oncolytic herpes simplex viruses (oHSVs) in cancer treatment. oHSV particles are injected into tumor cells, with one virus infecting one tumor cell. The virus replicates in the tumor cell, resulting in the direct killing of the neoplastic cell, release of virions, and infection of other tumor cells. Normal cells may also be infected, but the virus is unable to replicate or kill non-neoplastic cells. The dying tumor cells release soluble tumor antigens (Ags), viral Ags, cytokines, chemokines, and damage-associated molecular pattern factors, which can promote innate immunity and recruit innate immune cells. The tumor Ags and cytokine/chemokine profile can induce an adaptive immune response through cross-presentation of tumor Ag and can promote tumor-specific T cell responses capable of recognizing and eradicating tumor cells expressing these Ags. The cycle is counterbalanced by innate immunoregulatory pathways that dampen T cell responses and by adaptive antiviral immune responses that may clear herpes infection. From [264]

These findings open new avenues for exploring the immunotherapeutic potential of HSV-1 in the context of Glioblastoma treatment and warrant further investigation into the underlying mechanisms driving this observed immune response.

Discussion

CNS has been considered for long time an “immune privileged” organ that must be protected from immune system, particularly from immune cell entry for a variety of reasons including the fact that immune–related inflammatory reactions could generate within the brain oedema and thus intracranial hypertension ([265]). To guarantee this immune privileged situation a peculiar setting of intracranial circulation is put in place and constitutes the basis of the so called blood brain barrier (BBB) ([266]). Nevertheless, the recent discovery of a CNS lymphatic system in the meninges has debunked the long-held dogma of brain as an immune privileged organ ([267]). Intra and extra cranial lymphatic vessels are responsible for draining brain tissue fluid and transporting it into the bloodstream via arachnoid granulations. Pathological stimuli, such as the growth of tumors, induce modifications in BBB. Normally characterized by selective permeability, the BBB undergoes changes that facilitate the infiltration of several types of immune cells. Recently it has been also demonstrated the presence of a local source of functional immune cells resident in the bone marrow of the skull that can be mobilized into the brain ([268]).

This makes it possible to envisage anti-tumor strategies based on stimulation of immunity and consequent recruitment of anti-tumor lymphocytes at the site of intracranial tumors.

Following this concept and taking advantage of our previous findings demonstrating that CIITA-driven MHC class II expressing tumors can serve as potent stimulators of an anti-tumor response ([209,210,212–214,269]], we investigated whether glioblastoma cells can be rendered immunogenic and rescue an anti-tumor response after genetic modification with CIITA. The results presented here clearly demonstrate that in the GL261 mouse glioblastoma model this is indeed the case.

The GL261 glioblastoma model has been widely utilized to assess the behaviour and the sensitivity of glioblastoma to various therapeutic strategies ([270,271]), including immune-based approaches with anti-check point inhibitor antibodies ([272]). However, attempts to modify glioblastoma tumor cells to render them stronger stimulators of a specific anti-tumor response have never been tried before.

CIITA-driven MHC class II gene expression made GL261 cells highly immunogenic as witnessed by the fact that tumors cells were rejected or strongly retarded in their growth when injected orthotopically into the mouse brain. The abundant infiltrating T lymphocyte content was the proof of the strong immunogenic nature of this cell line.

Most importantly, animals vaccinated and protected from tumor growth by administration of GL261-CIITA tumor cells, displayed a protective anamnestic response when challenged with parental GL261 tumor cells in the opposite hemisphere. Indeed, parental tumor cells were completely rejected or extremely retarded in their growth and established minimal tumors as compared to naive animals. Particularly, in these control non-vaccinated mice a restricted T cell population was marginally observed, compared to challenged GL261, where an abundant lymphoid compartment was distributed throughout the neoplastic bed, sign of complete tumor remission. These results confirm that immune cells generated after GL261-CIITA vaccination can move across the brain and reach specific targets outside the original site of recognition. Within this frame, kinetic results revealed that GL261-CIITA tumor cells were rapidly arrested in their growth ad day 7 as a consequence of rapid immune recognition after the activation of the adaptive immune response.

To evaluate the efficacy of our vaccination strategy with GL261-CIITA in eliciting a long-lasting protection, an Overall Survival (OS) study was performed. The Kaplan-Meier survival analysis confirmed a significant prolonged OS in mice intracranially injected with GL261-CIITA with a median OS corresponding to 60 days.

Conversely, mice injected with parental GL261 shown an overall state of neoplastic cachexia, with a median OS of 26 days. Notably, 33% of GL261-CIITA injected mice resulted tumor free after 110 days post injection.

Thus, GL261-CIITA vaccination elicits a strong memory immune response able to protect against tumor growth.

These surviving mice were further intracranially challenged with the parental tumor in the opposite brain hemisphere. Results of this experiment showed that they were all resistant to parental tumor growth with a complete tumor regression in 80% of cases. This protection from tumor challenge was accompanied by the recruitment of a prominent memory CD4+ and CD8+ lymphocytic infiltrate. Altogether, these findings suggest a long term driven protection against the parental tumor, elicited by a long memory adaptive immune response. The improvement in overall survival in the GL261- CIITA and the long term driven protection against GL261 suggests the potential therapeutic benefits of CIITA-based immunotherapy in GBM.

Similarly, in order to better simulate the intricate network of interactions among glioma cells in the TME, GL261 and Gl261-CIITA murine glioblastoma lines were cultured *in vitro* to generate neurospheres (NS). GL261-NS and GL261-NS-CIITA were then implanted into C57BL/6 mice to assess the impact of CIITA on a more complex glioma model that better recapitulate the immunosuppressive feature of human glioblastoma. Histological analysis revealed that GL261-NS brain gliomas were highly infiltrating and more rapidly lethal than GL261-AC. Immunohistochemistry studies demonstrated the presence of tumor microenvironment with a marked immunosuppressive pattern. On the contrary, GL261-NS-CIITA tumor cells were distinctively retarded in their *in vivo* growth. Immunohistology confirmed in 50% of cases a strong T cell response, mainly distributed along the tumor margin together with a prominent myeloid compartment, forming an immunological barrier that prevents the tumor develop. Overall, the approach of GBM neurospheres while showing a better similarity with the characteristics of human GBM growth *in vivo*, basically confirmed the fact that their modification with CIITA was instrumental in render them immunogenic and prone to be rejected or strongly retarded in their growth as a consequence of the stimulation of an adaptive immunity.

Based on the above results, a crucial point of my thesis was to assess whether the adaptive immunity generated in the GL261 GBM model system after modification with CIITA could be extendable to other murine GBM cell lines. To this end a detailed characterization of CT-2A tumor cell line has been conducted. In contrast to the GL261 model, CT-2A cells are much more tumorigenic and with higher propensity to invasiveness and strong immunosuppressive microenvironment. These features make CT-2A a versatile model more similar to human GBM ([243]).

CT-2A transduced with CIITA, showed strong expression of MHC-II cell surface molecules. After enrichment for MHC-II expression and stabilization of this phenotype by selection and/or cloning CT-2A-CIITA cells were injected orthotopically in mouse brains. As for GL261-CIITA, CT-2A-CIITA cells were rejected or strongly reduced in their growth *in vivo* in 60% of injected mice as result of the generation of an adaptive immune response, again characterized by intense infiltration of the tumor area by T cells. In contrast, injection of parental CT-2A cells generated fast growing tumors characterized by a very limited lymphocyte and myeloid presence distributed within the lesion. Of interest, tumors developing in those 40% of animals that escaped the generation of a protective immunity after injection of CT-2A-CIITA cells, showed severe downmodulation of MHC-II expression and signs of a suppressive immune microenvironment as it has been already observed in previous investigations from our group ([210]). Altogether, these results establish the generality of the anti-tumor protection by modification of tumor cells with CIITA also in case of GBM and, as observed in other cases of tumor rejection, the acquisition of a surrogate antigen presenting cell function of CIITA-modified GBM cells *in vivo* ([209,212,214]).

Is this generalized protection from GBM tumor take and growth the consequence of an adaptive immune response against tumor antigens that are shared between distinct GBM cells? If this were the case, then vaccination against one GBM-CIITA tumor cell line should protect, at least in part, from the challenge with another GBM unmodified cell line. Thus, I evaluated whether the vaccination with GL261-CIITA was effective in protecting the mice from challenge with CT-2A parental cells. This was indeed the case as GL261 vaccinated mice rejected CT-2A tumor cells. Rejection was accompanied by a complete phenotype reversal from an immunosuppressive to a more immunogenic tumor microenvironment as witnessed by the analysis of a series

of markers specific for cell types of both brain tissue and lymphoid and myeloid cell lineages.
At variance with the control groups injected with the wild type tumors showing a restricted myeloid repertoire of CD68+ and CD11b+ cells, very few infiltrating T lymphocytes, and a limited participation of microglial cells. CIITA-expressing tumor cells disclosed an abundant lymphoid compartment, distributed inside the tumor surface (when present) and along the peritumoral lining with a concomitant participation of peritumoral vessels, where lymphocytes were directed towards the tumor site by diapedesis. A rich myeloid repertoire was present, forming a physical barrier against tumor growth. In absence of tumor cells, a residual fibrotic distortion was invaded by a rich myeloid and lymphoid cellular infiltrate, as consequence of complete tumor remission.
These results are of particular importance because the establish for the first time the existence of shared immunogenic antigens between two distinct GBM cell lines amenable to an identification by molecular analysis of the corresponding immunopeptidomes (see below, section future studies).
Replication competent oncolytic viruses (OVs) are selectively anticancer and immunotherapeutic agents that are specifically able to infect, replicate, and destroy tumor cells by multiple mechanisms and without damaging normal tissue. Several types of Ovs are presently tested in clinical trials for anti-tumor activity in various types of cancers including GBM. To increase the armamentarium of OVs use in GBM and with the idea to associate in near future OVs treatment with CIITA transduction to synergize the immune stimulation in GBM clinical setting, in collaboration with the University of Padova, I tested an HSV-1 oncolytic virus (oHSV-1) in our GL261 GBM model. An EGFP modified version of oHSV-1 was used first to infect GL261 cells *in vitro* to measure the lytic potential of the virus and then to inject it *in vivo* into the brain of animals previously injected with GL261 tumor cells. Results were more than encouraging since oHSV-1-treated mice showed and overall survival significantly prolonged (146.15% increase in survival rate) with respect to similar mice treated only with PBS. As previous work of several groups has shown, treatment of tumors with OVs *in vivo* can generate not only tumor cell lysis but also an efficient anti-tumor immune response. Thus, I decided to investigate whether oHSV-1-treated mice showing a prolonged overall survival were capable to reject and/or retard tumor growth when challenged with GL261 in the opposite hemisphere. Of extreme interest, all the mice challenged completely rejected the tumor. The immunological correlates of protection were the rapid and sustained infiltration with myeloid and particularly lymphoid cells, the latter with a clear T cell phenotype. Thus, it appears likely that treatment of tumors with oHSV-1 induces cell death liberating in the inflamed tumor milieu relevant immunogenic tumor antigens captured by antigen presenting cells responsible of the following activation and further maturation of tumor-specific CD4+ and particularly CD8+ T cells. It should be stressed again the fact that challenged mice were injected in the opposite brain hemisphere with respect to the primary GL261 tumor injection. This is a clear indication that the adaptive immune response generated by the treatment with oHSV-1 overcomes the limitations of BBB and allows migration of anti-tumor effector cells, at least within the brain.
Overall, these data open new avenues for exploring the immunotherapeutic potential of HSV-1 in the context of Glioblastoma treatment and warrant further investigation into the underlying mechanisms driving this observed immune response.

Future perspectives

Our previous and present results described in this thesis clearly demonstrate the strong immunogenic potential of tumor cells expressing CIITA-driven MHC-II cell surface molecules and establish the surrogate antigen presenting cell function of such modified tumor cells. The corollary of our findings is the existence of tumor-associated peptide antigens which can now be disclosed to tumor specific CD4+ TH cells for scrutiny. As a matter of fact, our CIITA vaccination strategy provided the basis to purify HLA-II bound peptides from hepatocarcinoma of affected patients, select them and use them for the preparation of a therapeutic anti-tumor vaccine, together with HLA-I bound tumor specific peptides (www.hepavac.eua) ([273]).

We will like to follow the same strategy within the contest of GBM. Within this frame, thanks to the collaboration with Dr. Bassani-Sternberg (from Ludwig Cancer Institute in Lausanne), we have generated stable CIITA transfectants of primary human GBM cell lines from three patients with different haplotypes. These human GBM cultured cell lines HROG02, HROG17, and RA, expressing MHC class II molecules (induced by CIITA transduction), underwent an immunopeptidomic analysis to identify their HLA-II-bound peptides. In total, 32,690 unique HLA-II peptides have been identified. To validate the identified peptides as true HLA-II ligands, their association with the various HLA alleles present in the three cell lines was carefully characterized. This allowed for the identification of 279 HLA-II ligands ([173]). Recent more in depth studies of the HLA-II immunopeptidome performed within the contest of my thesis, identified, tumor specific peptides from 7 proteins shared among the three different cell lines: Dedicator of cytokinesis protein 7 (DOCK7), Ephrin type-A receptor2 (EPHA2), Receptor tyrosine-protein kinase erbB-2 (ERBB2), Hepatocyte growth factor receptor (MET), 60S ribosomal proteinL7a (RPL7A), Structural maintenance of chromosomes protein 4 (SMC4) and Tenascin. Interestingly, up to now we did not identify mutated peptides.

On the basis of the above results, we now intend to enlarge the number of human GBM cell lines from fresh tumors. Tumor samples will be obtained from post-surgical specimens of GBM grade IV after patients informed/written consent and approval by Regione Lombardia Ethical Committees. After efficient CIITA transfection, GBM primary cells will be analysed through immunopeptidomics to define the nature and the sequence of HLA-II-bound peptides that are specific for GBM and not shared with other tumors. The aim will be to expand the pool of primary human GBM, in order to identify a broader range of tumor antigens expressed in GBM and presented by HLA-II from different subjects and different HLA-II genotype. We will use specific software such as MixMHC2pred and NetMHCIIpan ([274]) to predict, based on the patient's class II HLA alleles, peptide sequences derived from those previously listed proteins that we have found to be specifically expressed in GBMs, which have binding affinity for those alleles.

Overall, the characterization of the MHC-II immunopeptidome of CIITA-driven MHC class II-expressing tumor cells will permit to set up a multipeptide vaccine preparation that, possibly complemented by additional therapeutical approaches such as oHSV-1 treatment, could be used as therapeutic vaccine against GBM. Studies are now underway to construct oHSV-1 vectors that can accommodate the CIITA full sequence. It is our hope that such an engineered vector could synergize the antitumor action of the oncovirus with a more sustained tumor antigen presentation provided by CIITA-induced MHC-II expression in the tumor.

Another aspect related to my thesis, whose investigation is actually in the preliminary steps, relates to the role of the tumor suppressor ZBTB18 in the immune response against GBM. The transcriptional repressor ZBTB18 not only induces the expression of an array of cancer specific antigens, but is also an important suppressor of mesenchymal GBM and a negative modulator of *de novo* lipogenesis, elements in general considered a hallmark of cancer ([33,38,275]). Moreover, ZBTB18 also reduces the secretion of important cytokines, which affects the behaviour of tumor associated macrophages limiting their pro-tumorigenic phenotype and inducing the expression of pro-inflammatory genes (Ferrarese et al, in revision). Based on the described previous studies as well as more preliminary evidence, our groups planned to investigate the

cooperation between ZBTB18 and CIITA in enhancing an immune response against the tumor. Particularly, I am now exploring the role of ZBTB18 in altering the GBM tumor microenvironment, particularly focusing on infiltrating T cells. Preliminary results by immunofluorescence analysis indicate a discrete increase of CD8 and CD4 T cell infiltration. The second aim is focused on the expression of both ZBTB18 and CIITA in GBM cells to increase the expression and visibility of GBM specific antigens specifically recognized by T helper cells. GL261-CIITA and CT2A-CIITA are being transduced with a viral vector (pV-eGFP) containing ZBTB18. CT2A cell line was more permissive to the viral infection and to expression of both CIITA and ZBTB18. Our immediate future goal is now to assess the *in vivo* behavior of the double transfectant as compared to the single CIITA or ZBTB18 transfectants followed by the study of the quality and quantity of MHC-II immunopeptidome of CT2A-CIITA-ZBTB18 and to compare it to the one of CT2A-CIITA cells. I believe these studies will contribute to a better clarification of the immunological role of ZBTB18 in GBM and possibly to novel strategies of intervention to increase the immune response of GBM patients against the tumor.

References

1. Quail, D. F., and Joyce, J. A. (2017) The microenvironmental landscape of brain tumors. Cancer Cell 31, 326–341.

2. Louis, D. N.; Ohgaki, H.; Wiestler, O. D.; Cavenee, W. K.; Burger, P. C.; Jouvet, A.; Scheithauer, B. W.; Kleihues, P. The 2007 WHO Classification of Tumours of the Central Nervous System. Acta Neuropathol 2007, 114, 97-109.

3. Gil-Salú et al. "[Survival Analysis Following the Addition of Temozolomide to Surgery and Radiotherapy in Patients with Glioblastoma Multiforme]." In: Neurocirugia (Astur) 15.2 (1st Apr. 2004), pp. 144–150.

4. Ozge Petek Erpolat et al. "Outcome of Newly Diagnosed Glioblastoma Patients Treated by Radiotherapy plus Concomitant and Adjuvant Temozolomide: A Long-Term Analysis". In: Tumori 95.2 (1st Mar. 2009), pp. 191–197. ISSN: 0300-8916. DOI: 10.1700/422.5008. pmid: 19579865.

5. Ohgaki H. Epidemiology of brain tumors. In: Verma M, editor. Methods of Molecular Biology, Cancer Epidemiology. vol. 472 ed. Totowa, NJ: Humana Press; 2009. p. 323-242.

6. Fisher JL, Schwartzbaum JA, Wrensch M, Wiemels JL. Epidemiology of brain tumors. Neurol Clin. 2007 Nov;25(4):867,90, vii.

7. Bondy ML, Scheurer ME, Malmer B, Barnholtz-Sloan JS, Davis FG, Il'yasova D, et al. Brain tumor epidemiology: Consensus from the brain tumor epidemiology consortium. Cancer. 2008 Oct 1;113(7 Suppl):1953-68.

8. Alcantara Llaguno SR, Wang Z, Sun D, Chen J, Xu J, Kim E et al. Adult lineage-restricted CNS progenitors specify distinct glioblastoma subtypes. Cancer Cell 2015; 28:429–440.

9. Vescovi, R. Galli, B.A. Reynolds, Brain tumour stem cells, Nat. Rev. Cancer 6 (2006) 225–236. ; J.D. Lathia, S.C. Mack, E.E. Mulkearns-Hubert, C.L. Valentim, J.N. Rich, Cancer stem cells in glioblastoma, Genes Dev. 29 (2015) 1203–1217.

10. Blough, M.R. Westgate, D. Beauchamp, J.J. Kelly, O. Stechishin, A.L. Ramirez, et al., Cairncross, sensitivity to temozolomide in brain tumor initiating cells, Neuro Oncol 12 (2010) 756–760.

11. Kriegstein A, Alvarez-Buylla A. The glial nature of embryonic and adult neural stem cells. Annu Rev Neurosci (2009) 32:149–84. doi: 10.1146/ annurev.neuro.051508.135600.

12. Sanai N, Tramontin AD, Quinones-Hinojosa A, Barbaro NM, Gupta N, Kunwar S, et al. Unique astrocyte ribbon in adult human brain contains neural stem cells but lacks chain migration. Nature (2004) 427(6976):740–4.doi: 10.1038/nature02301.

13. Boldrini M, Fulmore CA, Tartt AN, Simeon LR, Pavlova I, Poposka V, et al. Human Hippocampal Neurogenesis Persists throughout Aging. Cell Stem Cell (2018) 22(4):589–99.e5. doi: 10.1016/j.stem.2018.03.015.

14. Hopewell, E.A. Wright, The importance of implantation site in cerebral carcinogenesis in rats, Cancer Res. 29 (1969) 1927–1932.

15. Nishide, Y. Nakatani, H. Kiyonari, T. Kondo, Gliomagenesis from transformed neural stem cells depleted of prominin1-expressing cells, PLoS One 4 (2009) e6869.

16. Hide, T. Takezaki, Y. Nakatani, H. Nakamura, J. Kuratsu, T. Kondo, Combination of a ptgs2 inhibitor and an epidermal growth factor receptor-signaling inhibitor prevents tumorigenesis of oligodendrocyte lineage-derived glioma-initiating cells, Stem Cells 29 (2011) 590–599.

17. Hide, T. Takezaki, Y. Nakatani, H. Nakamura, J. Kuratsu, T. Kondo, Sox11 prevents tumorigenesis of glioma-initiating cells by inducing neuronal differentiation, Cancer Res. 69 (2009) 7953–7959.

18. Kondo, M. Raff, Oligodendrocyte precursor cells reprogrammed to become multipotential CNS stem cells, Science 289 (2000) 1754–1757.

19. Kondo, M. Raff, Chromatin remodeling and histone modification in the conversion of oligodendrocyte precursors to neural stem cells, Genes Dev. 18 (2004) 2963–2972.

20. Bachoo, E.A. Maher, K.L. Ligon, N.E. Sharpless, S.S. Chan, M.J. You, et al., Epidermal growth factor receptor and Ink4a/Arf: convergent mechanisms governing terminal differentiation and transformation along the neural stem cell to astrocyte axis, Cancer Cell 1 (2002) 269–277.

21. Liu, J.C. Sage, M.R. Miller, R.G. Verhaak, S. Hippenmeyer, H. Vogel, et al., Mosaic analysis with double markers reveals tumor cell of origin in glioma, Cell 146 (2011) 209–221.

22. Kondo T. Glioblastoma-initiating cell heterogeneity generated by the cell-of-origin, genetic/epigenetic mutation and microenvironment. Semin Cancer Biol. 2022 Jul;82:176-183. doi: 10.1016/j.semcancer.2020.12.003. Epub 2021 Jan 13. PMID: 33453403.

23. Snuderl M, Fazlollahi L, Le LP, Nitta M, Zhelyazkova BH, Davidson CJ, et al. Article mosaic amplification of multiple receptor tyrosine kinase genes in glioblastoma. Cancer Cell 2011;20:810–7.

24. Patel AP, Tirosh I, Trombetta JJ, Shalek AK, Gillespie SM, Wakimoto H, et al. Single-cell RNA-seq highlights intratumoral heterogeneity in primary glioblastoma. Science 2014;344:1396–401.

25. Suzuki H, Aoki K, Chiba K, Sato Y, Shiozawa Y, Shiraishi Y, et al. Mutational landscape and clonal architecture in grade II and III gliomas. Nat Genet 2015;47:458–68.

26. Brennan CW, Verhaak RG, McKenna A, Campos B, Noushmehr H, Salama SR, Zheng S, Chakravarty D, Sanborn JZ, Berman SH, Beroukhim R, Bernard B, Wu CJ, Genovese G, Shmulevich I, Barnholtz-Sloan J, Zou L, Vegesna R, Shukla SA, Ciriello G, Yung WK, Zhang W, Sougnez C, Mikkelsen T, Aldape K, Bigner DD, Van Meir EG, Prados M, Sloan A, Black KL, Eschbacher J, Finocchiaro G, Friedman W, Andrews DW, Guha A, Iacocca M, O'Neill BP, Foltz G, Myers J, Weisenberger DJ, Penny R, Kucherlapati R, Perou CM, Hayes DN, Gibbs R, Marra M, Mills GB, Lander E, Spellman P, Wilson R, Sander C, Weinstein J, Meyerson M, Gabriel S, Laird PW, Haussler D, Getz G, Chin L; TCGA Research Network. The somatic genomic landscape of glioblastoma. Cell. 2013 Oct 10;155(2):462-77. doi: 10.1016/j.cell.2013.09.034. Erratum in: Cell. 2014 Apr 24;157(3):753. PMID: 24120142; PMCID: PMC3910500.

27. Verhaak RG, Hoadley KA, Purdom E, Wang V, Qi Y, Wilkerson MD, Miller CR, Ding L, Golub T, Mesirov JP, Alexe G, Lawrence M, O'Kelly M, Tamayo P, Weir BA, Gabriel S, Winckler W, Gupta S, Jakkula L, Feiler HS, Hodgson JG, James CD, Sarkaria JN, Brennan C, Kahn A, Spellman PT, Wilson RK, Speed TP, Gray JW, Meyerson M, Getz G, Perou CM, Hayes DN; Cancer Genome Atlas Research Network. Integrated genomic analysis identifies clinically relevant subtypes of glioblastoma characterized by abnormalities in PDGFRA, IDH1, EGFR, and NF1. Cancer Cell. 2010 Jan 19;17(1):98-110. doi: 10.1016/j.ccr.2009.12.020. PMID: 20129251; PMCID: PMC2818769.

28. Ceccarelli M, Barthel FP, Malta TM, Sabedot TS, Salama SR, Murray BA, Morozova O, Newton Y, Radenbaugh A, Pagnotta SM, Anjum S, Wang J, Manyam G, Zoppoli P, Ling S, Rao AA, Grifford M, Cherniack AD, Zhang H, Poisson L, Carlotti CG Jr, Tirapelli DP, Rao A, Mikkelsen T, Lau CC, Yung WK, Rabadan R, Huse J,

Brat DJ, Lehman NL, Barnholtz-Sloan JS, Zheng S, Hess K, Rao G, Meyerson M, Beroukhim R, Cooper L, Akbani R, Wrensch M, Haussler D, Aldape KD, Laird PW, Gutmann DH; TCGA Research Network; Noushmehr H, Iavarone A, Verhaak RG. Molecular Profiling Reveals Biologically Discrete Subsets and Pathways of Progression in Diffuse Glioma. Cell. 2016 Jan 28;164(3):550-63. doi: 10.1016/j.cell.2015.12.028. PMID: 26824661; PMCID: PMC4754110.

29. Cancer Genome Atlas Research Network. Comprehensive genomic characterization defines human glioblastoma genes and core pathways. Nature. 2008 Oct 23;455(7216):1061-8. doi: 10.1038/nature07385. Epub 2008 Sep 4. Erratum in: Nature. 2013 Feb 28;494(7438):506. PMID: 18772890; PMCID: PMC2671642.

30. Wang, L., Hu, L., Zhou, X. et al. Exosomes secreted by human adipose mesenchymal stem cells promote scarless cutaneous repair by regulating extracellular matrix remodelling. Sci Rep 7, 13321 (2017). https://doi.org/10.1038/s41598-017-12919-x.

31. Sottoriva A, Spiteri I, Piccirillo SG, Touloumis A, Collins VP, Marioni JC, Curtis C, Watts C, Tavaré S. Intratumor heterogeneity in human glioblastoma reflects cancer evolutionary dynamics. Proc Natl Acad Sci U S A. 2013 Mar 5;110(10):4009-14. doi: 10.1073/pnas.1219747110. Epub 2013 Feb 14. PMID: 23412337; PMCID: PMC3593922.

32. Neftel C, Laffy J, Filbin MG, Hara T, Shore ME, Rahme GJ, Richman AR, Silverbush D, Shaw ML, Hebert CM, Dewitt J, Gritsch S, Perez EM, Gonzalez Castro LN, Lan X, Druck N, Rodman C, Dionne D, Kaplan A, Bertalan MS, Small J, Pelton K, Becker S, Bonal D, Nguyen QD, Servis RL, Fung JM, Mylvaganam R, Mayr L, Gojo J, Haberler C, Geyeregger R, Czech T, Slavc I, Nahed BV, Curry WT, Carter BS, Wakimoto H, Brastianos PK, Batchelor TT, Stemmer-Rachamimov A, Martinez-Lage M, Frosch MP, Stamenkovic I, Riggi N, Rheinbay E, Monje M, Rozenblatt-Rosen O, Cahill DP, Patel AP, Hunter T, Verma IM, Ligon KL, Louis DN, Regev A, Bernstein BE, Tirosh I, Suvà ML. An Integrative Model of Cellular States, Plasticity, and Genetics for Glioblastoma. Cell. 2019 Aug 8;178(4):835-849.e21. doi: 10.1016/j.cell.2019.06.024. Epub 2019 Jul 18. PMID: 31327527; PMCID: PMC6703186.

33. Fedele V, Dai F, Masilamani AP, Heiland DH, Kling E, Gätjens-Sanchez AM, Ferrarese R, Platania L, Soroush D, Kim H, Nelander S, Weyerbrock A, Prinz M, Califano A, Iavarone A, Bredel M, Carro MS. Epigenetic Regulation of ZBTB18 Promotes Glioblastoma Progression. Mol Cancer Res. 2017 Aug;15(8):998-1011. doi: 10.1158/1541-7786.MCR-16-0494. Epub 2017 May 16. PMID: 28512252; PMCID: PMC5967621.

34. Bhat KPL, Balasubramaniyan V, Vaillant B, Ezhilarasan R, Hummelink K, Hollingsworth F, Wani K, Heathcock L, James JD, Goodman LD, Conroy S, Long L, Lelic N, Wang S, Gumin J, Raj D, Kodama Y, Raghunathan A, Olar A, Joshi K, Pelloski CE, Heimberger A, Kim SH, Cahill DP, Rao G, Den Dunnen WFA, Boddeke HWGM, Phillips HS, Nakano I, Lang FF, Colman H, Sulman EP, Aldape K. Mesenchymal differentiation mediated by NF-κB promotes radiation resistance in glioblastoma. Cancer Cell. 2013 Sep 9;24(3):331-46. doi: 10.1016/j.ccr.2013.08.001. Epub 2013 Aug 29. PMID: 23993863; PMCID: PMC3817560.

35. Halliday J, Helmy K, Pattwell SS, Pitter KL, LaPlant Q, Ozawa T, Holland EC. In vivo radiation response of proneural glioma characterized by protective p53 transcriptional program and proneural-mesenchymal shift. Proc Natl Acad Sci U S A. 2014 Apr 8;111(14):5248-53. doi: 10.1073/pnas.1321014111. Epub 2014 Mar 24. PMID: 24706837; PMCID: PMC3986190.

36. Phillips HS, Kharbanda S, Chen R, Forrest WF, Soriano RH, Wu TD, Misra A, Nigro JM, Colman H, Soroceanu L, Williams PM, Modrusan Z, Feuerstein BG, Aldape K. Molecular subclasses of high-grade glioma predict prognosis, delineate a pattern of disease progression, and resemble stages in neurogenesis. Cancer Cell. 2006 Mar;9(3):157-73. doi: 10.1016/j.ccr.2006.02.019. PMID: 16530701.

37. Bhat KP, Salazar KL, Balasubramaniyan V, Wani K, Heathcock L, Hollingsworth F, James JD, Gumin J, Diefes KL, Kim SH, Turski A, Azodi Y, Yang Y, Doucette T, Colman H, Sulman EP, Lang FF, Rao G, Copray S,

Vaillant BD, Aldape KD. The transcriptional coactivator TAZ regulates mesenchymal differentiation in malignant glioma. Genes Dev. 2011 Dec 15;25(24):2594-609. doi: 10.1101/gad.176800.111. PMID: 22190458; PMCID: PMC3248681.

38. Carro MS, Lim WK, Alvarez MJ, Bollo RJ, Zhao X, Snyder EY, Sulman EP, Anne SL, Doetsch F, Colman H, Lasorella A, Aldape K, Califano A, Iavarone A. The transcriptional network for mesenchymal transformation of brain tumours. Nature. 2010 Jan 21;463(7279):318-25. doi: 10.1038/nature08712. Epub 2009 Dec 23. PMID: 20032975; PMCID: PMC4011561.

39. Kelly KF, Daniel JM. POZ for effect-POZ-ZF transcription factors in cancer and development. Trends Cell Biol 2006;16:578–87.

40. Hill AD, Chang BS, Hill RS, et al. A 2-Mb critical region implicated in the microcephaly associated with terminal 1q deletion syndrome. Am J Med Genet 2007;143A:1692–8.

41. Tatard VM, Xiang C, Biegel JA, Dahmane N. ZNF238 is expressed in postmitotic brain cells and inhibits brain tumor growth. Cancer Res. 2010 Feb 1;70(3):1236-46. doi: 10.1158/0008-5472.CAN-09-2249. Epub 2010 Jan 26. PMID: 20103640.

42. Xiang C, Baubet V, Pal S, Holderbaum L, Tatard V, Jiang P, Davuluri RV, Dahmane N. RP58/ZNF238 directly modulates proneurogenic gene levels and is required for neuronal differentiation and brain expansion. Cell Death Differ. 2012 Apr;19(4):692-702. doi: 10.1038/cdd.2011.144. Epub 2011 Nov 18. PMID: 22095278; PMCID: PMC3307985.

43. Ohtaka-Maruyama C, Hirai S, Miwa A, Heng JI, Shitara H, Ishii R, Taya C, Kawano H, Kasai M, Nakajima K, Okado H. RP58 regulates the multipolar-bipolar transition of newborn neurons in the developing cerebral cortex. Cell Rep. 2013 Feb 21;3(2):458-71. doi: 10.1016/j.celrep.2013.01.012. Epub 2013 Feb 7. PMID: 23395638.

44. Okado H, Ohtaka-Maruyama C, Sugitani Y, Fukuda Y, Ishida R, Hirai S, Miwa A, Takahashi A, Aoki K, Mochida K, Suzuki O, Honda T, Nakajima K, Ogawa M, Terashima T, Matsuda J, Kawano H, Kasai M. The transcriptional repressor RP58 is crucial for cell-division patterning and neuronal survival in the developing cortex. Dev Biol. 2009 Jul 15;331(2):140-51. doi: 10.1016/j.ydbio.2009.04.030. Epub 2009 May 3. PMID: 19409883.

45. Cohen JS, Srivastava S, Farwell Hagman KD, Shinde DN, Huether R, Darcy D, Wallerstein R, Houge G, Berland S, Monaghan KG, Poretti A, Wilson AL, Chung WK, Fatemi A. Further evidence that de novo missense and truncating variants in ZBTB18 cause intellectual disability with variable features. Clin Genet. 2017 May;91(5):697-707. doi: 10.1111/cge.12861. Epub 2016 Oct 10. PMID: 27598823.

46. de Munnik SA, García-Miñaúr S, Hoischen A, van Bon BW, Boycott KM, Schoots J, Hoefsloot LH, Knoers NV, Bongers EM, Brunner HG. A de novo non-sense mutation in ZBTB18 in a patient with features of the 1q43q44 microdeletion syndrome. Eur J Hum Genet. 2014 Jun;22(6):844-6. doi: 10.1038/ejhg.2013.249. Epub 2013 Nov 6. PMID: 24193349; PMCID: PMC4023223.

47. Depienne C, Nava C, Keren B, Heide S, Rastetter A, Passemard S, Chantot-Bastaraud S, Moutard ML, Agrawal PB, VanNoy G, Stoler JM, Amor DJ, Billette de Villemeur T, Doummar D, Alby C, Cormier-Daire V, Garel C, Marzin P, Scheidecker S, de Saint-Martin A, Hirsch E, Korff C, Bottani A, Faivre L, Verloes A, Orzechowski C, Burglen L, Leheup B, Roume J, Andrieux J, Sheth F, Datar C, Parker MJ, Pasquier L, Odent S, Naudion S, Delrue MA, Le Caignec C, Vincent M, Isidor B, Renaldo F, Stewart F, Toutain A, Koehler U, Häckl B, von Stülpnagel C, Kluger G, Møller RS, Pal D, Jonson T, Soller M, Verbeek NE, van Haelst MM, de Kovel C, Koeleman B, Monroe G, van Haaften G; DDD Study; Attié-Bitach T, Boutaud L, Héron D, Mignot C. Genetic and phenotypic dissection of 1q43q44 microdeletion syndrome and neurodevelopmental phenotypes

associated with mutations in ZBTB18 and HNRNPU. Hum Genet. 2017 Apr;136(4):463-479. doi: 10.1007/s00439-017-1772-0. Epub 2017 Mar 10. PMID: 28283832; PMCID: PMC5360844.

48. van der Schoot V, de Munnik S, Venselaar H, Elting M, Mancini GMS, Ravenswaaij-Arts CMA, Anderlid BM, Brunner HG, Stevens SJC. Toward clinical and molecular understanding of pathogenic variants in the ZBTB18 gene. Mol Genet Genomic Med. 2018 May;6(3):393-400. doi: 10.1002/mgg3.387. Epub 2018 Mar 24. PMID: 29573576; PMCID: PMC6014478.

49. Xie B, Khoyratty TE, Abu-Shah E, F Cespedes P, MacLean AJ, Pirgova G, Hu Z, Ahmed AA, Dustin ML, Udalova IA, Arnon TI. The Zinc Finger Protein Zbtb18 Represses Expression of Class I Phosphatidylinositol 3-Kinase Subunits and Inhibits Plasma Cell Differentiation. J Immunol. 2021 Apr 1;206(7):1515-1527. doi: 10.4049/jimmunol.2000367. Epub 2021 Feb 19. PMID: 33608456; PMCID: PMC7980533.

50. Wang R, Bhatt AB, Minden-Birkenmaier BA, Travis OK, Tiwari S, Jia H, Rosikiewicz W, Martinot O, Childs E, Loesch R, Tossou G, Jamieson S, Finkelstein D, Xu B, Labelle M. ZBTB18 restricts chromatin accessibility and prevents transcriptional adaptations that drive metastasis. Sci Adv. 2023 Jan 6;9(1):eabq3951. doi: 10.1126/sciadv.abq3951. Epub 2023 Jan 6. PMID: 36608120; PMCID: PMC9821869.

51. Anastassiou D, et al. Human cancer cells express Slug-based epithelial-mesenchymal transition gene expression signature obtained in vivo. BMC Cancer. 2011; 11:529. [PubMed: 22208948.

52. Cheng WY, et al. A multi-cancer mesenchymal transition gene expression signature is associated with prolonged time to recurrence in glioblastoma. PLoS One. 2012; 7(4):e34705. [PubMed: 22493711].

53. Bazzocco S, Dopeso H, Martínez-Barriocanal Á, Anguita E, Nieto R, Li J, García-Vidal E, Maggio V, Rodrigues P, de Marcondes PG, Schwartz S Jr, Aaltonen LA, Sánchez A, Mariadason JM, Arango D. Identification of ZBTB18 as a novel colorectal tumor suppressor gene through genome-wide promoter hypermethylation analysis. Clin Epigenetics. 2021 Apr 23;13(1):88. doi: 10.1186/s13148-021-01070-0. PMID: 33892786; PMCID: PMC8063439.

54. Malta TM, de Souza CF, Sabedot TS, et al. Glioma CpG island methylator phenotype (G-CIMP): biological and clinical implications. Neuro-oncology. 2017;20(5):608-620.

55. Cancer Genome Atlas Research, N., Brat, D.J., Verhaak, R.G., Aldape, K.D., Yung, W.K., Salama, S.R., Cooper, L.A., Rheinbay, E., Miller, C.R., Vitucci, M., et al. (2015). Comprehensive, Integrative Genomic Analysis of Diffuse Lower-Grade Gliomas. N Engl J Med 372, 2481-2498.

56. Eckel-Passow, J.E., Lachance, D.H., Molinaro, A.M., Walsh, K.M., Decker, P.A., Sicotte, H., Pekmezci, M., Rice, T., Kosel, M.L., Smirnov, I.V., et al. (2015). Glioma Groups Based on 1p/19q, IDH, and TERT Promoter Mutations in Tumors. N Engl J Med 372, 2499-2508.

57. Schumacher T, Bunse L, Pusch S, Sahm F, Wiestler B, Quandt J, Menn O, Osswald M,Oezen I, Ott M, Keil M, BalßJ, Rauschenbach K, Grabowska AK, Vogler I, Diekmann J,Trautwein N, Eichmüller SB, Okun J, StevanovićS, Riemer AB, Sahin U, Friese MA,Beckhove P, von Deimling A, Wick W, Platten M. A vaccine targeting mutant IDH1induces antitumour immunity. Nature 2014;512:324–327. DOI: 10.1038/nature13387.

58. Gullick. “Prevalence of Aberrant Expression of the Epidermal Growth Factor Receptor in Human Cancers.” In: Br. Med. Bull. 47.1 (1st Jan.1991), pp. 87–98.

59. Appin CL, Brat DJ. Molecular pathways in gliomagenesis and their relevance to neuropathologic diagnosis. Adv Anat Pathol. Jan 2015;22(1):50-58.

60. Brennan CW, Verhaak RG, McKenna A, et al. The somatic genomic landscape of glioblastoma. Cell. Oct 10 2013;155(2):462-477.

61. Labussière M, Boisselier B, Mokhtari K, Di Stefano AL, Rahimian A, Rossetto M,Ciccarino P, Saulnier O, Paterra R, Marie Y, Finocchiaro G, Sanson M. Combined analysis of TERT, EGFR, and IDH status defines distinct prognostic glioblastoma classes. Neurology 2014;83:1200–1206. DOI: 10.1212/WNL.

62. Jiao Y, Killela PJ, Reitman ZJ, Rasheed AB, Heaphy CM, de Wilde RF, Rodriguez FJ,Rosemberg S, Oba-Shinjo SM, Nagahashi Marie SK, Bettegowda C, Agrawal N, Lipp E, Pirozzi C, Lopez G, He Y, Friedman H, Friedman AH, Riggins GJ, Holdhoff M, Burger P, Mc Lendon R, Bigner DD, Vogelstein B, Meeker AK, Kinzler KW, Papadopoulos N, Diaz LA, Yan H. Frequent ATRX, CIC, FUBP1 and IDH1 mutations refine the classification of malignant gliomas. Oncotarget 2012;3:709–722. DOI: 10.18632/oncotarget.588.

63. Reuss DE, Sahm F, Schrimpf D, Wiestler B, Capper D, Koelsche C, Schweizer L, Korshunov A, Jones DT, Hovestadt V, Mittelbronn M, Schittenhelm J, Herold-Mende C, Unterberg A, Platten M, Weller M, Wick W, Pfister SM, von Deimling A. ATRX and IDH1-R132H immunohistochemistry with subsequent copy number analysis and IDH sequencing as a basis for an “integrated” diagnostic approach for adult astrocytoma, oligodendroglioma and glioblastoma. Acta Neuropathol. 2015;129:133–146. DOI:10.1007/s00401-014-1370-3.

64. Tabatabai G, Stupp R, van den Bent MJ, Hegi ME, Tonn JC, Wick W, Weller M. Molecular diagnostics of gliomas: the clinical perspective. Acta Neuropathol. 2010;120:585–592. DOI: 10.1007/s00401-010-0750-6.

65. Hegi ME, Janzer RC, Lambiv WL, Gorlia T, Kouwenhoven MC, Hartmann C, vonDeimling A, Martinet D, Besuchet Schmutz N, Diserens AC, Hamou MF, Bady P, Weller M, van den Bent MJ, Mason WP, Mirimanoff RO, Stupp R, Mokhtari K, Wesseling P, European Organisation for Research and Treatment of Cancer Brain Tumour and Radiation Oncology Groups; National Cancer Institute of Canada Clinical Trials Group. Presence of an oligodendroglioma-like component in newly diagnosed glioblastoma identifies a pathogenetically heterogeneous subgroup and lacks prognostic value: central pathology review of the EORTC_26981/NCIC_CE.3 trial. Acta Neuropathol:2012;123:841–852. DOI: 10.1007/s00401-011-0938-4.

66. Rong L, Li N, Zhang Z. Emerging therapies for glioblastoma: current state and future directions. J Exp Clin Cancer Res. 2022 Apr 15;41(1):142. doi: 10.1186/s13046-022-02349-7. PMID: 35428347; PMCID: PMC9013078.

67. Wen PY, Kesari S. Malignant gliomas in adults. N Engl J Med. 2008 Jul 31;359(5):492-507.

68. Manuale dei casi clinici AIMS. AIMS (2020).

69. Roger Stupp et al. “Radiotherapy plus Concomitant and Adjuvant Temozolomide for Glioblastoma.” In: N. Engl. J. Med. 352.10 (10th Mar. 2005),pp. 987–996. DOI: 10.1056/NEJMoa043330.

70. Gunjur A, Lau E, Taouk Y, Ryan G. Early post-treatment pseudo-progression amongst glioblastoma multiforme patients treated with radiotherapy and temozolomide: a retrospective analysis. J Med Imaging Radiat Oncol. Dec 2011;55(6):603-610.

71. Newlands et al. “Temozolomide: A Review of Its Discovery, Chemical Properties, Pre-Clinical Development and Clinical Trials.” In: Cancer Treat. Rev. 23.1 (1st Jan. 1997), pp. 35–61.

72. Henry S. Friedman, Tracy Kerby and Hilary Calvert. “Temozolomide and Treatment of Malignant Glioma”. In: Clin Cancer Res 6.7 (1st July 2000), pp. 2585–2597. ISSN: 1078-0432, 1557-3265. pmid: 10914698.

73. Newlands et al. “Phase I Trial of Temozolomide (CCRG 81045: M&B 39831: NSC 362856).” In: Br J Cancer 65.2 (Feb. 1992), pp. 287–291.ISSN: 0007-0920. pmid: 1739631.

74. Valtonen, S.; Timonen, U.; Toivanen, P.; Kalimo, H.; Kivipelto, L.; Heiskanen, O.; Unsgaard, G.; Kuurne, T. Interstitial chemotherapy with carmustine-loaded polymers for high-grade gliomas: a randomized double-blind study. Neurosurgery 1997, 41, 44-8; discussion 48-9.

75. Westphal, M.; Hilt, D. C.; Bortey, E.; Delavault, P.; Olivares, R.; Warnke, P. C.; Whittle, I. R.; Jaaskelainen, J.; Ram, Z. A phase 3 trial of local chemotherapy with biodegradable carmustine (BCNU) wafers (Gliadel wafers) in patients with primary malignant glioma. Neuro Oncol 2003, 5, 79-88.

76. van den Bent MJ, Brandes AA, Taphoorn MJ, et al. Adjuvant procarbazine, lomustine, and vincristine chemotherapy in newly diagnosed anaplastic oligodendroglioma: long-term follow-up of EORTC brain tumor group study 26951. Journal of clinical oncology : official journal of the American Society of Clinical Oncology. Jan 20 2013;31(3):344-350.

77. Branter J, Basu S, Smith S. Tumour treating fields in a combinational therapeutic approach. Oncotarget. (2018) 9:36631–44. doi: 10.18632/oncotarget.26344.

78. Van Meir EG, Hadjipanayis CG, Norden AD, Shu HK, Wen PY, Olson JJ. Exciting new advances in neuro-oncology: The avenue to a cure for malignant glioma. CA Cancer J Clin. 2010 May-Jun;60(3):166-93.

79. Wang, J., Cazzato, E., Ladewig, E., Frattini, V., Rosenbloom, D.I., Zairis, S., Abate, F., Liu, Z., Elliott, O., Shin, Y.J., et al. (2016). Clonal evolution of glioblastoma under therapy. Nat Genet 48, 768-776.

80. Touat M, Idbaih A, Sanson M, Ligon KL. Glioblastoma targeted therapy: updated approaches from recent biological insights. Annals of Oncology: Official Journal of the European Society for Medical Oncology. 2017;28(7):1457–1472. [PubMed: 28863449].

81. Adams GP, Weiner LM. Monoclonal antibody therapy of cancer. Nat Biotechnol. 2005 Sep;23(9):1147-57.

82. Loew S, Schmidt U, Unterberg A, Halatsch ME. The epidermal growth factor receptor as a therapeutic target in glioblastoma multiforme and other malignant neoplasms. Anticancer Agents Med Chem. 2009 Jul;9(6):703-15.

83. Sathornsumetee S, Rich JN. Designer therapies for glioblastoma multiforme. Ann N Y Acad Sci. 2008 Oct;1142:108-32.

84. Martens, N.O. Schmidt, C. Eckerich, et al., A novel one-armed anti-c-Met antibody inhibits glioblastoma growth in vivo, Clin. Cancer Res. 12 (20 Pt 1) (2006) 6144–6152, https://doi.org/10.1158/1078-0432.CCR-05-1418.

85. Jahangiri, M. De Lay, L.M. Miller, et al., Gene expression profile identifies tyrosine kinase c-Met as a targetable mediator of antiangiogenic therapy resistance, Clin. Cancer Res. 19 (7) (2013) 1773–1783, https://doi.org/10.1158/1078-0432.CCR-12-1281.

86. Offenhäuser C, Al-Ejeh F, Puttick S, Ensbey KS, Bruce ZC, Jamieson PR, et al. EphA3 pay-loaded antibody therapeutics for the treatment of glioblastoma.Cancers. (2018) 10:E519. doi: 10.3390/cancers10120519.

87. Koul D, Fu J, Shen R, LaFortune TA, Wang S, Tiao N, et al. Antitumor activity of NVP-BKM120-a selective pan class I PI3 kinase inhibitor showed differential forms of cell death based on p53 status of glioma cells. Clin Cancer Res. (2012) 18:184–95. doi: 10.1158/1078-0432.CCR-11- 1558.

88. Wen PY, Touat M, Alexander BM, Mellinghoff IK, Ramkissoon S, McCluskey CS, et al. Buparlisib in patients with recurrent glioblastoma harboring phosphatidylinositol 3-kinase pathway activation: an open-label, multicenter, multi-arm, phase II trial. J Clin Oncol. (2019) 37:741–50. doi: 10.1200/JCO.18.01207.

89. Narita Y. Bevacizumab for glioblastoma. Ther Clin Risk Manag. 2015 Dec 1;11:1759-65. doi: 10.2147/TCRM.S58289. PMID: 26664126; PMCID: PMC4671800.

90. Brandes AA, Finocchiaro G, Zagonel V, Reni M, Caserta C, Fabi A, Clavarezza M, Maiello E, Eoli M, Lombardi G, Monteforte M, Proietti E, Agati R, Eusebi V, Franceschi E. AVAREG: a phase II, randomized, noncomparative study of fotemustine or bevacizumab for patients with recurrent glioblastoma. Neuro-Oncology. 2016;18(9):1304–1312. [PubMed: 26951379].

91. Diaz RJ, Ali S, Qadir MG, De La Fuente MI, Ivan ME, Komotar RJ. The role of bevacizumab in the treatment of glioblastoma. Journal of Neuro-Oncology. 2017;133(3):455–467. [PubMed: 28527008].

92. Chan LS, Daruwalla J, Christophi C. Selective targeting of the tumour vasculature. ANZ J Surg. 2008 Nov;78(11):955-67.

93. Chi AS, Sorensen AG, Jain RK, Batchelor TT. Angiogenesis as a therapeutic target in malignant gliomas. Oncologist. 2009 Jun;14(6):621-36.

94. Hanna C, Kurian KM, Williams K, Watts C, Jackson A, Carruthers R, Strathdee K, Cruickshank G, Dunn L, Erridge S, Godfrey L, Jefferies S, McBain C, Sleigh R, McCormick A, Pittman M, Halford S, Chalmers AJ. Pharmacokinetics, safety and tolerability of olaparib and temozolomide for recurrent glioblastoma: results of the phase I OPARATIC trial. Neuro-Oncology. 2020.

95. TIH, Jose J. PARP inhibitor cyanine dye conjugate with enhanced cytotoxic and antiproliferative activity in patient derived glioblastoma cell lines. Bioorganic & Medicinal Chemistry Letters. 2020;30(14):127252. [PubMed: 32527552].

96. Wu S, Gao F, Zheng S, Zhang C, Martinez-Ledesma E, Ezhilarasan R, Ding J, Li X, Feng N, Multani A, Sulman EP, Verhaak RG, de Groot JF, Heffernan TP, Yung WKA, Koul D. EGFR Amplification Induces Increased DNA Damage Response and Renders Selective Sensitivity to Talazoparib (PARP Inhibitor) in Glioblastoma. Clinical Cancer Research: An Official Journal of the American Association for Cancer Research. 2020;26(6):1395–1407. [PubMed: 31852834].

97. Shafiee F, Aucoin MG, Jahanian-Najafabadi A. Targeted Diphtheria Toxin-Based Therapy: A Review Article. Front Microbiol. 2019 Oct 18;10:2340. doi: 10.3389/fmicb.2019.02340. PMID: 31681205; PMCID: PMC6813239.

98. Sapra P, Allen TM. Ligand-targeted liposomal anticancer drugs. Prog Lipid Res. 2003 Sep;42(5):439-62.

99. Chirasani SR, Markovic DS, Synowitz M, Eichler SA, Wisniewski P, Kaminska B, et al. Transferrin-receptor-mediated iron accumulation controls proliferation and glutamate release in glioma cells. J Mol Med. 2009 Feb;87(2):153-67.

100. Husain SR, Puri RK. Interleukin-13 receptor-directed cytotoxin for malignant glioma therapy: From bench to bedside. J Neurooncol. 2003 Oct;65(1):37-48.

101. Chen C, Zhu S, Zhang X, Zhou T, Gu J, Xu Y, Wan Q, Qi X, Chai Y, Liu X, Chen L, Yan J, Hua Y, Lin F. Targeting the synthetic vulnerability of PTEN-deficient glioblastoma cells with MCL1 inhibitors. Molecular Cancer Therapeutics. 2020.

102. Mecca C, Giambanco I, Donato R, Arcuri C. Targeting mTOR in Glioblastoma: Rationale and Preclinical/Clinical Evidence. Disease Markers. 2018;2018:9230479. [PubMed: 30662577].

103. Heimberger, J.H. Sampson, Immunotherapy coming of age: what will it taketo make it standard of care for glioblastoma? Neuro Oncol. 13 (1) (2011) 3–13,https://doi.org/10.1093/neuonc/noq169.

104. Aspelund A, Antila S, Proulx ST, Karlsen TV, Karaman S, Detmar M, et al. A dural lymphatic vascular system that drains brain interstitial fluid and macromolecules. J Exp Med (2015) 212:991–9. doi: 10.1084/jem.20142290.

105. Louveau A, Harris TH, Kipnis J. Revisiting the mechanisms of CNS immune privilege. Trends Immunol (2015) 36:569–77. doi: 10.1016/j.it.2015.08.006.

106. Lim M, Xia Y, Bettegowda C, Weller M. Current state of immunotherapy for glioblastoma. Nat Rev Clin Oncol (2018) 15(7):422–42. doi: 10.1038/s41571-018-0003-5.

107. Sampson JH, Gunn MD, Fecci PE, Ashley DM. Brain immunology and immunotherapy in brain tumours. Nat Rev Cancer (2020) 20(1):12–25. doi: 10.1038/s41568-019-0224-7.

108. Korman AJ, Garrett-Thomson SC, Lonberg N. The foundations of immune checkpoint blockade and the ipilimumab approval decennial. Nat Rev Drug Discovery (2022) 21(7):509–28. doi: 10.1038/s41573-021-00345-8.

109. Cloughesy TF, Mochizuki AY, Orpilla JR, Hugo W, Lee AH, Davidson TB, et al.Neoadjuvant anti-PD-1 immunotherapy promotes a survival benefit with intratumoral and systemic immune responses in recurrent glioblastoma. Nat Med (2019) 25(3):477–86. doi: 10.1038/s41591-018-0337-7.

110. Reardon DA, Brandes AA, Omuro A, Mulholland P, Lim M, Wick A, Baehring J, Ahluwalia MS, Roth P, Bahr O, Phuphanich S, Sepulveda JM, De Souza P, Sahebjam S, Carleton M, Tatsuoka K, Taitt C, Zwirtes R, Sampson J, Weller M. Effect of Nivolumab vs Bevacizumab in Patients With Recurrent Glioblastoma: The CheckMate 143 Phase 3 Randomized Clinical Trial. JAMA Oncol.2020;6(7):1003–1010. [PubMed: 32437507].

111. Duerinck J, Schwarze JK, Awada G, Tijtgat J, Vaeyens F, Bertels C, et al.Intracerebral administration of CTLA-4 and PD-1 immune checkpoint blocking monoclonal antibodies in patients with recurrent glioblastoma: a phase I clinical trial. J Immunother Cancer (2021) 9(6):e002296. doi: 10.1136/jitc-2020-002296.

112. Brown NF, Ng SM, Brooks C, Coutts T, Holmes J, Roberts C, et al. A phase II open label, randomised study of ipilimumab with temozolomide versus temozolomide alone after surgery and chemoradiotherapy in patients with recently diagnosed glioblastoma: the Ipi-Glio trial protocol. BMC Cancer (2020) 20(1):198. doi: 10.1186/ s12885-020-6624-y.

113. Vom Berg J, Vrohlings M, Haller S, Haimovici A, Kulig P, Sledzinska A, et al. Intratumoral IL-12 combined with CTLA-4 blockade elicits T cell-mediated glioma rejection. J Exp Med. 2013;210:2803–11.

114. Sharma P, Allison JP. Dissecting the mechanisms of immune checkpoint therapy. Nat Rev Immunol. 2020;20:75–6.

115. Jena, B., Dotti, G. & Cooper, L. J. N. Redirecting T- cell specificity by introducing a tumor- specific chimeric antigen receptor. Blood 116, 1035–1044 (2010).

116. Guedan S, Ruella M, June CH. Emerging cellular therapies for Cancer. Annu Rev Immunol. 2019;37:145–71.

117. O'Rourke DM, Nasrallah MP, Desai A, Melenhorst JJ, Mansfield K, Morris-sette JJD, et al. A single dose of peripherally infused EGFRvIII-directed CAR T cells mediates antigen loss and induces adaptive resistance in patients with recurrent glioblastoma. Sci Transl Med. 2017;9:eaaa0984.

118. Ahmed N, Brawley V, Hegde M, Bielamowicz K, Kalra M, Landi D, Robertson C, Gray TL, Diouf O, Wakefield A, Ghazi A, Gerken C, Yi Z, Ashoori A, Wu MF, Liu H, Rooney C, Dotti G, Gee A, Su J, Kew Y, Baskin D, Zhang YJ, New P, Grilley B, Stojakovic M, Hicks J, Powell SZ, Brenner MK, Heslop HE, Grossman R, Wels WS, Gottschalk S. HER2-Specific Chimeric Antigen Receptor-Modified Virus-Specific T Cells for Progressive Glioblastoma: A Phase 1 Dose-Escalation Trial. JAMA Oncol. 2017;3(8):1094–1101. [PubMed: 28426845].

119. Bielamowicz K, Fousek K, Byrd TT, Samaha H, Mukherjee M, Aware N, Wu MF, Orange JS, Sumazin P, Man TK, Joseph SK, Hegde M, Ahmed N. Trivalent CAR T cells overcome interpatient antigenic variability in glioblastoma. Neuro Oncol. 2018;20(4):506–518. [PubMed: 29016929].

120. Tang X, Zhao S, Zhang Y, Wang Y, Zhang Z, Yang M, Zhu Y, Zhang G, Guo G, Tong A, Zhou L. B7-H3 as a Novel CAR-T Therapeutic Target for Glioblastoma. Mol Ther Oncolytics. 2019;14:279–287. [PubMed: 31485480].

121. Jin L, Tao H, Karachi A, Long Y, Hou AY, Na M, Dyson KA, Grippin AJ, Deleyrolle LP, Zhang W, Rajon DA, Wang QJ, Yang JC, Kresak JL, Sayour EJ, Rahman M, Bova FJ, Lin Z, Mitchell DA, Huang J. CXCR1- or CXCR2-modified CAR T cells co-opt IL-8 for maximal antitumor efficacy in solid tumors. Nat Commun. 2019;10(1):4016. [PubMed: 31488817].

122. Choi BD, Yu X, Castano AP, Bouffard AA, Schmidts A, Larson RC, et al. CAR-T cells secreting BiTEs circumvent antigen escape without detectable toxicity. Nat Biotechnol. 2019;37:1049–58.

123. Reardon DA, Desjardins A, Vredenburgh JJ, O'Rourke DM, Tran DD, Fink KL, Nabors LB, Li G, Bota DA, Lukas RV, Ashby LS, Duic JP, Mrugala MM, Cruickshank S, Vitale L, He Y, Green JA, Yellin MJ, Turner CD, Keler T, Davis TA, Sampson JH, Re ACTti. Rindopepimut with Bevacizumab for Patients with Relapsed EGFRvIIIExpressing Glioblastoma (ReACT): Results of a Double-Blind Randomized Phase II Trial. Clin Cancer Res. 2020;26(7):1586–1594. [PubMed: 32034072].

124. Phuphanich S, Wheeler CJ, Rudnick JD, Mazer M, Wang H, Nuno MA, et al. Phase I trial of a multi-epitope-pulsed dendritic cell vaccine for patients with newly diagnosed glioblastoma. Cancer Immunol Immunother. 2013;62:125–35.

125. Miranda W.Yu, Daniela F.Quail Immunotherapy for Glioblastoma: Current Progress and Challenges, Front. Immunol., 13 May 2021 | https://doi.org/10.3389/fimmu.2021.676301.

126. Learn et al. Genetic Analysis of Intracranial Tumors in a Murine Model of Glioma Demonstrate a Shift in Gene Expression in Response to Host Immunity. J neuroimmunol. 2007 Jan; 182(1-2): 63-72 doi: 10.1016/j.jneuroim.2006.09.016.

127. Santos PM, Butterfield LH. Dendritic Cell-Based Cancer Vaccines. J Immunol. 2018;200(2):443–449. [PubMed: 29311386].

128. Liau LM, Ashkan K, Tran DD, Campian JL, Trusheim JE, Cobbs CS, Heth JA, Salacz M, Taylor S, D'Andre SD, Iwamoto FM, Dropcho EJ, Moshel YA, Walter KA, Pillainayagam CP, Aiken R, Chaudhary R, Goldlust SA, Bota DA, Duic P, Grewal J, Elinzano H, Toms SA, Lillehei KO, Mikkelsen T, Walbert T, Abram SR, Brenner AJ, Brem S, Ewend MG, Khagi S, Portnow J, Kim LJ, Loudon WG, Thompson RC, Avigan DE, Fink KL, Geoffroy FJ, Lindhorst S, Lutzky J, Sloan AE, Schackert G, Krex D, Meisel HJ, Wu J, Davis RP, Duma C, Etame AB, Mathieu D, Kesari S, Piccioni D, Westphal M, Baskin DS, New PZ, Lacroix M, May SA, Pluard TJ, Tse V, Green RM, Villano JL, Pearlman M, Petrecca K, Schulder M, Taylor LP, Maida AE, Prins RM, Cloughesy TF, Mulholland P,

Bosch ML. First results on survival from a large Phase 3 clinical trial of an autologous dendritic cell vaccine in newly diagnosed glioblastoma. J Transl Med. 2018;16(1):142. [PubMed: 29843811].

129. Agarwalla, P., Barnard, Z., Fecci, P., Dranoff, G., & Curry, W. T. (2012). Sequential Immunotherapy by Vaccination with GM-CSF Expressing Glioma Cells and CTLA-4 Blockade Effectively Treats Established Murine Intracranial Tumors. Journal of Immunotherapy (Hagerstown, Md. : 1997), 35(5), 385–389. http://doi.org/10.1097/CJI.0b013e3182562d59.

130. Ommeren, Randy, Staudt, Michael, Xu, Hu, Hebb, Matthew, 2016. Advances in HSP27 and HSP90-targeting strategies for glioblastoma, 10.1007/s11060-016-2070-8 - Journal of Neuro-Oncology.

131. Reale, A., Vitiello, A., Conciatori, V., Parolin, C., Calistri, A., and Palù, G. (2019). Perspectives on immunotherapy via oncolytic viruses. Infect Agent Cancer 14. doi: 10.1186/s13027-018-0218-1.

132. Schietinger A, Philip M, and Liu RB, et al (2010) Bystander killing of cancer requires the cooperation of CD4+ and CD8+ T cells during the effector phase J Exp Med 207(11) 2469–2477 https://doi.org/10.1084/jem.20092450 PMID: 20921286 PMCID: 2964573.

133. Peters C, Grandi P, and Nigim F (2019) Updates on oncolytic virus immunotherapy for cancers Mol Ther Oncolytics 12 259–262 https://doi.org/10.1016/j.omto.2019.01.008 PMID: 33072862 PMCID: 7536361.

134. Hiraoka K, et al. Retroviral replicating vector-mediated gene therapy achieves long-term control of tumor recurrence and leads to durable anticancer immunity. Neuro-oncology. 2017;19(7):918–929.

135. Halfmann, C.T.; Sears, R.M.; Katiyar, A.; Busselman, B.W.; Aman, L.K.; Zhang, Q.; O'Bryan, C.S.; Angelini, T.E.; Lele, T.P.;Roux, K.J. Repair of nuclear ruptures requires barrier-to-autointegration factor. J. Cell Biol. 2019, 218, 2136–2149.

136. Nemunaitis J, et al. A phase I trial of intravenous infusion of ONYX-015 and enbrel in solid tumor patients. Cancer Gene Ther. 2007;14(11):885–893.

137. Wojton J, Kaur B. Impact of tumor microenvironment on oncolytic viral therapy. Cytokine Growth Factor Rev. 2010;21(2-3):127–134.

138. Yaacov B, et al. Extracellular matrix constituents interfere with Newcastle disease virus spread in solid tissue and diminish its potential oncolytic activity. J Gen Virol. 2012;93(pt 8):1664–1672.

139. Martinez-Quintanilla J, He D, Wakimoto H, Ale-many R, Shah K. Encapsulated stem cells loaded with hyaluronidase-expressing oncolytic virus for brain tumor therapy. Mol Ther. 2015;23(1):108–118.

140. Russell, S.J.; Peng, K.W.; Bell, J.C. Oncolytic virotherapy. Nat. Biotechnol. 2012, 30, 658–670.

141. Harrow S, Papanastassiou V, Harland J, Mabbs R, Petty R, Fraser M, et al. HSV1716 injection into the brain adjacent to tumour following surgical resection of high-grade glioma: Safety data and long-term survival. Gene Ther (2004) 11:1648–58. doi: 10.1038/sj.gt.3302289.

142. Markert JM, Liechty PG, Wang W, Gaston S, Braz E, Karrasch M, et al.Phase Ib trial of mutant herpes simplex virus G207 inoculated pre-and post-tumor resection for recurrent GBM. Mol Ther (2009) 17:199–207. doi: 10.1038/mt.2008.228.

143. Markert JM, Razdan SN, Kuo HC, Cantor A, Knoll A, Karrasch M, et al. A phase 1 trial of oncolytic HSV-1, G207, given in combination with radiation for recurrent GBM demonstrates safety and radiographic responses. Mol Ther (2014) 22:1048–55. doi: 10.1038/mt.2014.22.

144. Taguchi S, Fukuhara H, Homma Y, Todo T. Current status of clinical trials assessing oncolytic virus therapy for urological cancers. Int J Urol (2017) 24:342–51. doi: 10.1111/iju.13325.

145. Nakashima, H.; Nguyen, T.; Kasai, K.; Passaro, C.; Ito, H.; Goins, W.F.; Shaikh, I.; Erdelyi, R.; Nishihara, R.; Nakano, I.; et al.Toxicity and Efficacy of a Novel Gadd34-Expressing Oncolytic Hsv-1 for the Treatment of Experimental Glioblastoma. Clin.Cancer Res. 2018, 24, 2574–2584.

146. Daiichi-Sankyo. Daiichi sankyo submits application for oncolytic virus teserpaturev (g47d) for treatment of patients with malignant glioma in japan. (2021).

147. Kambara, H.; Okano, H.; Chiocca, E.A.; Saeki, Y. An Oncolytic HSV-1 Mutant Expressing ICP34.5 under Control of a Nestin Promoter Increases Survival of Animals Even When Symptomatic from a Brain Tumor. Cancer Res. 2005, 65, 2832–2839.

148. Cheema TA, Wakimoto H, Fecci PE, et al. Multifaceted oncolytic virus therapy for glioblastoma in an immunocompetent cancer stem cell model. Proc Natl Acad Sci U S A. 2013;110 (29):12006–12011.

149. Zhang W, Fulci G, Wakimoto H, et al. Combination of oncolytic herpes simplex viruses armed with angiostatin and IL-12 enhances antitumor efficacy in human glioblastoma models. Neoplasia. 2013;15(6):591–599.

150. Barnard Z, Wakimoto H, Zaupa C, et al. Expression of FMS-like tyrosine kinase 3 ligand by oncolytic herpes simplex virus type I prolongs survival in mice bearing established syngeneic intracranial malignant glioma. Neurosurgery. 2012; 71(3):741–748.

151. Tamura K, Wakimoto H, Agarwal AS, et al. Multimechanistic tumor targeted oncolytic virus overcomes resistance in brain tumors. Mol Ther. 2013;21(1):68–77.

152. Jahan N, Lee JM, Shah K, Wakimoto H. Therapeutic targeting of chemoresistant and recurrent glioblastoma stem cells with a proapoptotic variant of oncolytic herpes simplex virus. Int J Cancer. 2017;141(8):1671–1681.

153. Saha D, Martuza RL, Rabkin SD. Macrophage polarization contributes to glioblastoma eradication by combination immunovirotherapy and immune checkpoint blockade. Cancer Cell. 2017;32(2):253–267.e5.

154. Gambini E, Reisoli E, Appolloni I, Gatta V, Campadelli-Fiume G, Menotti L and Malatesta P: Replication-competent herpes simplex virus retargeted to HER2 as therapy for high-grade glioma. Mol Ther 20: 994-1001, 2012.

155. Reale A, Krutzke L, Cadamuro M, Vitiello A, von Einem J, Kochanek S, Palù G, Parolin C, Calistri A. Human Monocytes Are Suitable Carriers for the Delivery of Oncolytic Herpes Simplex Virus Type 1 In Vitro and in a Chicken Embryo Chorioallantoic Membrane Model of Cancer. Int J Mol Sci. 2023 May 25;24(11):9255. doi: 10.3390/ijms24119255. PMID: 37298206; PMCID: PMC10253092.

156. Bikfalvi A, da Costa CA, Avril T, Barnier JV, Bauchet L, Brisson L, et al. Challenges in glioblastoma research: focus on the tumor microenvironment. Trends Cancer (2023) 9(1):9–27. doi: 10.1016/j.trecan.2022.09.005.

157. Gieryng A, Pszczolkowska D, Walentynowicz KA, Rajan WD, Kaminska B. Immune microenvironment of gliomas. Lab Invest (2017) 97(5):498–518. doi: 10.1038/labinvest.2017.19.

158. De Vleeschouwer S, Bergers G. Glioblastoma: to target the tumor cell or the microenvironment? In: De Vleeschouwer S, editor. Glioblastoma. Brisbane (AU (2017).doi: 10.15586/codon.glioblastoma.2017.ch16.

159. Pratibha Sharma, Ashley Aaroe, Jiyong Liang, Vinay K Puduvalli, Tumor microenvironment in glioblastoma: Current and emerging concepts, Neuro-Oncology Advances, Volume 5, Issue 1, January-December 2023, vdad009, https://doi.org/10.1093/noajnl/vdad009.

160. Woroniecka KI, Rhodin KE, Chongsathidkiet P, Keith KA, Fecci PE. T-cell dysfunction in glioblastoma: applying a new framework. Clin Cancer Res (2018) 24 (16):3792–802. doi: 10.1158/1078-0432.CCR-18-0047.

161. Maddison K, Graves MC, Bowden NA, Fay M, Vilain RE, Faulkner S, et al. Low tumour-infiltrating lymphocyte density in primary and recurrent glioblastoma. Oncotarget (2021) 12(21):2177–87. doi: 10.18632/oncotarget.28069.

162. Zhang C, Cheng W, Ren X, Wang Z, Liu X, Li G, et al. Tumor purity as an underlying key factor in glioma. Clin Cancer Res (2017) 23(20):6279–91. doi: 10.1158/1078-0432.CCR-16-2598.

163. Weathers, S.P.; de Groot, J. VEGF Manipulation in Glioblastoma. Oncology 2015, 29, 720–727 ; Zhang, I.; Alizadeh, D.; Liang, J.; Zhang, L.; Gao, H.; Song, Y.; Ren, H.; Ouyang, M.; Wu, X.; D'Apuzzo, M.; et al. Characterization of Arginase Expression in Glioma-Associated Microglia and Macrophages. PLoS ONE 2016,11, e0165118.

164. Da Fonseca, A.C.; Amaral, R.; Garcia, C.; Geraldo, L.H.; Matias, D.; Lima, F.R. Microglia in Cancer: For Good or for Bad? Adv. Exp. Med. Biol. 2016, 949, 245–261.

165. Kalluri, R. & Zeisberg, M. Fibroblasts in cancer. Nature Rev. Cancer 6, 392–401 (2006).

166. Haile, L.A.; Greten, T.F.; Korangy, F. Immune suppression: The hallmark of myeloid derived suppressor cells.Immunol. Investig. 2012, 41, 581–594.

167. Li, H.; Han, Y.; Guo, Q.; Zhang, M.; Cao, X. Cancer-expanded myeloid-derived suppressor cells induce anergy of NK cells through membrane-bound TGF-beta 1. J. Immunol. 2009, 182, 240–249.

168. Waldron, T.J.; Quatromoni, J.G.; Karakasheva, T.A.; Singhal, S.; Rustgi, A.K. Myeloid derived suppressor cells: Targets for therapy. Oncoimmunology 2013, 2, e24117.

169. Srivastava, M.K.; Sinha, P.; Clements, V.K.; Rodriguez, P.; Ostrand-Rosenberg, S. Myeloid-derived suppressor cells inhibit T-cell activation by depleting cystine and cysteine. Cancer Res. 2010, 70, 68–77.

170. Dubinski, D.; Wolfer, J.; Hasselblatt, M.; Schneider-Hohendorf, T.; Bogdahn, U.; Stummer, W.; Wiendl, H.; Grauer, O.M. CD4+ T effector memory cell dysfunction is associated with the accumulation of granulocytic myeloid-derived suppressor cells in glioblastoma patients. Neuro-Oncology 2016, 18, 807–818.

171. Zagzag, D.; Salnikow, K.; Chiriboga, L.; Yee, H.; Lan, L.; Ali, M.A.; Garcia, R.; Demaria, S.; Newcomb, E.W. Downregulation of Major Histocompatibility Complex Antigens in Invading Glioma Cells: Stealth Invasion of the Brain. Lab. Investig. 2005, 85,328–341.

172. Brown, N.F.; Carter, T.J.; Ottaviani, D.; Mulholland, P. Harnessing the Immune System in Glioblastoma. Br. J. Cancer 2018, 119,1171–1181.

173. Forlani, G.; Michaux, J.; Pak, H.; Huber, F.; Marie Joseph, E.L.; Ramia, E.; Stevenson, B.J.; Linnebacher, M.; Accolla, R.S.; Bassani-Sternberg, M. CIITA-Transduced Glioblastoma Cells Uncover a Rich Repertoire of Clinically Relevant Tumor-Associated HLA-II Antigens. Mol. Cell. Proteom. 2021, 20, 100032.

174. Anderson, A. C., Joller, N. & Kuchroo, V. K. Lag-3, Tim-3, and TIGIT: co-inhibitory receptors with specialized functions in immune regulation. Immunity 44, 989–1004 (2016).

175. Singer, M. et al. A distinct gene module for dysfunction uncoupled from activation in tumor-infiltrating T cells. Cell 166, 1500–1511.e9 (2016).

176. Nduom EK, Weller M, Heimberger AB. Immunosuppressive mechanisms in glioblastoma. Neuro Oncol (2015) 17 Suppl 7(Suppl 7):vii9–vii14. doi: 10.1093/neuonc/nov151.

177. Da Ros M, De Gregorio V, Iorio AL, Giunti L, Guidi M, de Martino M, et al. Glioblastoma chemoresistance: the double play by microenvironment and blood-brain barrier. Int J Mol Sci (2018) 19(10):2879. doi: 10.3390/ijms19102879.

178. Scapini, P. et al. CXCL1/macrophage inflammatory protein-2-induced angiogenesis in vivo is mediated by neutrophil-derived vascular endothelial growth factor-A1. J. Immunol. 172, 5034–5040 (2004).

179. Benelli, R. et al. Neutrophils as a key cellular target for angiostatin: implications for regulation of angiogenesis and inflammation. FASEB J. 16, 267–269 (2002).

180. Frisch J, Angenendt A, Hoth M, Prates Roma L, Lis A. STIM-Orai channels and reactive oxygen species in the tumor microenvironment. Cancers (Basel). 2019;11(4):457.

181. Masternak K, Muhlethaler-Mottet A, Villard J, Zufferey M, Steimle V, Reith W. CIITA is a transcriptional coactivator that is recruited to MHC class II promoters by multiple synergistic interactions with an enhanceosome complex. Genes Dev 2000;14(9):1156e66.

182. Fontes JD, Kanazawa S, Nekrep N, Peterlin BM. The class II transactivator CIITA is a transcriptional integrator. Microbes Infect 1999;1(11):863e9.

183. Accolla, R.S. Human B cell variants immunoselected against a single Ia antigen subset have lost expression of several Ia antigen subsets. J. Exp. Med. 1983, 157, 1053–1058.

184. Steimle, V.; Otten, L.A.; Zufferey, M.; Mach, B. Complementation cloning of an MHC class II transactivator mutated in hereditary MHC class II deficiency (or bare lymphocyte syndrome). Cell 1993, 75, 135–146.

185. Steimle, V., Siegrist, C.A., Mottet, A., Lisowska-Grospierre, B., and Mach, B. (1994). Regulation of MHC class II expression by interferon-gamma mediated by the transactivator gene CIITA. Science 265, 106-109.

186. Forlani G, Shallak M, Gatta A, Shaik AKB, Accolla RS. The NLR member CIITA: Master controller of adaptive and intrinsic immunity and unexpected tool in cancer immunotherapy. Biomed J. 2023 Oct;46(5):100631. doi: 10.1016/j.bj.2023.100631. Epub 2023 Jul 17. PMID: 37467968; PMCID: PMC10505679.

187. Chou WC, Jha S, Linhoff MW, Ting JP. The NLR gene family: from discovery to present day. Nat Rev Immunol 2023;23(7):472.

188. Almeida-da-Silva CLC, Savio LEB, Coutinho-Silva R, Ojcius DM. The role of NOD-like receptors in innate immunity. Front Immunol 2023;14:1122586.

189. Harton JA, Ting JP. Class II transactivator: mastering the art of major histocompatibility complex expression. Mol Cell Biol 2000;20(17):6185e94.

190. Cressman DE, O'Connor WJ, Greer SF, Zhu XS, Ting JP.Mechanisms of nuclear import and export that control thesubcellular localization of class II transactivator. J Immunol2001;167(7):3626e34.

191. Reith W, Mach B. The bare lymphocyte syndrome and the regulation of MHC expression. Annu Rev Immunol 2001;19:331e73.

192. Muhlethaler-Mottet A, Otten LA, Steimle V, Mach B.Expression of MHC class II molecules in different cellular and functional compartments is controlled by differential usage of multiple promoters of the transactivator CIITA. EMBO J1997;16(10):2851e60.

193. Griscelli C, Lisowska-Grospierre B, Mach B. Combined immunodeficiency with defective expression in MHC class II genes. Immunodefic Rev 1989;1(2):135e53.

194. Zhao, M., Flynt, F.L., Hong, M., Chen, H., Gilbert, C.A., Briley, N.T., Bolick, S.C., Wright, K.L., and Piskurich, J.F. (2007). MHC class II transactivator (CIITA) expression is upregulated in multiple myeloma cells by IFN-gamma. Mol Immunol 44, 2923-2932.

195. Mellins ED, Stern LJ. HLA-DM and HLA-DO, key regulators of MHC-II processing and presentation. Curr Opin Immunol (2014) 26:115–22. doi:10.1016/j.coi.2013.11.005.

196. Singer DS, Devaiah BN. CIITA and its dual roles in MHC gene transcription. Front Immunol 2013;4:476.

197. Wright, K. L., Ting, J. P., 2006b. Epigenetic regulation of MHCII and CIITA genes. Trends Immunol. 2, 405-12.

198. Boss JM, Jensen PE. Transcriptional regulation of the MHC class II antigen presentation pathway. Curr Opin Immunol 2003;15(1):105e11.

199. Kanazawa S, Okamoto T, Peterlin BM. Tat competes with CIITA for the binding to P-TEFb and blocks the expression of MHC class II genes in HIV infection. Immunity 2000;12(1):61e70.

200. Bhat, K.P.; Turner, J.D.; Myers, S.E.; Cape, A.D.; Ting, J.P.; Greer, S.F. The 19S proteasome ATPase Sug1 plays a critical role in regulating MHC class II transcription. Mol. Immunol. 2008, 45, 2214–2224.

201. Reith, W.; LeibundGut-Landmann, S.; Waldburger, J.M. Regulation of MHC class II gene expression by the class II transactivator. Nat. Rev. Immunol. 2005, 5, 793–806.

202. Germain RN, Margulies DH. The biochemistry and cellular biology of antigen processing and presentation. Annu Rev Immunol 1993; 11:403-50; PMID:8476568.; http://dx.doi.org/10.1146/annurev.iy.11.040193.02155.

203. Bonifaz LC, Bonnyay DP, Charalambous A, Darguste DI, Fujii S,Soares H, Brimnes MK, Moltedo B, Moran TM, Steinman RM. In vivo targeting of antigens to maturing dendritic cells via the DEC-205 receptor improves T cell vaccination. J Exp Med 2004; 199:815-24; PMID:15024047; http://dx.doi.org/10.1084/jem.20032220.

204. Steinman RM. Dendritic cells: versatile controllers of the immune system. Nature Med 2007; 13:1155-9; PMID:17917664; http://dx.doi.org/10.038/nm643.

205. Pardoll DM, Topalian SL. The role of CD4C T cell responses in anti-tumor immunity. Curr Opin Immunol 1998; 10:588-94;PMID:9794842; http://dx.doi.org/10.1016/S0952-7915(98)80228-8.

206. Hung K, Hayashi R, Lafond-Walker A, Lowenstein C, Pardoll DM,Levitsky H. The central role of CD4C T cells in the antitumor immune response. J Exp Med 1998; 188:2357-68; PMID:9858522; http://dx.doi.org/10.1084/jem.188.12.2357.

207. Boon T, Cerottini JC, Van den Eynde B, Van der Bruggen P, Van PelA. Tumor antigens recognized by T lymphocytes. Annu Rev Immunol 1994; 12:337-65; PMID:8011285; http://dx.doi.org/10.1146/annurev.iy.12.040194.02005.

208. Dunn JP, Old LJ, Schreiber RD. The three Es of cancer immunoediting. Annu Rev Immunol 2004; 22:329-60; PMID:15032581; http://dx.doi.org/10.1146/annurev.immunol.22.012703.104803.

209. Frangione, V., Mortara, L., Castellani, P., De Lerma Barbaro, A., andAccolla, R. S. (2010) CIITA-driven MHC-II positive tumor cells: Preventive vaccines and superior generators of antitumor CD4+ T lymphocytes for immunotherapy. Int. J. Cancer 127, 1614 – 1624.

210. Meazza, R., Comes, A., Orengo, A. M., Ferrini, S., and Accolla, R. S. (2003) Tumor rejection by gene transfer of the MHC class II transactivator in murine mammary adenocarcinoma cells. Eur. J. Immunol. 33, 1183 – 1192.

211. Accolla RS, Jotterand-Bellomo M, Scarpellino L, Maffei A, Carra G, Guardiola J. aIr-1, a newly found locus on mouse chromosome 16 encoding a trans-acting activator factor for MHC class II gene expression. The Journal of experimental medicine 1986;164(1):369-74.

212. Mortara, L., Castellani, P., Meazza, R., Tosi, G., De Lerma Barbaro, A.,Procopio, F. A., Comes, A., Zardi, L., Ferrini, S., and Accolla, R. S. (2006)CIITA-induced MHC class II expression in mammary adenocarcinoma leads to a Th1 polarization of the tumor microenvironment, tumor rejection, and speci fi c antitumor memory. Clin. Cancer Res. 12, 3435 – 3443.

213. Accolla RS, Lombardo L, Abdallah R, Raval G, Forlani G, Tosi G. Boosting the MHC class II-restricted tumor antigen presentation to CD4C T helper cells: a critical issue for triggering protective immunity and re-orienting the tumor microenvironment toward an anti-tumor state. Frontiers Oncol 2014; 4:32; PMID:23986750; http://dx.doi.org/10.3389/fonc.2014.00032.

214. Bou Nasser Eddine F, Forlani G, Lombardo L, Tedeschi A, Tosi G, Accolla RS. CIITA-driven MHC class II expressing tumor cells can efficiently prime naive CD4(+)TH cells in vivo and vaccinate the host against parental MHC-II-negative tumor cells. Oncoimmunology (2017) 6:e1261777. doi: 10.1080/2162402X.2016.1261777.

215. Accolla RS, Ramia E, Tedeschi A, Forlani G. CIITA-driven MHC class II expressing tumor cells as antigen presenting cell performers: Toward the construction of an optimal anti-tumor vaccine. Front Immunol (2019) 10:1806. doi: 10.3389/fimmu.2019.01806.

216. Celesti F, Gatta A, Shallak M, Chiaravalli AM, Cerati M, Sessa F, et al. Protective anti-tumor vaccination against glioblastoma expressing the MHC class II transactivator CIITA. Front Immunol 2023;14:1133177.

217. Tosi G, Pilotti E, Mortara L, De Lerma Barbaro A, Casoli C, Accolla RS. 2006. Inhibition of human T cell leukemia virus type 2 replication by the suppressive action of class II transactivator and nuclear factor Y. Proc Natl Acad Sci U S A 103:12861–12866. doi: 10.1073/pnas.0601589103.

218. Forlani G, Abdallah R, Accolla RS, Tosi G. The major histocompatibility complex class II transactivator CIITA inhibits the persistent activation of NF-kB by the human T cell lymphotropic virus type 1 tax-1 oncoprotein. J Virol (2016) 90:3708– 21. doi: 10.1128/JVI.03000-15.

219. Forlani G, Turrini F, Ghezzi S, Tedeschi A, Poli G, Accolla RS, et al. The MHC-II transactivator CIITA inhibits tat function and HIV-1 replication in human myeloid cells. J Trans Med (2016) 14:94. doi: 10.1186/s12967-016-0853-5.

220. Angela M. Pierce, Amy K. Keating; Creating Anatomically Accurate and Reproducible Intracranial Xenografts of Human Brain Tumors (2014). Jove doi:10.3791/52017.

221. Viale G, Fusco N. Pathology after neoadjuvant treatment e How to assess residual disease. Elsevier. 2021; The Breast 62 (2022) S25eS28. https://doi.org/10.1016/j.breast.2021.11.009.

222. Provenzano E, et al. Standardization of pathologic evaluation and reporting of postneoadjuvant specimens in clinical trials of breast cancer: recommendations from an international working group. Modern Pathology. (2015) 28, 1185–1201. doi:10.1038/modpathol.2015.74.

223. Sahoo S, Susan C. Pathology of Breast Carcinomas After Neoadjuvant Chemotherapy, An Overview With Recommendations on Specimen Processing and Reporting. Arch Pathol Lab Med—Vol 133, 2009.

224. Ma, Y. H., Mentlein, R., Kneich, F., Kruse, M. L., Mehdorn, H. M., and HeldFeindt, J. (2008). Expression of stem cell markers in human astrocytomas of different WHO grades. J Neurooncol 86, 31–45.

225. Grabowski MM et al (2021) Immune suppression in gliomas. J Neurooncol 151(1):3–12. https:// doi. org/ 10. 1007/ S11060-020-03483-Y.

226. Springer, T. A. 1990. Adhesion receptors of the immune system. Nature 346:425.

227. Vremec, D., Zorbas, M., Scollay, R., Saunders, D. J., Ardavin, C. F., Wu, L. and Shortman, K. 1992. The surface phenotype of dendritic cells purified from mouse thymus and spleen: investigation of the CD8 expression by a subpopulation of dendritic cells. J. Exp. Med.176:47.

228. Nielsen, H. V., Christensen, J. P., Andersson, E. C., Marker, O. and Thomsen, A. R. 1994. Expression of type 3 complement receptor on activated CD8+ T cells facilitates homing to inflammatory sites. J. Immunol. 153:2021.

229. Stankov, V. Belakaposka-Srpanova, N. Bitoljanu, L. Cakar, Z. Cakar, G. Rosoklija, Visualisation of Microglia with the use of Immunohistochemical Double Staining Method for CD-68 and Iba-1 of Cerebral Tissue Samples in Cases of Brain Contusions, Pril (Makedon Akad Nauk Umet Odd Med Nauki) 36 (2015) 141-145.

230. Holness, C. L. & Simmons, D. L. Molecular cloning of CD68, a human macrophage marker related to lysosomal glycoproteins. Blood 81, 1607–1613 (1993).

231. Steinert, G. et al. Immune escape and survival mechanisms in circulating tumor cells of colorectal cancer. Cancer Res. 74, 1694–1704. https://doi.org/10.1158/0008-5472.CAN-13-1885 (2014).

232. Troiano, G. et al. Prognostic significance of CD68(+) and CD163(+) tumor associated macrophages in head and neck squamous cell carcinoma: A systematic review and metaanalysis. Oral.Oncol. 93,6675. https://doi.org/10.1016/j.oraloncology.2019.04.019 (2019).

233. De Palma, M. & Lewis, C. E. Macrophage regulation of tumor responses to anticancer therapies. Cancer Cell 23, 277–286. https://doi.org/10.1016/j.ccr.2013.02.013 (2013).

234. Vitale, I., Manic, G., Coussens, L. M., Kroemer, G. & Galluzzi, L. Macrophages and metabolism in the tumor microenvironment. Cell. Metab. 30, 36–50. https://doi.org/10.1016/j.cmet.2019.06.001 (2019).

235. Zhu, J. et al. The role of tumor associated macrophages in the tumor microenvironment: Mechanism and functions. Anticancer Agents Med. Chem. 16, 1133–1141. https://doi.org/10.2174/1871520616666160520112622 (2016).

236. Bennett, M. L., Bennett, F. C., Liddelow, S. A., Ajami, B., Zamanian, J. L., Fernhoff, N. B., et al. (2016). New tools for studying microglia in the mouse and human CNS. Proc. Natl. Acad. Sci. U.S.A. 113, E1738–E1746. doi: 10.1073/pnas. 1525528113.

237. Satoh, J., Kino, Y., Asahina, N., Takitani, M., Miyoshi, J., Ishida, T., et al. (2016). TMEM119 marks a subset of microglia in the human brain. Neuropathology 36, 39–49. doi: 10.1111/neup.12235.

238. Ruan, C., Sun, L., Kroshilina, A., Beckers, L., De Jager, P., Bradshaw, E. M., et al. (2020). A novel Tmem119-tdTomato reporter mouse model for studying microglia in the central nervous system. Brain Behav. Immun. 83, 180–191. doi: 10.1016/j.bbi.2019.10.009.

239. Seyfried, T.N.; El-Abbadi, M.; Roy, M.L. Ganglioside distribution in murine neural tumors. Mol. Chem. Neuropathol. 1992, 17,147–167.

240. Martínez-Murillo, R.; Martínez, A. Standardization of an orthotopic mouse brain tumor model following transplantation of CT-2A astrocytoma cells. Histol. Histopathol. 2007, 22, 1309–1326.

241. Marsh J, Mukherjee P, Seyfried TN. Akt-dependent proapoptotic effects of dietary restriction on late-stage management of a phosphatase and tensin homologue/tuberous sclerosis complex 2-deficient mouse astrocytoma. Clin Cancer Res. 2008;14(23):7751–7762.

242. Binello E, Qadeer ZA, Kothari HP, Emdad L, Germano IM. Stemness of the CT-2A Immunocompetent mouse brain tumor model: characterization in vitro. J Cancer. 2012;3:166–174.

243. Woroniecka, K.; Chongsathidkiet, P.; Rhodin, K.; Kemeny, H.; Dechant, C.; Farber, S.H.; Elsamadicy, A.A.; Cui, X.; Koyama, S.;Jackson, C.; et al. T-cell exhaustion signatures vary with tumor type and are severe in glioblastoma. Clin. Cancer Res. 2018, 24,4175–4186.

244. Shelton LM, Mukherjee P, Huysentruyt LC, Urits I, Rosenberg JA, Seyfried TN. A novel pre-clinical in vivo mouse model for malignant brain tumor growth and invasion. J Neurooncol. 2010;99(2):165–176.

245. Comba, S. M. Faisal, P. J. Dunn, A. E. Argento, T. C. Hollon, W. N. Al-Holou, M. L. Varela, D. B. Zamler, G. L. Quass, P. F. Apostolides, C. Abel, 2nd, C. E. Brown, P. E. Kish, A. Kahana, C. G. Kleer, S. Motsch, M. G. Castro, P. R. Lowenstein, Spatiotemporal analysis of glioma heterogeneity reveals COL1A1 as an actionable target to disrupt tumor progression. Nat Commun 13, 3606 (2022).

246. Jamous, A. Comba, P. R. Lowenstein, S. Motsch, Self-organization in brain tumors: How cell morphology and cell density influence glioma pattern formation. PLoS Comput Biol 16, e1007611 (2020).

247. Maas SLN, Abels ER, Van De Haar LL et al (2020) Glioblastoma hijacks microglial gene expression to support tumor growth. J Neuroinflammation 17:120. https:// doi. org/ 10. 1186/ s12974-020-01797-2.

248. Eng LF, Ghirnikar RS, Lee YL. Glial fibrillary acidic protein: GFAP-thirty-one years (1969–2000). Neurochem Res. 2000;25(9–10):1439–51.

249. Barthel PC, Staabs F, Li LY, Buthut M, Otto C, Ruprecht K, et al. Immunoreactivity to astrocytes in different forms of dementia: High prevalence of autoantibodies to GFAP. Brain Behav Immun Health. 2023;29: 100609.

250. McDermott DF, Atkins MB. PD-1 as a potential target in cancertherapy. Cancer Med. 2013;2(5):662–673.

251. Zhao H, Liao X, Kang Y. Tregs: where we are and what comes next? Front Immunol. (2017) 8:1578. doi: 10.3389/fimmu.2017.01578.

252. Ward-Hartstonge KA, Kemp RA. Regulatory T-cell heterogeneity and the cancer immune response. Clin Transl Immunol. (2017) 6:e154. doi: 10.1038/cti.2017.43.

253. Sivakumar H, Devarasetty M, Kram DE, Strowd RE and Skardal A (2020) Multi-Cell Type Glioblastoma Tumor Spheroids for Evaluating Sub-Population-Specific Drug Response. Front. Bioeng. Biotechnol. 8:538663.

254. Yi L, Zhou C, Wang B, Chen T, Xu M, Xu L, Feng H. Implantation of GL261 neurospheres into C57/BL6 mice: a more reliable syngeneic graft model for research on glioma-initiating cells. Int J Oncol. 2013 Aug;43(2):477-84. doi: 10.3892/ijo.2013.1962. Epub 2013 May 27. PMID: 23708048.

255. Pellegatta S, Poliani PL, Corno D, Menghi F, Ghielmetti F, Suarez-Merino B, et al. Neurospheres enriched in cancer stem-like cells are highly effective in eliciting a dendritic cell-mediated immune response against malignant gliomas. Cancer Res. 2006;66:10247–52. doi:10.1158/0008-5472.CAN-06-2048.

256. Eder K, Kalman B (2015) The Dynamics of interactions among immune and glioblastoma cells. Neuromol Med 17:335–352. https://doi.org/10.1007/s12017-015-8362-x.

257. Zong H, Parada LF, Baker SJ (2015) Cell of origin for malignant gliomas and its implication in therapeutic development. Cold Spring Harb Perspect Biol 7:a020610. https:// doi. org/ 10. 1101/ cshperspect.a020610.

258. Boche D, Perry VH and Nicoll JA: Review: Activation patterns of microglia and their identification in the human brain. Neuropathol Appl Neurobiol 39: 3-18, 2013.

259. Yu Y, Chen Y, Kim B, et al. Olig2 targets chromatin remodelers to enhancers to initiate oligodendrocyte differentiation. Cell 2013;152(1-2):248–61.

260. Lu F, Chen Y, Zhao C, et al. Olig2-dependent reciprocal shift in PDGF and EGF receptor signaling regulates tumor phenotype and mitotic growth in malignant glioma. Cancer Cell 2016;29(5):669–83.

261. Mehta S, Huillard E, Kesari S, et al. The central nervous system-restricted transcription factor Olig2 opposes p53 responses to genotoxic damage in neural progenitors and malignant glioma. Cancer Cell 2011;19(3):359–71.

262. Bowman RL, Klemm F, Akkari L et al (2016) Macrophage ontogeny underlies differences in tumor-specific education in brain malignancies. Cell Rep 17:2445–2459. https://doi.org/10.1016/j. celrep.2016.10.052.

263. Kevin P. Egan, Alexander G. Allen, Brian Wigdahl, Stephen R. Jennings, Modeling the pathology, immune responses, and kinetics of HSV-1 replication in the lip scarification model, Virology, Volume 514, 2018, Pages 124-133, ISSN 0042-6822, https://doi.org/10.1016/j.virol.2017.11.010.

264. Annual Review of Cancer Biology Vol. 2:155-173 (Volume publication date March 2018) First published as a Review in Advance on December 1, 2017 https://doi.org/10.1146/annurev-cancerbio-030617-050254.

265. Engelhardt B, Vajkoczy P, Weller RO. The movers and shapers in immune privilege of the CNS. Nat Immunol. 2017;18(2):123-31. doi: 10.1038/ni.3666.

266. Abbott NJ, Ronnback L. Hansson e: Astrocyte-endothelial interactions at the blood-brain barrier. Nat Rev Neurosci (2006) 7:41–53. doi: 10.1038/nrn1824, 5.

267. Louveau, A.; Smirnov, I.; Keyes, T.J.; Eccles, J.D.; Rouhani, S.J.; Peske, J.D.; Derecki, N.C.; Castle, D.;Mandell, J.W.; Lee, K.S.; et al. Structural and functional features of central nervous system lymphatic vessels.Nature 2015, 523, 337–341.

268. Cugurra A, Mamuladze T, Rustenhoven J, Dykstra T, Beroshvili G, Greenberg ZJ, et al. Skull and vertebral bone marrow are myeloid cell reservoirs for the meninges and CNS parenchyma. Sci (New York NY) (2021) 373:eabf7844. doi: 10.1126/science.abf7844.

269. Accolla RS, Tosi G. Adequate antigen availability: a key issue for novel approaches to tumor vaccination and tumor immunotherapy J Neuroimmune Pharmacol.2013;8:28-36. DOI: 10.1007/s11481-012-9423-7.

270. Szatmári T, Lumniczky K, Désaknai S, Trajcevski S, Hídvégi EJ, Hamada H, et al. Detailed characterization of the mouse glioma 261 tumor model for experimental glioblastoma therapy. Cancer Science. 2006;97(6):546-53. doi: 10.1111/j.1349-7006.2006.00208.x.

271. Ausman JI, FShapiro WR, Rall DP. Studies on the chemotherapy of experimental Bbrain tumors: development of an experimental model. Cancer Res. 1970;30:2394-400.

272. Reardon DA, Gokhale PC, Klein SR, Ligon KL, Rodig SJ, Ramkissoon SH, et al. Glioblastoma Eradication Following Immune Checkpoint Blockade in an Orthotopic, Immunocompetent Model. Cancer Immunology Research. 2016;4(2):124-35. doi: 10.1158/2326-6066.cir-15-0151.

273. Loffler, M.W., et al., Phase I/II Multicenter Trial of a Novel Therapeutic Cancer Vaccine, HepaVac-101, for Hepatocellular Carcinoma. Clin Cancer Res, 2022. 28(12): p. 2555-2566.

274. Reynisson B, Alvarez B, Paul S, Peters B, Nielsen M. NetMHCpan-4.1 and NetMHCIIpan-4.0: improved predictions of MHC antigen presentation by concurrent motif deconvolution and integration of MS MHC eluted ligand data. Nucleic acids research 2020;48(W1):W449-w54.

275. Ferrarese, R., et al., ZBTB18 inhibits SREBP-dependent lipid synthesis by halting CTBPs and LSD1 activity in glioblastoma. Life Sci Alliance, 2023. 6(1).